

INFORMATION TO USERS

This manuscript has been reproduced from the microfilm master. UMI films the text directly from the original or copy submitted. Thus, some thesis and dissertation copies are in typewriter face, while others may be from any type of computer printer.

The quality of this reproduction is dependent upon the quality of the copy submitted. Broken or indistinct print, colored or poor quality illustrations and photographs, print bleedthrough, substandard margins, and improper alignment can adversely affect reproduction.

In the unlikely event that the author did not send UMI a complete manuscript and there are missing pages, these will be noted. Also, if unauthorized copyright material had to be removed, a note will indicate the deletion.

Oversize materials (e.g., maps, drawings, charts) are reproduced by sectioning the original, beginning at the upper left-hand corner and continuing from left to right in equal sections with small overlaps.

Photographs included in the original manuscript have been reproduced xerographically in this copy. Higher quality 6" x 9" black and white photographic prints are available for any photographs or illustrations appearing in this copy for an additional charge. Contact UMI directly to order.

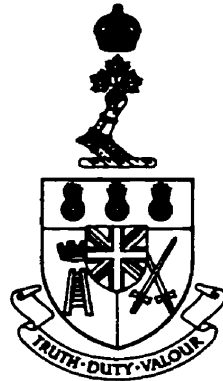
**Bell & Howell Information and Learning
300 North Zeeb Road, Ann Arbor, MI 48106-1346 USA**

UMI[®]
800-521-0600

**INVESTIGATION INTO THE SIGNIFICANCE
OF GEOMETRY ON
THE RADAR CROSS SECTION OF A SHIP**

by

**M. Losier, Lt(N), B.Eng
Canadian Armed Forces**



**DEPARTMENT OF
ELECTRICAL AND COMPUTER ENGINEERING**

ROYAL MILITARY COLLEGE OF CANADA

KINGSTON, ONTARIO



National Library
of Canada

Acquisitions and
Bibliographic Services

395 Wellington Street
Ottawa ON K1A 0N4
Canada

Bibliothèque nationale
du Canada

Acquisitions et
services bibliographiques

395, rue Wellington
Ottawa ON K1A 0N4
Canada

Your file *Votre référence*

Our file *Notre référence*

The author has granted a non-exclusive licence allowing the National Library of Canada to reproduce, loan, distribute or sell copies of this thesis in microform, paper or electronic formats.

The author retains ownership of the copyright in this thesis. Neither the thesis nor substantial extracts from it may be printed or otherwise reproduced without the author's permission.

L'auteur a accordé une licence non exclusive permettant à la Bibliothèque nationale du Canada de reproduire, prêter, distribuer ou vendre des copies de cette thèse sous la forme de microfiche/film, de reproduction sur papier ou sur format électronique.

L'auteur conserve la propriété du droit d'auteur qui protège cette thèse. Ni la thèse ni des extraits substantiels de celle-ci ne doivent être imprimés ou autrement reproduits sans son autorisation.

0-612-44851-7

Canada

**INVESTIGATION INTO THE SIGNIFICANCE
OF GEOMETRY ON
THE RADAR CROSS SECTION OF A SHIP**

by

Lt(N) M. Losier, B.Eng. (RMC)

Canadian Armed Forces

**A thesis submitted
to the School of Graduate Studies
in the
Department of Electrical and Computer Engineering
Royal Military College of Canada
Kingston, Ontario**

**In partial fulfilment of the requirements of
the degree
master of Engineering**

November 1997

COPYRIGHT

**“This thesis may be used within the Department of National Defense but copyright
for open publication remains the property of the author.”**


M. Losier

ABSTRACT

The radar cross section (RCS) of a warship plays an important role in its overall ability to survive in a hostile environment. The proliferation of sophisticated signal processors in today's radar systems, in particular missile seekers, makes it ever more difficult for warships to deceive or elude hostile intentions. The RCS has thus become a more predominant factor in the design of major warships across the world. There are three major means of determining the RCS of a complex object like a ship: scale modeling measurement, full-scale measurement and numerical modeling. This work concentrates on the significance of geometry in modeling an object numerically for RCS analysis. In this research, the object chosen to be modeled was the Canadian Patrol Frigate (CPF).

The work undertaken in this project was part of an effort directed by the Countermeasures Section of the Electronic Warfare Division of the Defense Research Establishment Ottawa. In essence, a computer aided design (CAD) model of the CPF suitable for RCS analysis was generated using a modified version of a software program called RAPPORT, which stands for Radar Signature and Prediction by Physical Optics and Ray Tracing. As the name implies, this software generated by the TNO Physics and Electronics Laboratory in the Netherlands is a high frequency method program which uses physical optics to predict the RCS of a complex object. Once complete, the model would be used to help ascertain the effectiveness of RCS reduction techniques prior to proceeding with expensive costs in time and resources related to installation.

In order to keep this document unclassified, the results presented concentrate on a single aspect of the findings made in this project, that being the importance of precision in generating the CAD model of the object to be analyzed.

ACKNOWLEDGMENTS

I would like to express my sincere appreciation to Dr. Y. Antar for his guidance, supervision and encouragement throughout this research and in the preparation of this thesis. I am equally grateful to Dr. S. Kashyap of the Defense Research Establishment Ottawa for taking the time to be co-advisor and allowing me to partake in an area of research not normally accessible to graduate students because of security classification issues.

I am also indebted:

To Dr. A. Louie of the Defense Research Establishment Ottawa for entertaining my countless emails so expediently by providing invaluable suggestions to facilitate the software conversions from DEC-FORTRAN to PC and for the numerous suggestions in modeling;

To Dr. K. Wheaton for his insight into the practical aspects of radar cross section reduction in the Canadian Navy; and

To my wife Sandra and my son Jonah for their patience and support without which I would not have been able to enjoy myself doing this research.

VITA

Name: Marcel Losier

Place and year of birth: Bathurst, New Brunswick, 1967

Education: Ecole Secondaire Népisiguit, Bathurst, New Brunswick, 1985

Collège militaire royal de St-Jean 1985-86

Royal Military College of Canada 1986-90;
BEng (Electrical Engineering) 1990

Royal Military College of Canada 1995-1997;
Post-Graduate Program

Experience: Joined Canadian Armed Forces as an ROTP candidate in 1985

Contact Training with the Canadian Patrol Frigate Leadyard in Saint-John, New Brunswick as a quality assurance inspector May to August 1988

On-Job-Training with the Defense Research Establishment Atlantic in Dartmouth, Nova Scotia in the Digital Signal Processing Section of the Underwater Acoustics Group January to May 1991

Trained as Maritime Engineer (MARE) Officer at the Combat Systems Engineering Division of the Canadian Forces Fleet School May 1991 to February 1992

Trained as Combat Systems Engineer, Phase VI Afloat, onboard HMCS ALGONQUIN, Halifax, Nova Scotia, February to September 1992. MARE 44C qualification September 1992

Employed as Combat Systems Engineer at the TRUMP Detachment, Halifax, Nova Scotia September 1992 to November 1993

Trained as Assistant Combat Systems Engineering Officer, A/CSEO, onboard HMCS IROQUOIS, Halifax, Nova Scotia, December 1993 - January 1995. Completed peacekeeping tour in the Adriatic Sea on Flagship for COMSNFL December 1993 to April 1994. MARE 44C.A8 qualification January 1995

Employed as Staff Officer Space and Electronic Warfare, SO SEW N34-6, in Maritime Command Headquarters, Halifax Nova Scotia January to July 1995

Employed as Squadron Commander for the Stone Frigate Military Academy, 1 Squadron, while completing the requirements of the Post-Graduate program part-time August 1995 to December 1997

Awards:

Second prize in the Kingston Chapter IEEE Student Paper Night, 1990

Westinghouse Award for Professional Excellence in Combat Systems Engineering Training, 1992

TABLE OF CONTENTS

Title	i
Abstract	ii
Acknowledgments	iii
Vita	iv
Table of Contents	vi
List of Figures and Plots	viii
List of Tables	xii
List of Terms and Acronyms	xiii
Chapter 1 INTRODUCTION	1-1
1.1 Background	1-1
1.2 Scope of Work	1-5
1.3 Outline	1-7
Chapter 2 RCS OVERVIEW	2-1
2.1 Radar Fundamentals	2-1
2.2 RCS Basics	2-2
2.3 RCS Prediction Techniques	2-14
2.4 Computational Methods	2-17
2.4.1 Geometric Optics	2-17
2.4.2 Physical Optics	2-19
2.4.3 Geometrical Theory of Diffraction	2-21

	2.4.4	Physical Theory of Diffraction	2-22
	2.4.5	Uniform Theory of Diffraction	2-23
	2.4.6	Method of Equivalent Currents	2-23
Chapter 3		RAPPORT MODELING	3-1
	3.1	RAPPORT - Basic Principles	3-1
	3.2	RAPPORT - Application	3-7
	3.3	RAPPORT - Limitations	3-10
	3.4	RAPPORT - Basic Performance Evaluation	3-13
Chapter 4		RESULTS	4-1
	4.1	Baseline Models	4-1
	4.2	RCS of Baseline Model	4-4
	4.3	Results of the Baseline Modifications	4-11
Chapter 5		DISCUSSION	5-1
	5.1	Validation of the Process.	5-1
	5.2	Review of Results	5-8
Chapter 6		CONCLUSION	6-1
		References and Bibliography	7-1

LIST OF FIGURES AND PLOTS

Figure 1-1	Picture of HMS WARRIOR	1-1
Figure 1-2	Concept of Surface Combatant of the 21 st Century - United States Navy	1-3
Figure 1-3	United States Navy Ships Conducting a Replenishment-at-Sea Illustrating the Relative Size Between an Aircraft Carrier, a Replenishment Ship and a Destroyer	1-4
Figure 1-4	Canadian Patrol Frigate HMCS CALGARY at Sea	1-5
Figure 2-1	Block Diagram of a Basic Radar System	2-2
Figure 2-2	Radar Cross Section of a Sphere	2-4
Figure 2-3	Radar Cross Section of a Flat Plate	2-5
Figure 2-4	Radar Cross Section of a 90° Dihedral Corner	2-6
Figure 2-5	Radar Cross Section of a 100° Dihedral Corner	2-7
Figure 2-6	Radar Cross Section of a Cone-Sphere	2-8
Figure 2-7	Radar Cross Section of a Typical Airplane	2-11
Figure 2-8	Radar Cross Section of a Typical Ship	2-12
Figure 2-9	Principal Radii of Curvature of a Doubly Curved Surface	2-18
Figure 2-10	Keller Cone of Diffracted Rays	2-21
Figure 2-11	Geometry for Wedge Diffraction	2-22
Figure 3-1	Representation of the Typical Scattering on an Object in Free Space	3-3
Figure 3-2	Scattering Mechanisms which Contribute to the Radar Cross Section of a Typical Ship	3-5
Figure 3-3	Software Flow Diagram of Radar Cross Section Process Utilized	3-9

Figure 3-4	MATLAB X-Y Plot of the Radar Cross Section Results for a 6.5" by 6.5" Flat Plate	3-17
Figure 3-5	SIGMAPLOT Polar Plot of the Radar Cross Section Results for a 6.5" by 6.5" Flat Plate	3-18
Figure 4-1	Scale Drawing of the Canadian Patrol Frigate	4-5
Figure 4-2	Canadian Patrol Frigate Baseline Model # 1	4-6
Figure 4-3	Canadian Patrol Frigate Baseline Model # 2	4-7
Figure 4-4	Radar Cross Section of the Canadian Patrol Frigate Baseline Model and Parameter File Information	4-8
Figure 4-5	Mainmast Supporting Structure Modification (modification 'b')	4-12
Figure 4-6	Solid Mainmast Modification (modification 'c')	4-13
Figure 4-7	Addition of the Starboard Side Boat Deck Flat Plate (modification 'e')	4-14
Plot 4-1	Radar Cross Section Difference Between Modification 'a' and Baseline Model of the Canadian Patrol Frigate	4-17
Plot 4-2	Radar Cross Section Difference Between Modification 'b' and Modification 'a' of the Canadian Patrol Frigate Model	4-18
Plot 4-3	Radar Cross Section Difference Between Modification 'c' and Modification 'b' of the Canadian Patrol Frigate Model	4-19
Plot 4-4	Radar Cross Section Difference Between Modification 'd' and Modification 'c' of the Canadian Patrol Frigate Model	4-20
Plot 4-5	Radar Cross Section Difference Between Modification 'e' and Modification 'd' of the Canadian Patrol Frigate Model	4-21
Plot 4-6	Radar Cross Section Difference Between Modification 'f' and Modification 'd' of the Canadian Patrol Frigate Model	4-22
Figure 4-8	Addition of Four VLSS Canisters on the Starboard Side (modification 'g') ..	4-24
Figure 4-9	Addition of the Hangar Port Aft Structure (modification 'k')	4-26

Plot 4-7	Radar Cross Section Difference Between Modification ‘g’ and Modification ‘f’ of the Canadian Patrol Frigate Model	4-27
Plot 4-8	Radar Cross Section Difference Between Modification ‘h’ and Modification ‘g’ of the Canadian Patrol Frigate Model	4-28
Plot 4-9	Radar Cross Section Difference Between Modification ‘i’ and Modification ‘h’ of the Canadian Patrol Frigate Model	4-29
Plot 4-10	Radar Cross Section Difference Between Modification ‘j’ and Modification ‘i’ of the Canadian Patrol Frigate Model	4-30
Figure 4-10	Modifications to the Hangar Aft End (modifications ‘l’ and ‘m’).	4-32
Figure 4-11	Addition of the Close-in-Weapon-System Mount (modification ‘o’)	4-33
Plot 4-11	Radar Cross Section Difference Between Modification ‘k’ and Modification ‘j’ of the Canadian Patrol Frigate Model	4-34
Plot 4-12	Radar Cross Section Difference Between Modification ‘l’ and Modification ‘j’ of the Canadian Patrol Frigate Model	4-35
Plot 4-13	Radar Cross Section Difference Between Modification ‘n’ and Modification ‘m’ of the Canadian Patrol Frigate Model	4-36
Plot 4-14	Radar Cross Section Difference Between Modification ‘n’ and Modification ‘l’ of the Canadian Patrol Frigate Model	4-37
Figure 4-12	Addition of the Funnel tail (modification ‘p’)	4-39
Plot 4-15	Radar Cross Section Difference Between Modification ‘o’ and Modification ‘n’ of the Canadian Patrol Frigate Model	4-41
Plot 4-16	Radar Cross Section Difference Between Modification ‘p’ and Modification ‘o’ of the Canadian Patrol Frigate Model	4-42
Plot 4-17	Radar Cross Section Difference Between Modification ‘q’ and Modification ‘p’ of the Canadian Patrol Frigate Model	4-43
Plot 4-18	Radar Cross Section Difference Between Modification ‘r’ and Modification ‘q’ of the Canadian Patrol Frigate Model	4-44
Plot 5-1	Radar Cross Section versus Elevation of Modification ‘k’	5-10

Plot 5-2 Radar Cross Section Difference Between Modification 'r' and Baseline Model of the Canadian Patrol Frigate Model 5-12

LIST OF TABLES

Table 2-1	Hierarchy of Scattering Shapes	2-10
Table 4-1	List of Modifications to the Baseline Model	4-10
Table 4-2	Impact of Modifications on the Radar Cross Section	4-45

LIST OF TERMS AND ACRONYMS

ATR	Automatic Target Recognition
CAD	Computer Aided Design
CIWS	Close-in-Weapon System, located on top of CPF Hangar
CPF	Canadian Patrol Frigate
DIDEC	Software program used to convert geometric files in formats for input to a variety of time domain and frequency domain electromagnetic interaction codes
DREO	Defense Research Establishment Ottawa
DXF	File format used as input to DIDEC, exported from AutoCAD
EFIE	Electric Field Integral Equation. Used in this research to denote the file format output from DIDEC and converted to *.002 file format for input into JUNCTION
FACET	File format output from JUNCTION and converted into *.PLAN file format for input into RAPPORT
GO	Geometric Optics
GTD	Geometrical Theory of Diffraction
HIST	RCS calculated by RAPPORT as a function of the number of reflections
ISAR	Complex square root of the RCS calculated by RAPPORT
OHGR	Osborne Head Gunnery Range, location of RCS measurement facility off Halifax
OPVAL	Operational Evaluation
MARE	Maritime Engineering
MULTI	RCS calculation by RAPPORT which includes multi-path
NCTR	Aerospace Non-cooperative Target Recognition
PLAN	File format used as input to RAPPORT

PO	Physical Optics
PTD	Physical Theory of Diffraction
RAM	Radar Absorbent Material
RAPPORT	Software program produced by TNO, stands for Radar Signature Analysis and Prediction by Physical Optics and Ray Tracing
RCS	Radar Cross Section
RMC	Royal Military College
ROTP	Regular Officer Training Plan
RPI	File format used to control the variables in the RAPPORT simulation
RPM	File format containing the material characteristics of the facets used by RAPPORT to compute the RCS
RPO	File format used as output from RAPPORT
SBR	Shooting and Bouncing Ray technique
STL	Stereo Lithography, file format used as input to RAPPORT
TNO	Netherlands Organization for Applied Scientific Research
TRUMP	Tribal Class Update and Modernization Project
USN	United States Navy
USNSM	United States Naval & Shipbuilding Museum
VISI	RAPPORT computation which produces the result of the visible area of the object for each reflection
VLSS	Vertical Launch Sea Sparrow
XPATCH	High-Frequency Electromagnetic-Scattering Prediction Code and Environment for Complex Three-Dimensional Objects

CHAPTER 1 INTRODUCTION

1.1 BACKGROUND

In the early days of naval warfare before the advent of radars and airplanes, ships could only be detected by one means, visually. Detection was severely limited by environmental conditions such as rain, fog and daylight. The curvature of the earth also limited the visual horizon making the height of a ship, usually dominated by the mast, the primary design factor with an impact on early detection by enemy ships. Of course the size, shape and color scheme of the ship were also important as would become the exhaust plume with the advent of steam propulsion and later gas turbines.

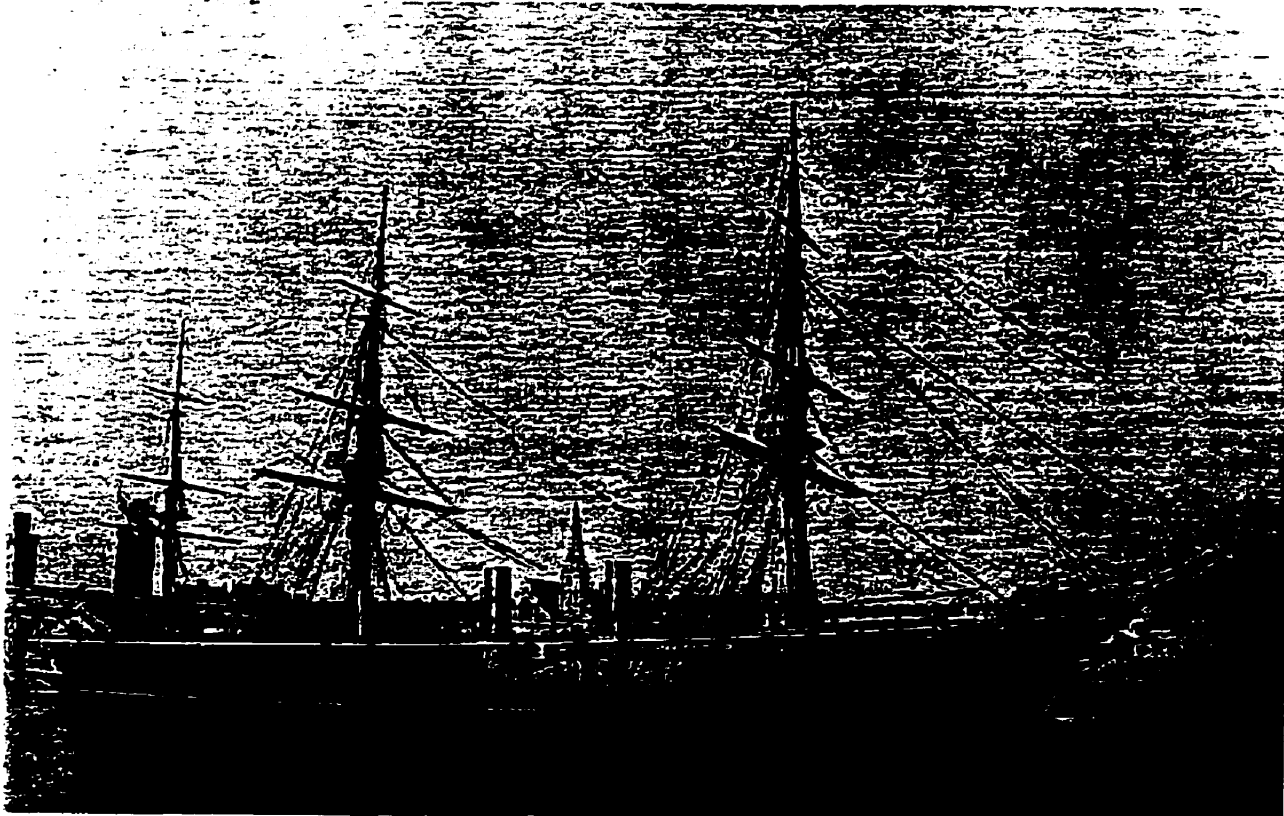


Figure 1-1 HMS WARRIOR 1860 - World's First Armored Iron Ship (from USNSM [1])

The origins of the radar can be traced back to Hertz as early as 1886 but it wasn't until the late 1930's that it saw any significant development. The invention of the first cavity magnetron by Randall and Boot in Britain overcame the major limitation of previous designs, high power at high frequencies [2]. This paved the way for efforts by Britain and the United States in 1940 which propelled radar development leaps and bounds.

The introduction of modern radar during the Second World War would take detection of enemy contacts into the next era. No longer would airplanes be limited by visual detection to classify and engage targets. Although sonar and radio intercept systems were also making their mark by this time, their impact on naval warfare was nowhere near as significant as that of the radar. Over the past 50 years, vast improvements have been made in the design of radar systems. The race towards technological supremacy in this area has brought forward the advent of electronic deception systems or jammers and off board decoys, primarily chaff. The integration of powerful signal processing techniques then enabled radars to use less and less power to detect targets in even the most difficult of environmental conditions, reducing the probability of counter detection. Finally, being able to package these sophisticated radars into missile seeker heads with integrated global positioning systems has forced ship builders to integrate radar cross section (RCS) management into the design of warships.

The improvements made over the last decade in signal processing techniques have rendered the detection of targets by radar increasingly more probable, even in what has become a noisy spectrum due to the proliferation of communication systems. The RCS of a warship has thus taken on a more significant role in ensuring survivability against enemy weapons, in particular missiles. New ship constructions in the defense industry around the world have been

making RCS management an important design criteria, in particular in smaller vessels where the benefits of signature reduction are greatest. The inclusion of a stealth design in a warship is depicted in Figure 1-2 by the Surface Combatant concept for the 21st Century of the United States Navy. In the Canadian Navy, RCS played an important part in the design and implementation of its latest class of warships, the Canadian Patrol Frigate (CPF). The ship provides a low profile over the water, thus making detection by other ships and low flying air contacts more difficult. The design also incorporates shaping to reduce the RCS, making it more stealthy to enemy radars.



Figure 1-2 Concept of Surface Combatant for the 21st Century - United States Navy (from Tappan [3])

The prime contractor for the CPF purchased twelve ship sets worth of radar absorbent material (RAM) tiles to further reduce the RCS of the CPF. For reasons beyond the scope of this discussion, it was deemed more appropriate to turn the ships over to the Canadian Navy without

having installed these RAM tiles. For the first few years of service, CPFs sent in operational areas were fitted with “mission fit” RCS reduction techniques which relied heavily on tie-on RAM panels in areas considered more important and practically treated.



Figure 1-3 United States Navy Ships Conducting a Replenishment-at-Sea Illustrating the Relative Size Between an Aircraft Carrier, a Replenishment Ship and a Destroyer (from USN [4])

In search for a more permanent solution, an Operational Evaluation (OPVAL) was initiated in the Spring of 1995 to determine the suitability of installing the RAM tiles which up to this point had been dormant in storage. That is to say, the Canadian Navy wanted to know if the operational benefits of reducing the CPF RCS by having these tiles installed would outweigh the cost of permanently mounting and maintaining them. The ultimate question was really one of putting a dollar value to the RCS reduction in dB which in turn would be used to estimate the improvement in probability of survival against enemy missiles. These estimates would take into

consideration the RCS of the ship as compared to that of the off board decoys under various operational conditions.

The OPVAL has since been terminated, again for reasons beyond the scope of this discussion, but the investigation into the requirement for a permanent CPF RCS reduction fit continues. This project is in essence an extension or subset of this ongoing effort by Dr. Satish Kashyap in the Countermeasures Section of the Electronic Warfare Division at the Defense Research Establishment Ottawa (DREO).



Figure 1-4 Canadian Patrol Frigate HMCS CALGARY at Sea (from USNSM [5])

1.2 SCOPE OF WORK

The initial scope of this thesis was to build a computer aided design (CAD) model of the CPF suitable for RCS analysis. Once complete, this model could be modified to assess the

effectiveness or suitability of applying RAM tiles on specified areas deemed to be RCS “hot spots”. For a number of reasons which will be discussed later in this report, the focus was scaled back partway through the research to that of investigating the significance of geometry on the RCS of ships. The results and discussion will thus concentrate on the more generic aspects of computer modeling as opposed to the specific merits of the efforts into a permanent RCS fit for the CPFs. Historically research in the field of RCS has been primarily conducted by defense related agencies and for the most part remains difficult to access. Results of related research in open literature is normally limited to aspects of a more generic nature. Although it is quite reasonable to assume that very similar research has been conducted by other countries, for the most part this project was initiated with little knowledge of the intricacies of modeling warships for RCS analysis. Such information would have allowed for a far more complete research into the RCS of the CPF but would have also rendered the potential findings unsuitable for open publication. Experience in the field of numerical modeling of ships for RCS analysis will nevertheless prove to be valuable in the overall goal of managing the RCS of the CPFs and subsequent naval platforms in Canada more effectively.

In order to achieve the initial aim of this research, the proposed methodology consisted of the following steps:

- a. study RCS theory, paying particular attention to modeling of complex shapes at high frequencies using computational methods such as Physical Optics, Geometry Optics and Physical Theory of Diffraction;
- b. study the use of the primary software tools required to conduct the research, namely AutoCAD, DIDEC, JUNCTION and RAPPORT;

- c. **generate and/or review basic models and validate the results to gain experience in the process;**
- d. **analyze the available results of the CPF models produced by DREO;**
- e. **improve on the DREO models of the CPF and perform the RCS computation; and**
- f. **document the results.**

These steps remain essentially unchanged except that the publication of results and discussion will be limited to what can remain open literature.

1.3 OUTLINE

This project will be described in six chapters. Chapter 1 has provided an introduction which included a brief history, the scope of work and the outline. Chapter 2 will review basic radar theory as it applies to RCS and cover pertinent aspects of RCS prediction techniques. Chapter 3 will describe the specifics of RCS modeling based on a software tool called RAPPORT. Chapter 4 will present the pertinent results and Chapter 5 will describe them more thoroughly. Finally Chapter 6 will provide concluding remarks.

CHAPTER 2 RCS OVERVIEW

2.1 RADAR FUNDAMENTALS

The term radar stands for radio detection and ranging which is quite appropriate for what is in essence a system which utilizes radio frequency (RF) signals to detect targets and determine their range. In basic terms, a radar determines the range R to a target using the equation below by clocking the time t it takes a known pulse of energy to get to a target and return.

$$R = ct/2 \tag{2.1}$$

where c is the speed of light.

The basic radar equation can be defined as follows:

$$P_r = (P_t G_t)/(4 \pi R^2) \times \sigma/(4 \pi R^2) \times A_e \tag{2.2}$$

- where:
- P_r is the return power;
 - G_t is the transmitter antenna gain;
 - R is the range between the transmitter and the target, assumed the same for the receiver;
 - σ is the RCS of the target; and
 - A_e is the aperture of the receive antenna.

This form of the equation relates the received power P_r , as the product of three distinct factors. The first term relates the power density at the target, the second term accounts for scattering by the target and attenuation of the power density back to the source and finally the effective aperture area of the receive antenna quantifies the portion of power density intercepted by the

radar [2]. The power received by a radar is evidently directly proportional to the RCS of the target.

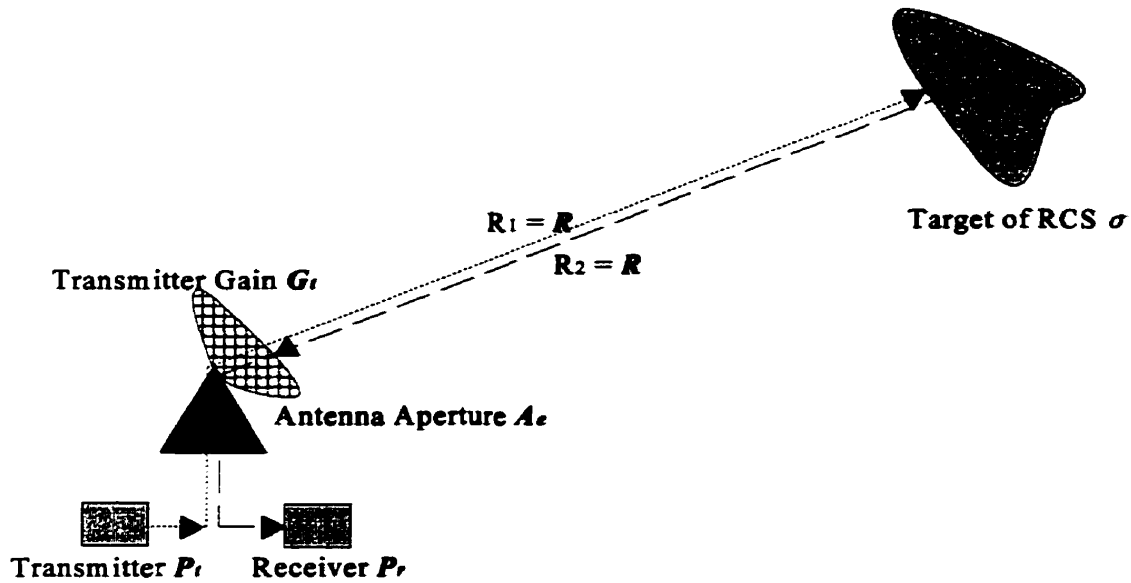


Figure 2-1 Block Diagram of a Basic Radar System

2.2 RCS BASICS

The dispersing of energy incident on an object from an electromagnetic wave in all directions is defined as scattering. The intensity of the energy scattered back towards the radar receiver constitutes the radar cross section of an object. For cases where the transmitter and the receiver are co-located the RCS is said to be monostatic, otherwise the RCS is bistatic. The RCS of a object can be defined as follows [2]:

$$\sigma = \lim_{R \rightarrow \infty} 4 \pi R^2 \frac{|\mathbf{E}_s|^2}{|\mathbf{E}_i|^2} \quad (2.3)$$

which relates the electric field scattered by the target back to the radar, E_s , with respect to the incident electric field E_i arriving at the target from the radar. The limit is included as a reminder that the relation applies in the far field and the remaining term normalizes the RCS to make it independent of the range.

The RCS is a function of target characteristics such as size, shape, composition and orientation with respect to the direction of arrival and the polarization of the incident wave.

There are four primary means of reducing the RCS of a target:

- a. passive cancellation;
- b. active cancellation;
- c. radar absorbent material (RAM); and
- d. shaping.

The last two applications are the ones of particular interest for this research. As the name implies, the use of RAM reduces the scattered energy by absorbing and dissipating it in the form of heat. On the other hand, shaping does not reduce the scattered energy as much as redistribute it. This effectively reduces the energy scattered in a particular direction of interest, generally towards the source, in favor of other directions. Shaping is a method more effectively used during the inception stage of ship construction but can be used throughout the life span of a ship with lesser success in cases where RAM is deemed unsuitable.

In order to appreciate the importance of shaping and geometry in the RCS of a complex object, a review of simple objects is essential. As the simplest three-dimensional body, the perfectly conducting sphere is often used as the basis for understanding the concept of RCS. Its geometry provides an invariance in echo with orientation but more importantly presents a

relatively simple exact solution to the wave equation by virtue of its surface coinciding with that of the spherical coordinate system. As shown in Figure 2-2, the RCS of the sphere is highly dependant on its electrical size, $ka = 2\pi a/\lambda$, with k being the wave number and a the radius of the sphere.

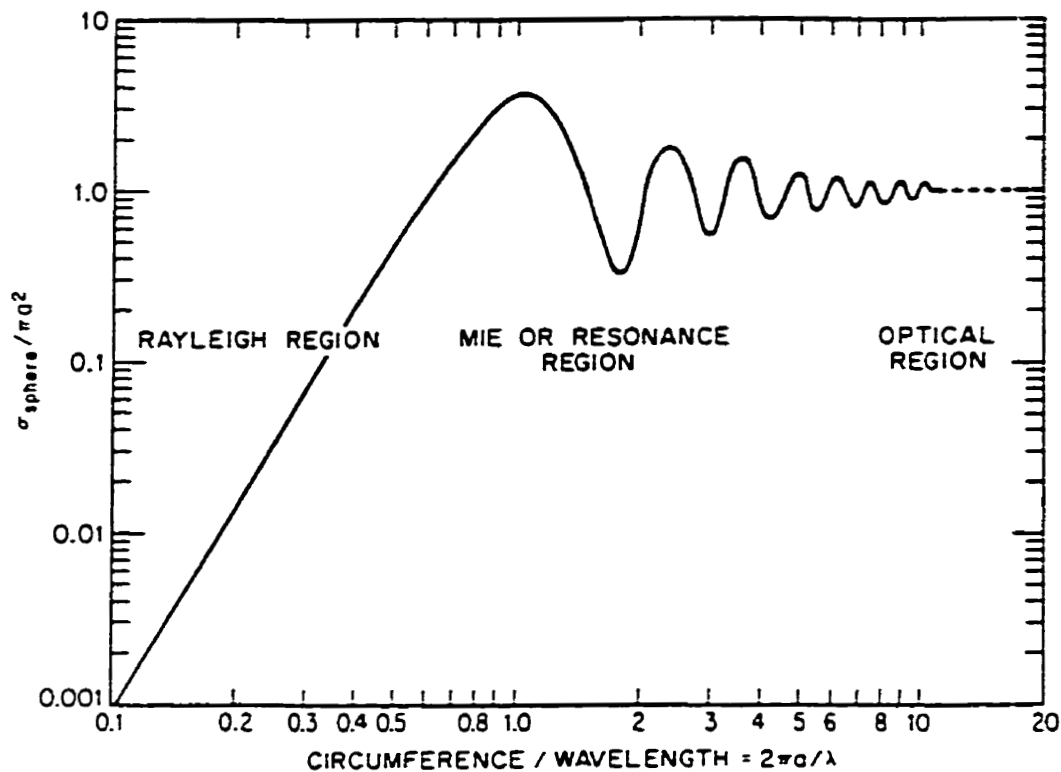


Figure 2-2 Log-Log Representation of the Radar Cross Section of a Sphere (from Knott [2])

The RCS of a perfectly conducting sphere can be divided into three distinct regions. In the Rayleigh Region objects are electrically small, $ka < 1$, and the normalized RCS rises quickly from a value of zero to a peak which overshoots unity. In the middle region, the RCS fluctuates around a normalized RCS of unity as a result of the contribution from the specular or forward reflections adding in and out of phase with the creeping waves which must travel different distances around the sphere as its size changes. This part of the curve is commonly referred to as

the Mie or Resonance Region. As the size of the sphere gets bigger, $ka > 10$, the attenuation of the creeping waves becomes more pronounced and the oscillations of the previous region diminish progressively. The term Optical Region is used to characterize this part of the curve as the RCS approximates the geometric optics value of πa^2 very closely.

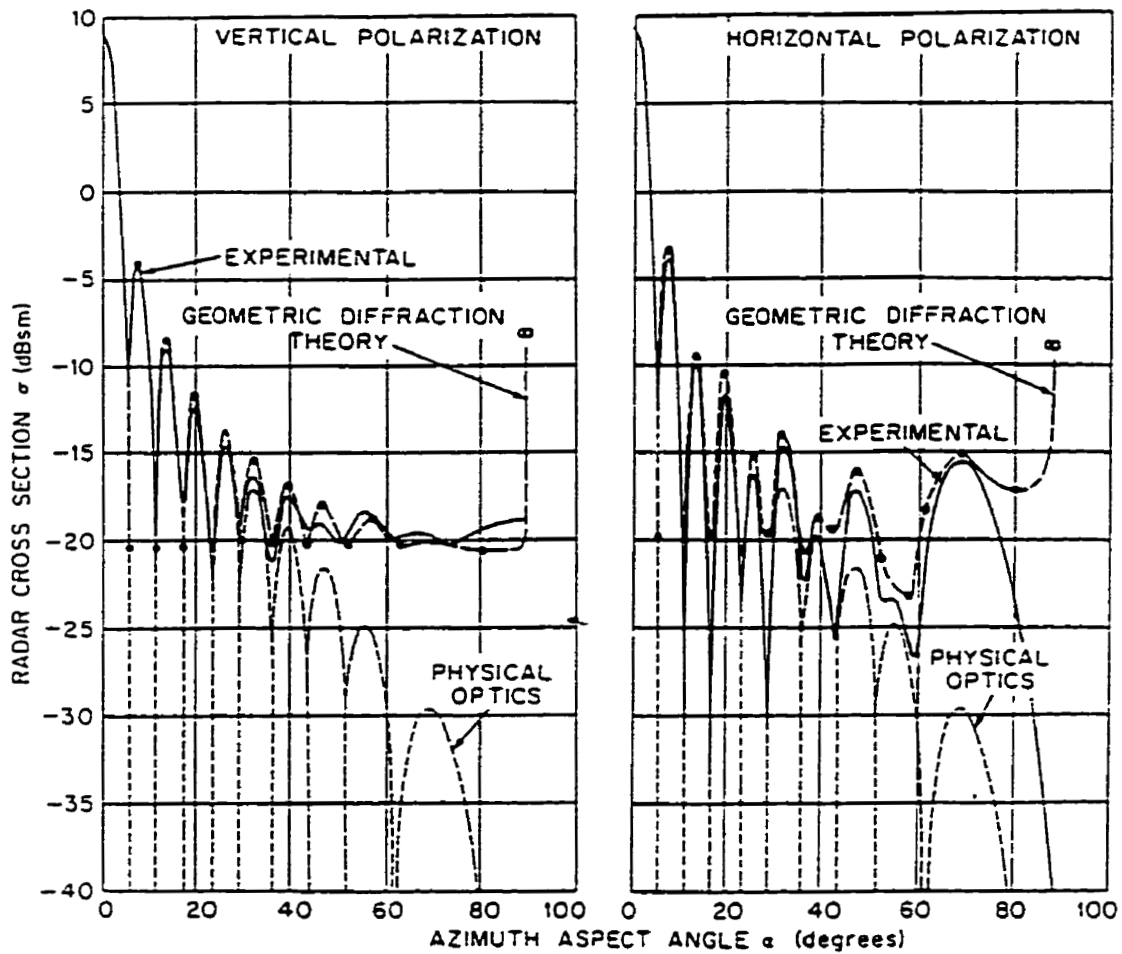


Figure 2-3 Radar Cross Section of a 6.5" Square Plate with $\lambda = 1.28"$ (from Skolnik [6])

The sphere is a great tool to provide insight into the concept of RCS but unfortunately complex objects are seldom formed uniquely of spheres. It is thus equally important to understand the RCS of more common shapes. The first example is the RCS of a flat plate. The

RCS for a plate of dimensions 5λ by 5λ is shown in Figure 2-3.

Figure 2-3 shows the results of experimentation as well as curves from two computational methods which will be described later, namely geometrical diffraction theory and physical optics. What is important to note here is that the RCS at normal incidence, $\alpha = 0^\circ$, has the greatest amplitude with the remainder of the return decreasing more or less as a sinc function. The magnitude of the return at normal incidence increases and the width of this main return decreases as the size of the plate increases. For very large flat areas, the main return is often referred to as a "spike".

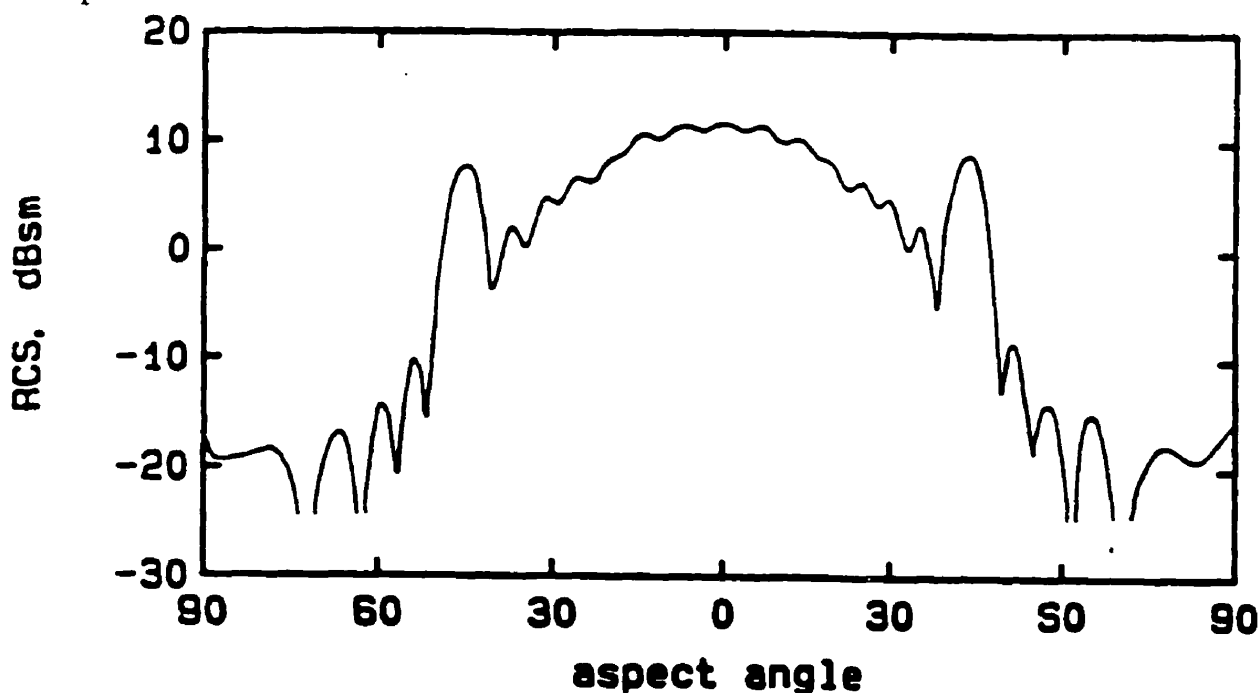


Figure 2-4 Radar Cross Section of a 90° Dihedral Corner Reflector with 17.9 cm Sides Measured at 9.4 GHz (from Knott [2])

The dihedral corner is the next shape of interest in our review of the RCS of simple objects. The results shown in Figure 2-4 and Figure 2-5 were measured using two plates of dimensions 5.6λ which is very close to that of the flat plate presented above. In the case of the

90° dihedral, the obvious difference in the return compared to the flat plate is the wider aspect angle of the main lobe. By simply changing the angle between the two plates to 100°, the RCS at normal incidence is greatly reduced but the return away from incidence is still quite significant. From these results, it is not difficult to understand the importance of minimizing the use of 90° dihedral corners on a warship. This is not easily accomplished when one takes into account the fact that the sea surface acts as the ground plane for the ship and forms one side of a dihedral for many areas of concern.

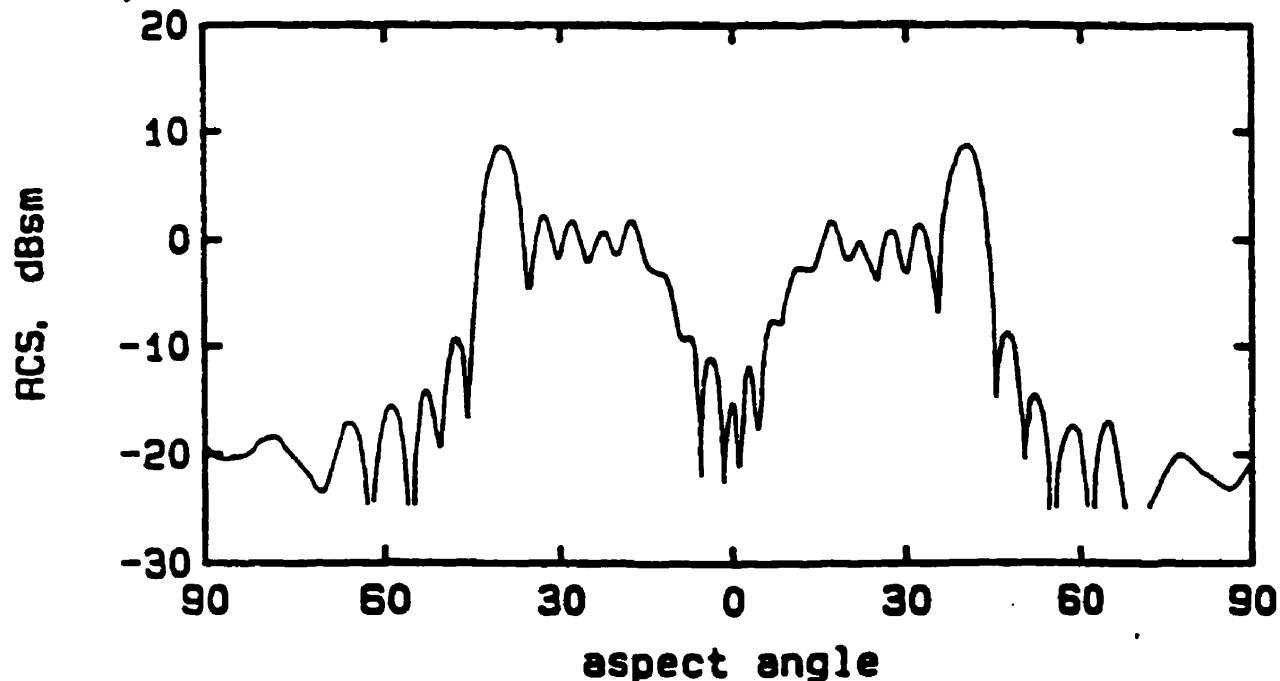


Figure 2-5 Radar Cross Section of a 100° Dihedral Corner Reflector with 17.9 cm Sides Measured at 9.4 GHz (from Knott [2])

The last shape to be reviewed is the cone-sphere for which typical measured results are presented in Figure 2-6. As can be seen in the figure, the spherical aspect of the object offers a very constant RCS in magnitude for azimuths covering roughly 85° to 275°. The discontinuity or change of aspect between the cone and the sphere results in a rather significant change in the RCS at roughly 80° and 280°. The remainder of the curve, accounting for the cone aspect of the

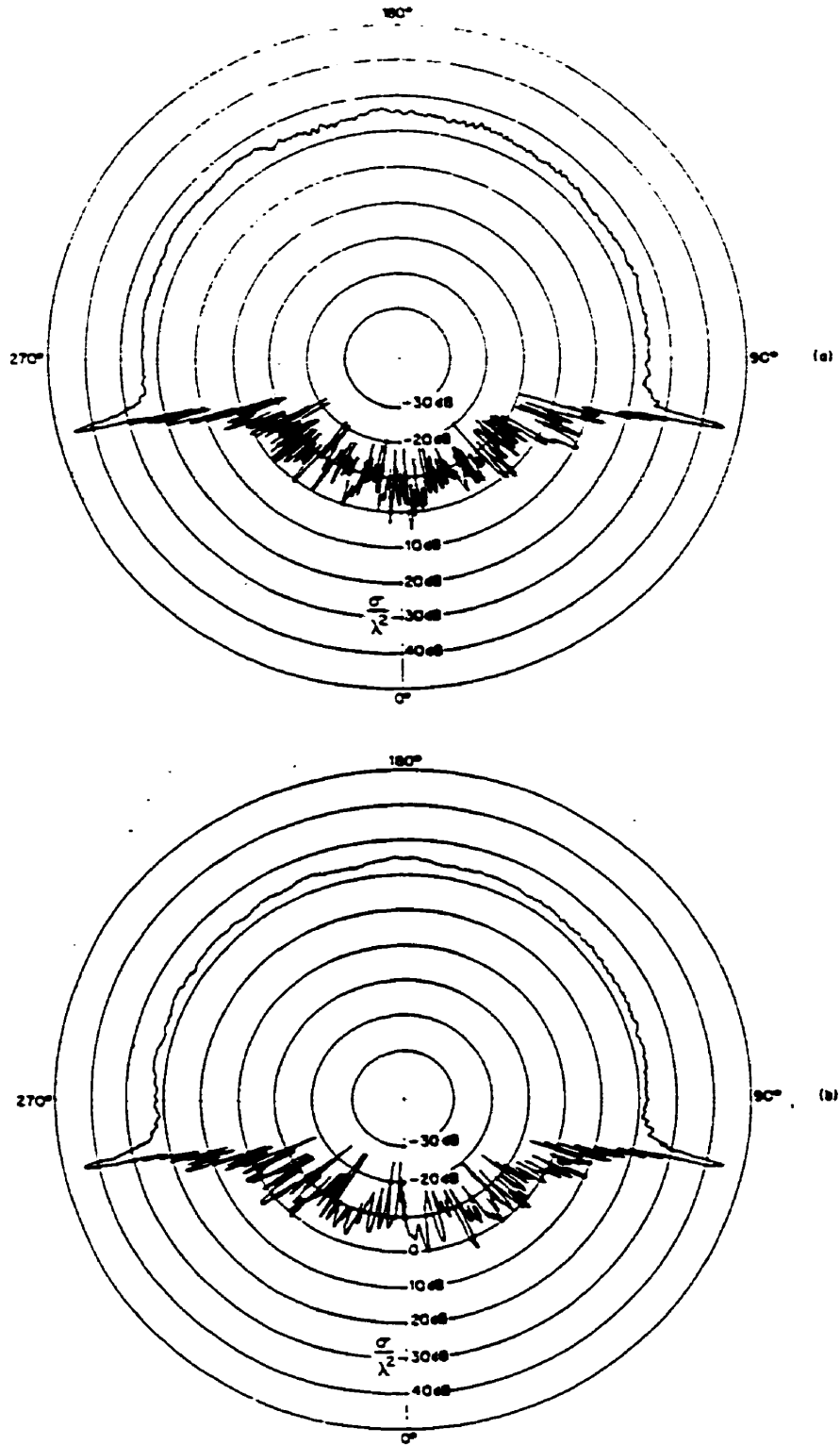


Figure 2-6 Radar Cross Section of a Large Cone-Sphere with 12.5° Half Angle and Radius Base = 10.4λ . (a) Horizontal (Perpendicular) Polarization, (b) Vertical (Parallel) Polarization (from Knott [2])

object, offers interesting insight into RCS. First of all, the return is dominated by a myriad of spikes of varying magnitudes as opposed to the smooth constant return provided by the spherical aspect of the shape. The magnitudes of the returns are also far lower than those of the spherical aspect of the sphere, even at 0° where the cone provides an identical two-dimensional surface area to that of the sphere. This further illustrates the importance of the shape or geometry of an object in dealing with RCS.

The significance of shaping in designing complex objects should be apparent based on the examples used above. The hierarchy of scattering shapes provided in Table 2.1 is a helpful guide in reducing the RCS of a complex object during the inception stage of a ship's design. This table can also prove useful in identifying potential scatterers of concern during the in-service phase of the ship.

Determining the RCS of complex objects is no trivial matter for several reasons. The most significant factor is the complexity of the surface profiles. Complex objects such as ships and airplanes contain numerous major scattering centers and countless less significant scatterers which go in and out of phase with each other continuously [2]. Figure 2-7 illustrates the spike dominated appearance of raw RCS measurement curves. In taking full-scale measurements, even slight changes in the position of the ship resulting from wind or seas produce variances in the RCS curves over time, making precise identification of the scattering centers very difficult. This explains why raw measured data is generally represented as a percentile level of the signals collected over windows of 1° - 5° to average out the curves. This is the case in the example presented in Figure 2-8 where 80, 50 and 20 percentile levels are drawn over 2° windows. The 80 percentile in fact represents the level at which 80% of the measured data samples fall below

Geometry	Type	Free- Deg.	Size Deg.	Formula	Remarks
	Square trihedral corner retro-reflector	r^2	L^4	Maximum $\sigma = \frac{170 \lambda^2}{L^2}$	Strongest return; high RCS due to triple reflection
	Right dihedral corner reflector	r^2	L^4	Maximum $\sigma = \frac{80 \lambda^2}{L^2}$	Second strongest; high RCS due to double reflection. Tapers off gradually from the maximum with changing θ and sharply with changing ϕ .
	Flat plate	r^2	L^4	Maximum $\sigma = \frac{4\pi a^2 L^2}{L^2}$ Normal incidence	Third strongest; High RCS due to direct reflection. Grows off sharply as incidence changes from normal.
	Cylinder	r^2	L^3	Maximum $\sigma = \frac{70 \pi \lambda^2}{L}$ Normal incidence	Prevalent cause of strong, broad RCS over varying aspect (θ). Grows off sharply as azimuth (ϕ) changes from normal. Can combine with flat plate to form dihedral corner reflector.
	Sphere	r^2	L^2	Maximum $\sigma = \pi a^2$ Normal incidence	Prevalent cause of strong, broad RCS from other than those due to large angles in target body. Energy contained in two directions.
Geometry	Type	Free- Deg.	Size Deg.	Formula	Remarks
	Straight edge normal incidence	r^0	L^2	$\sigma(0, \theta) \propto L^2$ θ - aspect θ_{inc} - interior dihedral angle between faces meeting at edge	Limiting case of 2-dimensional curved plate mechanism as radius becomes ∞ . Prevalent cause of strong, narrow RCS peaks from supersonic aircraft.
	Curved edge normal incidence	r^{-1}	L^1	$\sigma(0, \theta_{inc}) \propto L$ $\theta \geq 1$	Limiting case of 3-dimensional curved plate mechanism as principal radius becomes ∞ . The function f is the same as in mechanism 3.
	Cone	r^{-1}	L^0	$\sigma(\theta, \phi, \theta_0) \propto L^0$ θ, ϕ - interior angles of tip θ_0 - aspect angle	Limiting case of previous mechanism as a becomes ∞ . For $a=0$, the tip is that of a cone. For $a=0$, the tip is the corner of a thin sheet, or tip.
	Discontinuity of curvature along a straight line, normal incidence	r^{-2}	L^0	$\sigma \propto \frac{1}{\Delta \kappa} \left(\frac{L}{\lambda} \right)^2$ $\Delta \kappa$ - jump in reciprocal of d^2y/dx^2 - slope of surface w.r.t. incident ray	Strongest of an infinite sequence of discontinuities. Very weak mechanism which together with a sharp discontinuity of slope on RCS of cone sphere.
	Discontinuity of curvature of a curved edge	r^{-2}	L^{-1}	$\sigma(\theta, \phi) \propto \frac{1}{a^2} \left(\frac{L}{\lambda} \right)^2$ $f(\theta, \phi)$ - function of aspect a - radius of edge $\gg \lambda$	Important mechanism for traveling wave backscatter where RCS of discontinuity is augmented by gain of traveling wave structure. Dependences are based on dimensional considerations.
	Discontinuity of curvature along an edge	r^{-4}	L^{-2}	$\sigma(\theta, \phi) \propto \frac{1}{a^4} \left(\frac{L}{\lambda} \right)^4$ $f(\theta, \phi)$ - function of aspect	Important mechanism for traveling wave backscatter where RCS of discontinuity is augmented by gain of traveling wave structure. Dependences are based on dimensional considerations.

Table 2-1 Hierarchy of Scattering Shapes (from Knott [2])

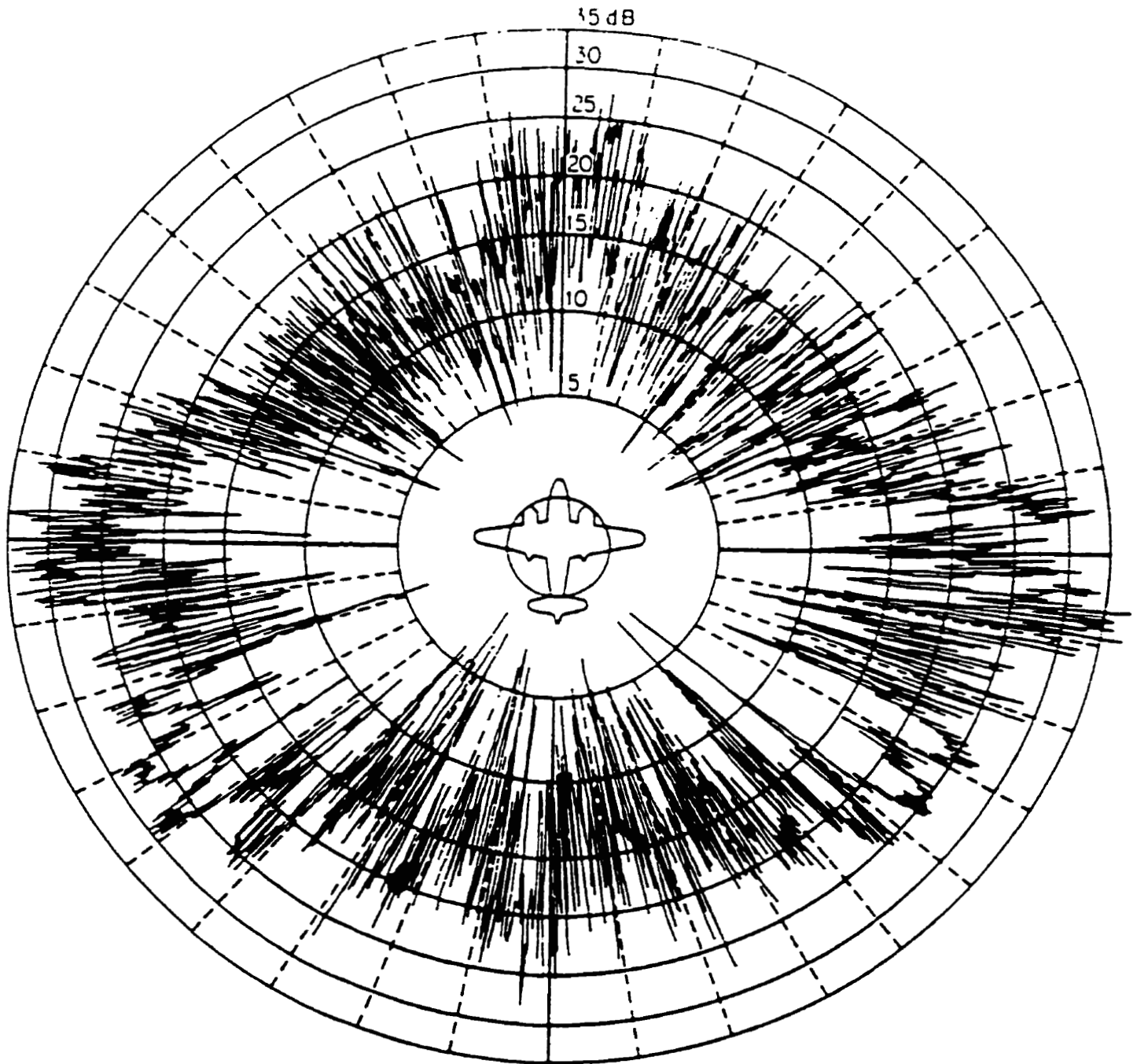
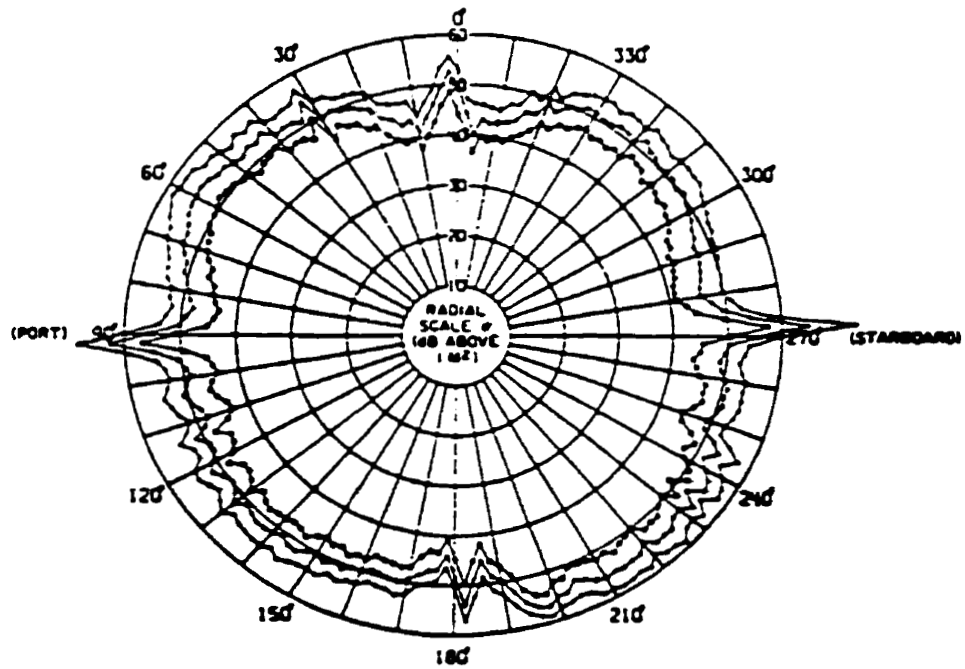
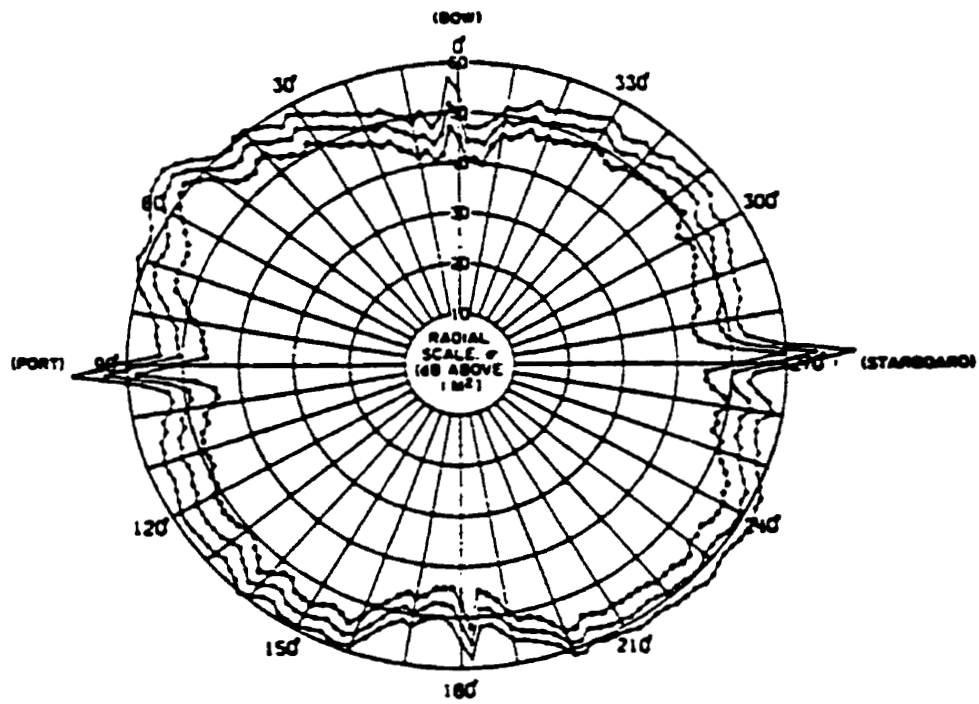


Figure 2-7 Radar Cross Section of the B-26 Two-Engine Bomber with $\lambda = 10$ cm as a Function of Azimuth Angle (from Skolnik [6])



(a)



(b)

Figure 2-8 RCS of a Large Auxiliary Ship at (a) S band (2800 MHz) and (b) X Band (9225 MHz), both with Horizontal Polarization (from Skolnik [6])

for a specific azimuth, thus excluding the top 20% of the sampled magnitudes [2]. This representation is far more valuable in determining the overall RCS of a complex object.

A quick analysis of the RCS presented in Figure 2-8 shows that a narrow spike can be found on both the Port and Starboard sides of the ship. Relying on the basic review of simple objects presented earlier, one can see that these narrow spikes are likely as a result of returns from large flat areas, in this particular case the ship's sides. The overall RCS remains surprisingly constant over most aspect angles except for the areas around the bow, stern and broadside.

As will be shown later, computational methods tend not to produce returns as constant with aspect angle as those obtained from measured data for two reasons. First, the modeling of complex ships generally results in simplifying the geometry. For example, a bulkhead may be modeled as being perfectly flat and vertical when in fact it has slight curvatures and an angle different from 90° with the deck. This contributes to vary the RCS, in some case rather significantly. The second contributing factor is the inclusion of small details. The methods used to model complex objects are generally based on geometric optics approximations which become invalid for small objects, $ka < 10$, although values as low as one wavelength can produce results within 1 or 2 dB over most aspect angles [6]. This forces the modeling of small objects to be either an improper representation of reality or as is more often the case have them not included at all because of the increase in complexity they pose. The absence of a significant number of small objects is not believed to impact the overall average RCS as much as deny the result curve of a more constant return with respect to the aspect angle. Accordingly, spikes from flat plates are not tapered down as much as they would normally be when small objects are included. The

exclusion of small objects means that returns in the vicinity are seen as being of lower levels than they might be in reality as a result of the simplified modeling for the affected reflection of energy.

2.3 RCS DETERMINATION TECHNIQUES

The most basic means of determining the RCS of an object is analytically. Unfortunately the complexity of solving the wave equations for RCS restricts this approach to simple objects such as spheres and cylinders. Alternatively, there are three main methods used to determine the RCS of a complex object such as the CPF:

- a. full-scale measurements;
- b. scale measurements; and
- c. computational prediction techniques.

For large objects such as ships, full-scale measuring is considered the most accurate technique since the data is taken in an environment which most closely resembles the operational theatre. This is due to the fact that measurements are acquired by either air or shore based radars over open ranges at sea. This enables accounting for effects such as reflections from the sea which would otherwise be difficult to predict. The two primary limitations of this method are the costly use of resources to conduct the measurements, necessitating the ship to be at sea, and the inability to predict the effectiveness of RAM treatment before installation. This technique is thus generally reserved as a final confirmation of a ship's RCS signature.

Scale measurements consist of building accurate representations of the object being modeled and determining the RCS using extremely high frequency emitters. For the CPF, a

0.0126 brass model was built by Thorn EMI which required the use of a laser operating at 890 GHz to determine the RCS at 11.2 GHz, 0.0126 multiplied by the source frequency [7,8]. The advantage of this method is that it allows for a very accurate determination of scattering centers as long as the model is a reliable representation of the ship. The construction of an accurate brass model is however an expensive proposition which doesn't lend itself well to changes in the configuration of the ship. The analysis is also generally limited to a single frequency as the number of available sources in the immediate frequency ranges of the models are scarce.

Finally the RCS of an object can be determined using computational prediction techniques. Although techniques which employ the method of moments can be used to compute the RCS of objects, the large memory requirements generally restrict their use to electrically small objects, less than one wavelength. The majority of the computational methods used to analyze the RCS of large objects such as ships ordinarily invoke either the application of simple ray tracing approximations similar to Snell's law or solving the Stratton-Chu integral formulation of Maxwell's equations by applying geometric optics approximations to simplify the calculations. These methods include but are not limited to geometric optics, physical optics, physical theory of diffraction, geometric theory of diffraction, uniform theory of diffraction and method of equivalent currents. These methods are for the most part lower bound restricted by the geometric optics approximation to objects of wavelengths greater than 10 although as indicated earlier the use of values down to as low as one wavelength are not unreasonable [2].

Computational prediction techniques, also referred to as high frequency techniques, benefit from the fact that complex bodies may be considered as a collection of independent scattering centers since collective interactions are very small at these frequencies. That is as long as the length of

these independent scattering bodies is large compared to the wavelength. The geometric details also play an important role in the application of these methods.

Computational prediction techniques rely on the construction of models representing the object to calculate the RCS, usually using CAD tools. Unlike scale modeling, these methods lend themselves very well to changes in the configuration of a ship throughout its life and can easily be used to assess the effectiveness of RAM treatment which can lead to installation cost and time savings. Once a model has been built, it can be used to compute the RCS for any frequency above the base frequency chosen to determine the minimum size of the construction lines in the model. The primary drawbacks of these methods are that the optical approximations which simplify the computation make it difficult to accurately model complex objects, such as ships. This is particularly true of modeling at frequencies below 10 GHz and practically unfeasible below 1 GHz. The lower bound size limitations of these methods apply not to the overall size of the object being modeled but rather to the lines which form the shapes utilized to represent it. On an object the size of a warship the use of dimensions no smaller than 3 centimeter, one wavelength at 10 GHz, makes it very difficult to accurately describe parts which require many lines to define their shape. Such is the case for spheres and cylinders, especially if they are electrically small themselves. Increasing the number of lines and shapes used to represent an object not only increases the complexity of the model but also impacts on the time required to compute the RCS. The modeling process is further restricted in practice to the use of simple objects. In the case of this project, the construction of the CPF was formed entirely of triangles.

2.4 COMPUTATIONAL METHODS

The software used to determine the RCS of the models built for this project is based on physical optics although it does use some of the principles of geometric optics to produce faster and more accurate results. The application of these two methods by RAPPOR will be covered in the next chapter. Geometric optics and physical optics will be the focus of this section as they form the building blocks for most computational methods. Methods such as the geometrical theory of diffraction, the physical theory of diffraction, the uniform theory of diffraction and the method of equivalent currents all offer variances of physical and geometric optics in solving the limitations of shadow boundaries and edges diffraction. These methods will be mentioned briefly out of interest as each provides its own advantages and limitations.

2.4.1 GEOMETRIC OPTICS

Geometric optics has its roots firmly planted into the same principles which govern classical optics. Snell's law explains that when a ray confronts a medium of differing refractive index, two rays are formed. One ray is reflected at the same angle from the surface normal as the angle of the incident ray. The second ray is transmitted across the boundary and into the second medium but at a different angle than that of the incident ray depending on the properties of the media on either side of the boundary. This bending of the angle is termed refraction. At the limit, a ray incident to a perfectly conducting surface would reflect all the energy, making the transmitted or refracted ray null.

The theory of geometric optics is based on the conservation of energy within a fictitious tube called a ray which combined in large numbers can approximate a wave. The behavior of

these rays forming a wave incident to a surface can be described using Snell's law. The energy intensity of rays which converge or diverge at the surface may be calculated from the curvatures of the reflective surface and the incident wave at a point called the specular point, where the surface normal points towards the radar. The final result is simply [2]:

$$\sigma = \pi a_1 a_2 \quad (2.4)$$

where a_1 and a_2 are the principle radii of curvature of the body at the specular point.

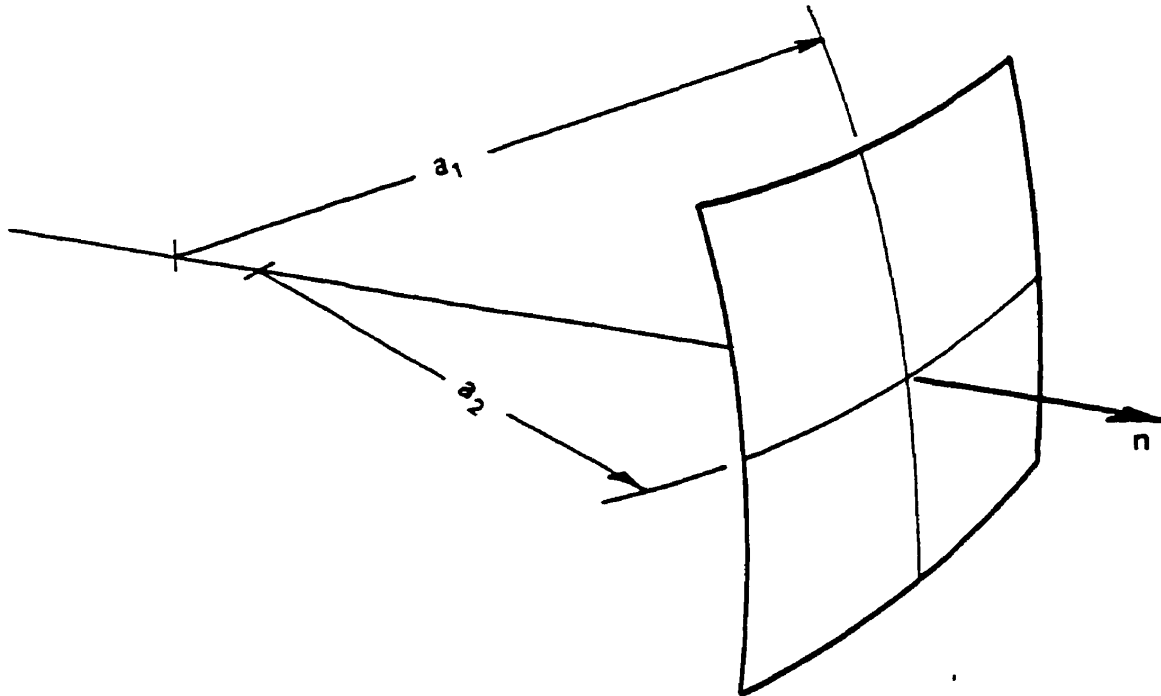


Figure 2-9 Principal Radii of Curvature of a Doubly Curved Surface (from Skolnik [6])

It is interesting to note that the results presented in equation (2.4) for the RCS are not a function of frequency. Of course the results consider the wavelength to be at the limit of zero and are only valid for electrically large objects. Using the sphere as an example, the values of a_1 and a_2 would be equal to the radius of the sphere which gives the same result as proposed earlier in section 2.2, that being $\sigma/\pi a^2 = 1$.

In addition to being limited to surfaces where the radii of curvature is large compared to the wavelength, this method requires two other conditions to be met. The first is that the specular point not be close to the edges of the surface as no provision is made to account for the effects of diffraction from edges. The second condition limits the application of this method to surfaces which are curved. A flat or singly curved surface results in one or both curvatures having an infinite radii and according to equation (2.4) this would make the RCS infinite, which is obviously not the case.

2.4.2 PHYSICAL OPTICS

The description of physical optics is very much an exercise in derivations using two simple approximations. The starting point is the transformation of Maxwell's equations to the form presented below, known as the Stratton-Chi integral equations [2,6,9]:

$$\mathbf{E}_s = \oint \{j\omega\mu(\mathbf{n} \times \mathbf{H})\psi + (\mathbf{n} \times \mathbf{E}) \times \nabla\psi + (\mathbf{n} \cdot \mathbf{E})\nabla\psi\} dS \quad (2.5a)$$

$$\mathbf{H}_s = \oint \{-j\omega\mu(\mathbf{n} \times \mathbf{E})\psi + (\mathbf{n} \times \mathbf{H}) \times \nabla\psi + (\mathbf{n} \cdot \mathbf{H})\nabla\psi\} dS \quad (2.5b)$$

where: $\mathbf{E}_s, \mathbf{H}_s$ scattered electric and magnetic fields;
 \mathbf{E}, \mathbf{H} total electric and magnetic fields;
 ω radian frequency;
 μ permeability; and
 \mathbf{n} unit surface normal erected at the surface patch dS .

and Green's function ψ is:

$$\psi = e^{jk_r}/4\pi r \quad (2.6)$$

with r being the distance measured from the surface patch dS to the point at which the scattered fields are desired. The first approximation is that of far-field which requires r to be large compared to any dimension used to describe the object being analyzed. The gradient of Green's function becomes [6]:

$$\nabla\psi = jk\psi_0\mathbf{s} \quad (2.7a)$$

$$\psi_0 = e^{-jk\mathbf{r}\cdot\mathbf{s}} e^{jkR}/4\pi R \quad (2.7b)$$

where \mathbf{s} is a unit vector pointing from an origin in or near the object to the far-field observation point, usually back towards the radar, and R is the distance from the origin of the object to the far-field observation point.

The second approximation is that of the surface being infinite and perfectly flat. The tangential field components $\mathbf{n} \times \mathbf{E}$ and $\mathbf{n} \times \mathbf{H}$ can thus be replaced by [6]:

$$\mathbf{n} \times \mathbf{E} = 0; \quad (2.8a)$$

$$\mathbf{n} \times \mathbf{H} = 2\mathbf{n} \times \mathbf{H}_i \text{ for illuminated surfaces; and} \quad (2.8b)$$

$$\mathbf{n} \times \mathbf{H} = 0 \quad \text{for shaded surfaces.} \quad (2.8c)$$

This simplifies equations (2.5) by making them a function entirely of the known incident field values. By evaluating one of these approximate integrals and substituting the result into equation (2.3), the RCS of a rectangular plate viewed in a principal plane can be expressed as [6]:

$$\sigma = 4\pi \left| (A \cos \theta) / \lambda \cdot (\sin(kl \sin \theta)) / (kl \sin \theta) \right|^2 \quad (2.9)$$

where A is the physical area of the plate, θ is the angle between its surface normal and the direction of the radar, and l is the length of the plate in the principal plane containing the surface

normal and the radar line of sight.

There are two problems with physical optics. The first is the breakdown of the second approximation which occurs when objects become electrically small, typical of high frequency methods. The second limitation is the failure to account for edge diffraction, as was the case for geometric optics. The results of this method are evidently quite good at normal incidence but get progressively less accurate as the angle θ increases.

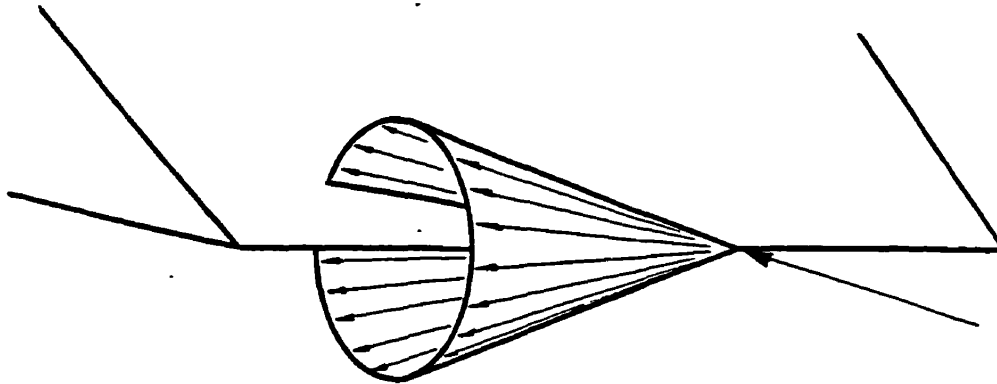


Figure 2-10 Keller's Cone of Diffraction Rays (from Skolnik [6])

2.4.3 GEOMETRICAL THEORY OF DIFFRACTION

The geometrical theory of edge diffraction was designed to address the problem of diffraction from edges or surface discontinuities, ignored by the both geometric and physical optics. This method consists of essentially assigning a phase and magnitude to the fields diffracted from surface discontinuities [2,6]. Up to this point, the reflection of rays was only considered to be possible in the plane of incidence containing the incident ray and the surface normal. Keller proposes that when a ray is incident to a edge, the result is a multitude of rays as shown in Figure 2-10.

The diffraction coefficients required to solve the solution offer the added feature of taking

into account the polarization of the incident ray, again ignored by physical optics. This method offers a definite improvement but the singularity of diffraction coefficients at certain aspects forces obvious false results.

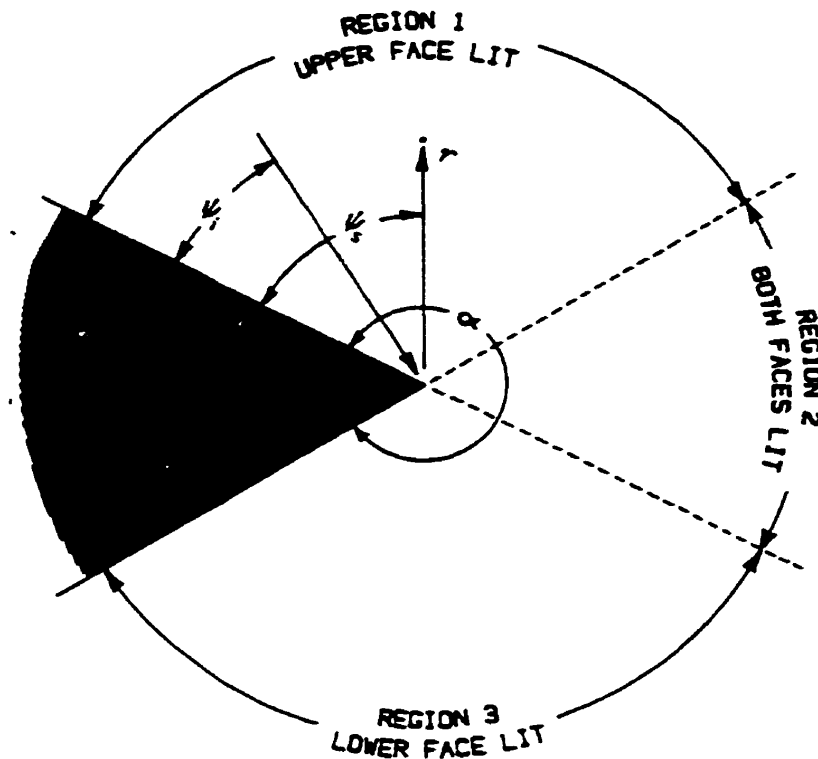


Figure 2-11 Geometry for Wedge Diffraction (from Skolnik [6])

2.4.4 PHYSICAL THEORY OF DIFFRACTION

The physical theory of diffraction attempts to improve on previous methods by addressing the singularity in diffraction coefficients mentioned in the geometrical theory of diffraction. This method, developed by Ufimtsev, also seeks to determine the diffraction coefficients at the edge but considers the coefficients as originating from two separate sources, the edge and the surface. By subtracting the contribution of the surface, the diffraction coefficients are thus those of the edge itself in the absence of any other source. Ufimtsev's diffraction coefficients are determined for not just one but three areas as depicted by Figure 2-11. This added characteristic creates

significant computational complications but the improvement over Keller's geometrical theory of diffraction make the effort well worthwhile [2,6].

Oddly enough, since Ufimtsev's coefficients are representative purely of the edge, having removed the surface contribution, the physical theory of diffraction must be combined with another method such as physical optics in order to account for the surface contributions.

2.4.5 UNIFORM THEORY OF DIFFRACTION

The uniform theory of diffraction is another attempt to improve upon the two basic high frequency techniques presented earlier. It looks to address the singularities of the diffraction coefficients confronted by the geometrical theory of diffraction but in a quite different approach from the physical theory of diffraction. The method removes the singularities by simply multiplying the diffraction coefficients by a Fresnel integral. However, this method fails to eliminate the caustic difficulties of the geometrical theory of diffraction where an infinity of rays may converge [2].

2.4.6 METHOD OF EQUIVALENT CURRENTS

The last of the high frequency techniques to be reviewed is the method of equivalent currents which seeks to address the caustics left unresolved by the geometric theory of diffraction. The premise for this method is the fact that any finite current distribution yields a finite result for the far field when that distribution is summed in a radiation integral. The challenge comes from determining suitable expressions for the current distribution. Ryan and Peters proposed such expressions as did Knott and Senior. The results offer improvements in two areas. Not only do the edge-diffracted fields remain finite in caustic directions but the

scattering direction is no longer limited to areas on the Keller cone, thus offering a more complete solution to the problem. The main limitation of this method is that the added computational requirements prohibits its implementation on complex bodies [2].

CHAPTER 3 RAPPORT MODELING

The primary tool used in this project to analyze the RCS of the CPF is a software program written by the Netherlands Organization for Applied Scientific Research (TNO) Physics and Electronics Laboratory called RAPPORT, which stands for Radar Signature Analysis and Prediction by Physical Optics and Ray Tracing. The purpose of this chapter will be to cover the basic principles, application and limitations of this software. RAPPORT is not a complete package when it comes to RCS prediction in that it requires several software tools to allow it to perform and depict the RCS of an object properly. In essence, RAPPORT inputs ASCII text, performs the RCS computations and outputs ASCII text. There are different ways to manipulate the ASCII text files depending on the processing platform used. This project made use of three software programs to generate the ASCII input and two for the output. In order to gain an appreciation for the effectiveness of the methodology proposed, RAPPORT will be compared briefly to XPATCH which is a similar software tool produced in the United States by a consortium comprising both military and civilian organizations.

3.1 RAPPORT - BASIC PRINCIPLES

As the name implies, RAPPORT uses physical optics and ray tracing to predict the RCS of complex objects. The application of physical optics is quite similar to the description provided in the previous chapter but the use of ray tracing in the acronym is somewhat misleading. RAPPORT uses the so-called ray tracing as a means of determining which patches of the object contribute to the RCS computation for a specific angle of incidence and observation point, taking into account both single and multiple reflections [9]. The fallacy is that the use of

ray tracing is nothing more than the application of Snell's law with respect to reflection. In any case, RAPPOR is essentially an improved physical optics method when it comes to estimating the RCS.

The building blocks used by RAPPOR to compute the RCS of complex objects are the same equations proposed earlier in physical optics, namely equations (2.3), (2.5) and (2.8). Equations (2.8) are only valid for a plane wave incident to a perfectly conducting infinite plane with the reflected wave being planar and its direction equal to the angle of the incident wave as determined by Snell's law. RAPPOR takes this concept one step further by accounting for a plane wave incident upon a non-perfectly conducting infinite plane, making the polarization of the incident wave a factor in the reflection coefficients for the reflected wave [9].

The following derivations are based on the pictorial representation of Figure 3-1. The fields incident to the surface may be broken into components in the plane of incidence E_p^i, H_p^i and components normal to the plane of incidence E_n^i, H_n^i . Equations (2.8) can then be expressed as [9]:

$$\mathbf{n} \times \mathbf{E}_n = (1 + R_n)\mathbf{n} \times \mathbf{E}_n^i; \quad (3.1a)$$

$$\mathbf{n} \times \mathbf{E}_p = (1 - R_p)\mathbf{n} \times \mathbf{E}_p^i; \quad (3.1b)$$

$$\mathbf{n} \times \mathbf{H}_n = (1 - R_n)\mathbf{n} \times \mathbf{H}_n^i; \text{ and} \quad (3.1c)$$

$$\mathbf{n} \times \mathbf{H}_p = (1 + R_p)\mathbf{n} \times \mathbf{H}_p^i \quad (3.1d)$$

where the Fresnel reflection coefficients R_n and R_p are defined as [9]:

$$R_n = [\mu_r \cos \theta_i - (\mu_r \epsilon_r - \sin^2 \theta_i)^{1/2}] / [\mu_r \cos \theta_i + (\mu_r \epsilon_r - \sin^2 \theta_i)^{1/2}]; \text{ and} \quad (3.2a)$$

$$R_p = [\epsilon_r \cos \theta_i - (\mu_r \epsilon_r - \sin^2 \theta_i)^{1/2}] / [\epsilon_r \cos \theta_i + (\mu_r \epsilon_r - \sin^2 \theta_i)^{1/2}] \quad (3.2b)$$

with θ_i representing the angle between the normal and the direction of the incident wave, and μ_r , ϵ_r characterizing the material of the surface being radiated. By substituting the Fresnel coefficients with the values for perfectly conducting material, $R_s = -1$ and $R_p = 1$, equations (3.1) reduce to the results of equations (2.8) presented earlier as expected. The formulation of equations (3.1) allows us to calculate the scattered field for both parallel and perpendicular polarizations of monostatic as well as bistatic radar systems.

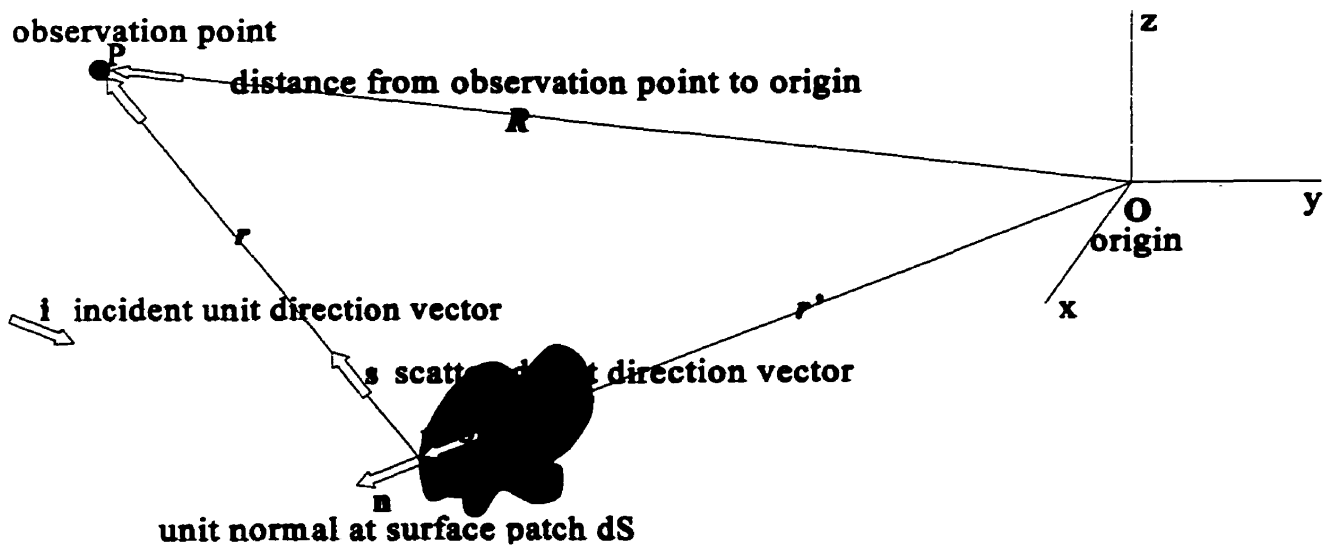


Figure 3-1 Representation of a Typical Scattering on an Object in Free Space (inspired by Brand [9])

The starting point in determining an expression to compute the RCS is equation (2.3).

The incident electric and magnetic fields, E^i and H^i , of this equation can be defined as [9]:

$$E^i = e_i E_o e^{i \cdot r}; \text{ and} \quad (3.3a)$$

$$H^i = h_i H_o e^{i \cdot r} \quad (3.3b)$$

where e_i and h_i are the incident unit direction vectors associated with electric and magnetic field

magnitudes E_o and H_o respectively. By combining equations (2.5), (3.2) and (3.3), the scattered perpendicular polarized component of the electric field can be described as [9]:

$$\mathbf{E}^s = -E_o [jke^{jkR}/(4\pi R)] \cdot \oint \mathbf{f}_n e^{j(\mathbf{l} \cdot \mathbf{s})} dS \quad (3.4a)$$

in which:

$$\mathbf{f}_n = (1 - R_n)(\mathbf{n} \cdot \mathbf{i}) \{ \mathbf{e}_i - (\mathbf{e}_i \cdot \mathbf{s}) \mathbf{s} \} + (1 + R_n) \{ (\mathbf{n} \cdot \mathbf{s}) \mathbf{e}_i - (\mathbf{s} \cdot \mathbf{e}_i) \mathbf{n} \} \quad (3.4b)$$

Similarly, the scattered parallel polarized component of the electric field can be described as [9]:

$$\mathbf{H}^s = -H_o [jke^{jkR}/(4\pi R)] \cdot \oint \mathbf{f}_p e^{j(\mathbf{l} \cdot \mathbf{s})} dS \quad (3.5a)$$

in which:

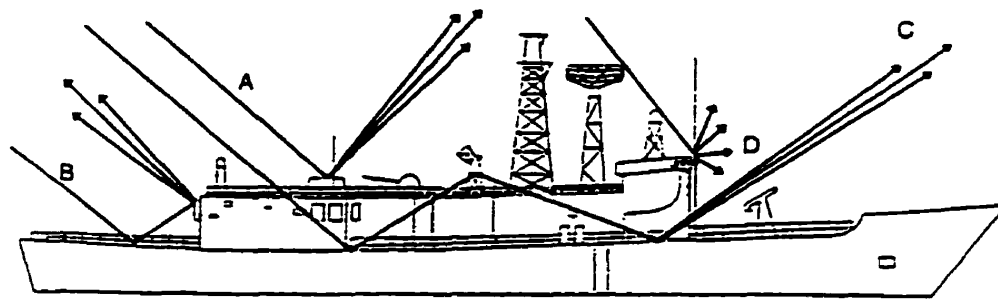
$$\mathbf{f}_p = (1 - R_p)(\mathbf{n} \cdot \mathbf{i}) \{ \mathbf{h}_i - (\mathbf{h}_i \cdot \mathbf{s}) \mathbf{s} \} + (1 + R_p) \{ (\mathbf{n} \cdot \mathbf{s}) \mathbf{h}_i - (\mathbf{s} \cdot \mathbf{h}_i) \mathbf{n} \} \quad (3.5b)$$

In both the above cases, equations (3.4a) and (3.5a), the enclosed surface integral is over the illuminated area of the surface.

These relations are valid for any combination of incident and scattered field angles, directions \mathbf{i} and \mathbf{s} , and thus valid for monostatic and bistatic cases. The scattered parallel and perpendicular polarized field relations can also account for surface materials which are not perfectly conducting by virtue of the Fresnel reflection coefficients described earlier. Each surface polygon forming the object being analysed can be given a different reflection characteristic. For example, all the polygons forming the ship's side or a specific "hot spot" on the structure might be given the properties of a layer of radar absorbent material to evaluate the effectiveness of several different radar cross section reduction plans prior to installation.

The final concept required to understand RAPPORT is that of multiple reflections.

Figure 3-2 gives a brief overview of the scattering mechanisms one might expect from a typical ship.



- A = single reflection
- B = double reflection
- C = triple reflection
- D = edge diffraction

Figure 3-2 Scattering Mechanisms which Contribute to the Radar Cross Section of a Typical Ship (from Brand [9])

The basic application of the physical optics equations only account for single reflections, defined as ray 'A' in Figure 3-2. By using ray-tracing, RAPPOR can also account for the patches which contribute to the RCS as a result of reflections from other patches rather than being limited to direct incidence from the source for any scattering angle. For example using ray 'B' in Figure 3-2, Snell's law of reflection can be employed to calculate the scattering angle of the reflection from the flight deck towards the hangar. In essence, this scattering angle acts as the incident angle to the patch(es) on the affected part of the hangar. The process continues for triple reflections and so on. Ray-tracing is thus important to RAPPOR in accounting for both multiple reflections and in determining which patches are being "illuminated" for any given incident field angle and observation point combination.

The equations detailed above to quantify the scattered fields are valid for any surface geometry. Unfortunately, the surface integrals in equations (3.4a) and (3.5a) are not easily solved

by computer. To simplify matters, RAPPOR accepts only polygons in the ASCII text input file to define the shape of the object being analysed. RAPPOR then simplifies the process even further by converting the polygons into triangles to facilitate solving of the integral. The following expressions are used specifically by RAPPOR in the computation of the RCS [9]:

$$\mathbf{E}^s = -E_o [jke^{jkR}/(4\pi R)] \sum_n(\Delta_i) \oint e^{j(\mathbf{i}-\mathbf{s})} dS; \text{ and} \quad (3.6a)$$

$$\mathbf{H}^s = -H_o [jke^{jkR}/(4\pi R)] \sum_p(\Delta_i) \oint e^{j(\mathbf{i}-\mathbf{s})} dS \quad (3.6b)$$

The summations are over the illuminated patches and the integrations are over the individual patches. The integrals can be evaluated using the following simplified expression [9]:

$$\oint e^{j(\mathbf{i}-\mathbf{s})} dS = [-1/jk] [1/|\mathbf{v} \times \mathbf{n}|^2] \cdot \sum (\mathbf{v} \times \mathbf{n}) \cdot \Delta \mathbf{a}_m [\sin(k\Delta \mathbf{a}_m \cdot \mathbf{v}/2)] / [\sin(k\Delta \mathbf{a}_m \cdot \mathbf{v}/2)] \exp[jk(\Delta \mathbf{a}_m + \Delta \mathbf{a}_{m+1}) \cdot \mathbf{v}/2] \quad (3.7)$$

where:

$$\mathbf{v} = \mathbf{i} - \mathbf{s}; \text{ and}$$

$$\Delta \mathbf{a}_m = (\mathbf{a}_{m+1} - \mathbf{a}_m)$$

The triangular patch is defined by vertices $\mathbf{a}_1, \mathbf{a}_2, \mathbf{a}_3, \mathbf{a}_4$, and $\mathbf{a}_4 = \mathbf{a}_1$. It is important to note that although RAPPOR accepts polygons in the ASCII text input file, the models generated in this project were comprised entirely of triangles. This is due to the fact that the RAPPOR input format used for this work required the outward normal of the polygons defining the object and the software utilized to generate the normals was valid only for triangles. This was not seen as a serious limitation given that RAPPOR internally converts all polygons into triangles in order to be able to make use of equation (3.7).

3.2 RAPPORT - APPLICATION

RAPPORT requires several different software tools to allow it to estimate the RCS of an object. These tools are dependant on the computer platform used and the type of display format desired. In generic terms, RAPPORT requires an input file describing the object geometry and outputs the RCS as a function of variables such as frequency, azimuth angle and elevation angle for example. The output file must then be manipulated in order to make it compatible with a software tool which can display the raw RCS data in a more meaningful display format. Figure 3-3 depicts the block diagram of the software used in this project with the applicable file formats.

The first step in creating a model for RCS analysis is the most important and time consuming of the process. It consists of “lifting-off” the vertices coordinates from drawings of the ship and entering them manually into AutoCAD, a commercial CAD software program. These coordinates could have been input directly into DIDEDEC but since the latter accepted one of the AutoCAD output file formats, it was deemed more suitable to take advantage of the more sophisticated CAD software to accomplish what amounts to being the most difficult aspect of the RCS analysis process.

DIDEDEC is a CAD software tool used to create wire grid, surface patch and cell models of complex structures for electromagnetic interaction analysis [10]. DIDEDEC can accept several different file formats and can even interface directly with a digitizing tablet but none of the alternatives available to build the model where deemed more appropriate than the method proposed in Figure 3-3. DIDEDEC was thus used simply to convert the model generated by AutoCAD into a format compatible with JUNCTION.

For its part, JUNCTION is primarily utilized to convert the DIDEDEC output into a file compatible with RAPPORT. The version of JUNCTION used was actually stripped of most of its traditional computational code and modified to perform essentially one task, that of calculating the outward normal for each facet or triangle forming the model. The modified version of JUNCTION also provided invaluable error checking capabilities, increasing the level of confidence in the AutoCAD model significantly.

The process up to this point was often repeated several times to ensure that the model was as accurate as possible prior to the actual RCS computations being performed. As indicated earlier, RAPPORT recognizes any polygon shaped element to construct the model but this capability was not used to its limit as it would have required software capable of specifically calculating the outward normal for shapes other than triangles. The model was consequently generated entirely of triangles but this was not seen as a major limitation since RAPPORT internally converts all polygons into triangles prior to the prescribed calculation process taking place. RAPPORT also accepts files in the STL (Stereo Lithography) format but this option was not used as the software tools compatible with this format were not readily available. It should be noted that TNO favors the STL format over the native PLAN format to perform RCS analysis of ships, presumably because of its compatibility with the design software used by the Deutsche Navy. The CPF was designed using CAD software which is now essentially outdated and not compatible with either the PLAN or STL format.

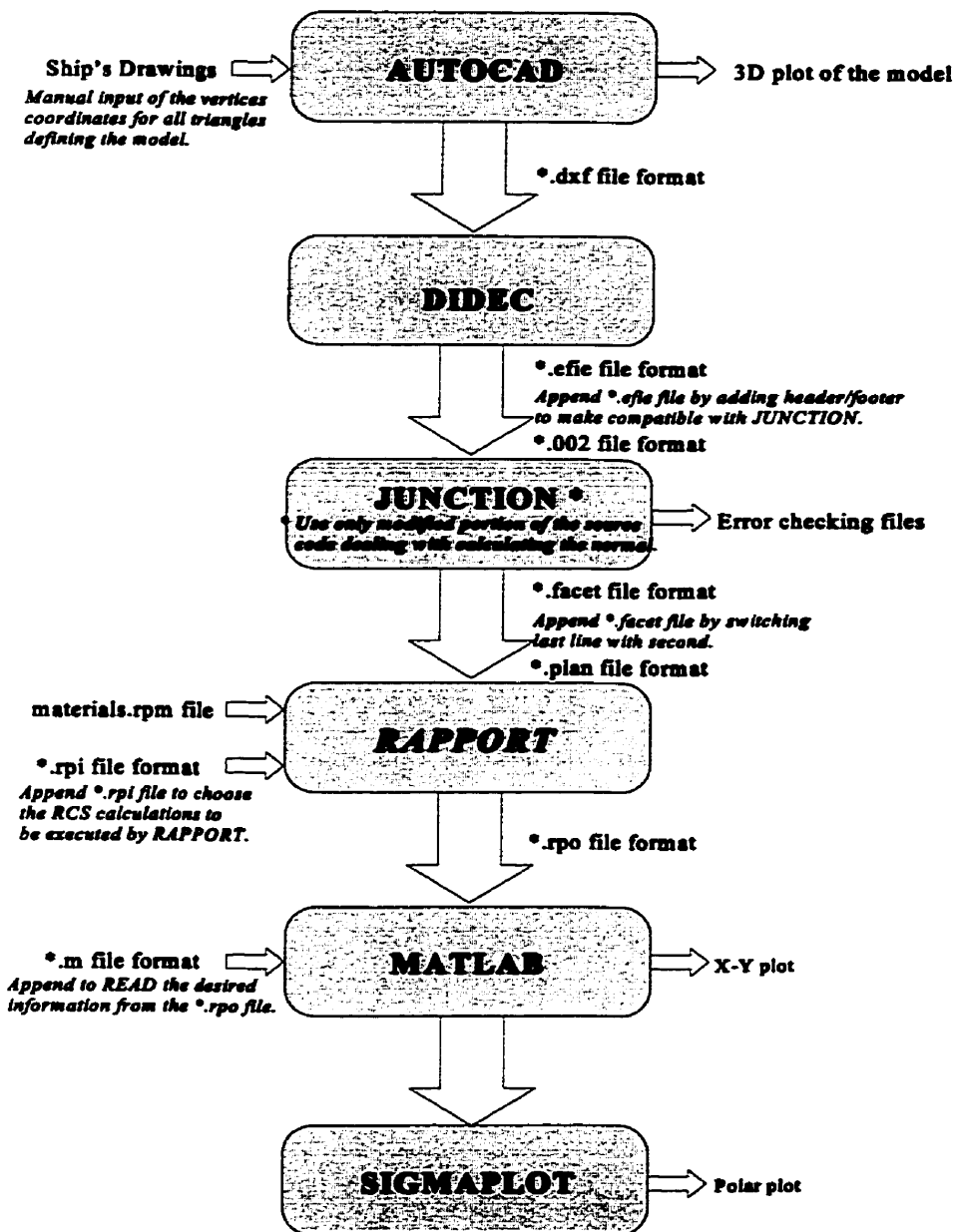


Figure 3-3 Software Flow Diagram of Radar Cross Section Process Utilized

The next step in the process is the actual RCS computation of the model generated. Aside from the PLAN file which describes the object geometry, RAPPOR also requires two other input files to function. The “materials.rpm” file contains the values of the material characteristics used to describe the model while the RPI input file, also known as the parameter

file, contains the data describing the type of simulation which is to be performed by RAPPOR on the object. RAPPOR is capable of producing the following results [9]:

- a. RCS, ISAR, HIST, MULTI or VISI;
- b. transmitter and receiver vertical or horizontal polarization;
- c. single or sweep frequency; and
- d. any combination of azimuth or elevation angles.

ISAR represents the complex square root of the RCS, HIST calculates the RCS as a function of the number of reflections, MULTI includes multi-path in the RCS calculation and finally VISI calculates the visible area for each reflection.

RAPPOR outputs the desired results in the RPO file which are in turn manipulated to accommodate a software tool suitable for graphical display of the data. In this project, a MATLAB M-file was written to allow the desired information to be extracted from the RPO file and plotted in an X-Y format. The information manipulated by MATLAB could also be transferred to another software program called SIGMAPLOT which is capable of producing a Theta-R polar plot of the results. This is generally the preferred format used to display RCS information as it can depict for example the magnitude of the RCS with respect to the azimuth angle for a fixed elevation angle. The process proposed in Figure 3-3 is presented in Section 3-4 using a flat plate as an example.

3.3 RAPPOR - LIMITATIONS

The version of RAPPOR used to compute the RCS of the CPF in this project was not identical to the one conceived by TNO. TNO generated their latest version of RAPPOR, V3.0,

using a UNIX-FORTRAN compiler. DREO incorporated improvements to TNO's source code of RAPPOR and made it compatible for the DEC-FORTRAN compiler used at DREO. Finally, the DREO source code was modified at the Royal Military College of Canada to make it suitable for compilation using FORTRAN 90. The time spent adapting RAPPOR's source code to FORTRAN 90 allowed the research to be carried out using a standard PC with a 90 MHz clock and 16 MB of memory. As one would expect, the time required to compute the RCS of a complex object like the CPF was greater using the PC version compared to the UNIX or DEC versions which ran on systems with much more memory and computational speed. However, the amount of time required by RAPPOR to perform the actual RCS computations was relatively small when compared to the amount of time required to build the model or even make relatively minor changes free of errors in AutoCAD. For example, adding an antenna mount to the structure could take the better part of a day while a basic RCS computation could be done in a manner of minutes. There is a point where decreasing the azimuth or elevation step size and/or increasing the number of frequencies considered in the simulation for small values of "maxsize" increased the computational time enough to warrant transmitting the PLAN file to DREO for computation. The use of a PC nevertheless remained more than adequate to carry-out all the other functions in the RCS process proposed in Figure 3-3.

The limitations imposed by RAPPOR on the shape of the basic elements forming the model was discussed in passing earlier. A complex object like a ship is formed of numerous objects of varying shapes and sizes. Limiting the modeling to the use of triangles or even polygons for that matter makes it practically impossible to represent the model with a high level of definition. In fact, this is arguably the single most important factor in the level of precision

achievable using numerical prediction techniques to determine the RCS of complex objects. For simple areas like the ship's side, triangles are more than suitable for the task. On the other hand, several triangles are required to model curved surfaces like antennas which are known to be major scatterers. Not only do curved surfaces require many triangles to generate models which are representative of reality but the increase in complexity also impacts negatively on the computational speed. These difficulties become even more prevalent as the objects being modeled get smaller in size, like stanchions for example.

The next issue of concern in producing an exact model involves the complexity of adding objects to the model. In this project, the starting point of the analysis was a model of the CPF consisting of the main hull, the superstructure, the funnel and the hangar. The RCS of the ship was analyzed after each major change to the baseline model. This provided invaluable insight into the RCS response of ships. Unfortunately this approach had two drawbacks. The first was the fact that adding items to the baseline was complex and time consuming in many cases. For example, sixteen rectangular canister shaped objects were added to the boat deck. Each canister required 18 lines to model it and approximately as many to integrate into the baseline model as each new vertex necessitated the formation of new triangles with its "surroundings".

The progressive addition of shapes or objects to the baseline was deemed beneficial although in hindsight it could have been done more efficiently. Once an object was added to the baseline, it became part of the new baseline. It would have been useful to have utilized some of AutoCAD's features which allow objects to be saved in separate files or layers. These features would also prove invaluable in evaluating RCS reduction techniques like shaping or radar absorbent material treatment. The application of the above suggestion is not entirely trivial as

the inclusion of layers must also take into account the interaction of the added lines and vertices to the model. In some cases, lines could have to be removed from the baseline model to allow objects to be placed overtop of them. This is a feature which is not easily accounted for automatically.

3.4 RAPPORT - BASIC PERFORMANCE EVALUATION

RAPPORT's ability to estimate the RCS of an object is documented in [9]. Due to the numerous modifications made to RAPPORT's source code and the differing approach used in this research to handle the input and output files, it was deemed worthwhile to present a brief evaluation to validate the process proposed in Figure 3-3. This validation will be presented in two phases. The first phase consists of quantifying RAPPORT's ability to evaluate the RCS of a perfectly conducting flat plate. The dimensions of the plate modeled are 6.5" by 6.5" and the wavelength chosen is $\lambda = 1.28"$, making the frequency 9.2 GHz [2,6]. The model of the plate created using AutoCAD consists of four lines describing the contour of the plate and one line joining opposite corners to convert the polygon into two triangles. The PLATE.PLAN file output by JUNCTION is presented below:

```

PLATE.PLAN
  2          ! FACES WITH AREA > 1 sq cm
1.0000000  0.0000000  0.0000000  ! FIRST FACE OF BODY    1
  1
  3
0.0000000 -0.1651000  0.1651000
0.0000000  0.0000000  0.0000000
0.0000000  0.0000000  0.1651000
1.0000000  0.0000000  0.0000000
  1
  3
0.0000000  0.0000000  0.0000000
0.0000000 -0.1651000  0.1651000
0.0000000 -0.1651000  0.0000000

```

The PLAN file has two faces representing the two triangles modeled in AutoCAD as

indicated in the second line of the PLAN file, the first line being the file name. The two triangles are defined by lines 3 through 8 and 9 through 14 with the last three lines of each set representing the vertices coordinates, the “3”s at line 5 and 11 indicate that both polygons have three vertices and the “1” indicates that the material code used for both facets is “1”, corresponding to perfectly conducting material in this particular case. The PLATE.RPI file used to choose the simulation parameters is as follows:

```
RCS computation of a 6.5" by 6.5" square plate
1                nr_objects
plate.plan      objectfile
3                number of reflections
0.25            maxsize
monostatic configuration
RCS
azimuth scan
    0            80            10.0000
    90           90            1.0000
SINGLE frequency
 9.221          9.221          0.1
vertical       transmitter polarization
vertical       receiver polarization
plate.rpo      resultfile
reset
```

The comments included in the PLATE.RPI file make it fairly straight forward to understand most of the text. The value of “maxsize” refers to the maximum size allowable for each facet with respect to the total area of the object. RAPPORT essentially subdivides facets which are greater than the “maxsize” prior to performing the RCS computations. This is an important factor in dealing with complex objects, like ships, since the greater the size of the facets, the less accurate the process of determining which facets contribute to the RCS because the ray-tracing algorithm determines if a facet contributes to the RCS by tracing back from its geometrical center [9]. In this specific case, the maximum allowable size of the triangles was set at 0.25 or 25% of the plate area which causes RAPPORT to re-generate the model of the flat

plate internally using 8 facets instead of the original 2 from the AutoCAD model to compute the RCS. Decreasing the value of "maxsize" greatly enhances the accuracy of the RCS results for complex objects within certain limitations. First of all increasing the number of facets by decreasing "maxsize" will increase the time required to execute the computation. The second factor deals with wavelength limitations relating to the theory presented in Chapter 2. Physical optics is a high-frequency method which is limited to sizes greater than ten wavelengths. By forming facets, in this case triangles, with dimensions of less than ten wavelengths, the results computed become essentially erroneous by virtue of failing to account for scattering mechanisms which become more prevalent for smaller sizes.

The results mandated in the PLATE.RPI file consist of a 0° to 80° azimuth scan in 10° increments at an elevation angle of 90° and frequency of 9.221 GHz. The results of the PLATE.RPO file are:

```

#-----
#-----          RAPPORT V3.0 -----
#-----
#-----          TNO Physics and Electronics Laboratory -----
#-----          Radar signature Analysis and Prediction -----
#-----                      by -----
#-----          Physical Optics and Ray Tracing -----
#-----
#-----          RAPPORT V3.0 -----
#-----
#
#TITLE OF CALCULATION
#-----
#RCS computation of a 6.5" by 6.5" flat plate
#
#PARAMETER FILE
#-----
#Parameters for the calculation were taken from the file:
#   plate.rpi
#
#EXTERNAL OBJECT DESCRIPTION
#-----

#The object description is taken from the file(s):
#   plate.pla          which contains          2 polygons
#The x-min and x-max of the object are          .00000          .00000

```

```

#The y-min and y-max of the object are      -.16510      .00000
#The z-min and z-max of the object are      .00000      .16510
#The area of the object equals              .02726
#
#INTERNAL OBJECT DESCRIPTION
#-----
#The polygons were transformed to triangular patches,
#with a relative maximum area of:          .25000
#This corresponds with a maximum radius of: .061529
#An object description with                8 patches is obtained.
#
#RAYTRACING INFORMATION
#-----
#The maximum number of reflections accounted for = 3
#
#TYPE OF CALCULATION
#-----
#Perform a monostatic calculation: transmitter and
#receiver are located at the same position
#
#TYPE OF RESULT
#-----
#The RCS after the total number of reflections.
#
#SCAN MODE
#-----
#An azimuth scan is performed,
#starting from azimuth angle              = .000000
#ending at azimuth angle                  = 80.000000
#with increment                           = 10.000000
#at a fixed elevation angle of 90.000000 degrees
#
#FREQUENCY INFORMATION
#-----
#The used frequency in GHz                = 9.22
#
#POLARIZATION
#-----
#Used transmitter polarization = v
#Used receiver polarization   = v
#
#-----
#----- RESULTS -----
#-----
#PLOTDATA
      .00      90.00      9.46
     10.00     90.00     -8.94
     20.00     90.00    -11.87
     30.00     90.00    -28.13
     40.00     90.00    -19.13
     50.00     90.00    -26.06
     60.00     90.00    -29.84
     70.00     90.00    -29.48
     80.00     90.00    -79.83

```

The three columns represent the azimuth angle, elevation angle and magnitude of the

RCS in dBsm or dBm². The X-Y plot of the above results using an azimuth increment of 0.5° instead of 10.0° is presented in Figure 3-4 and the polar plot in Figure 3-5. These results can be compared to the values presented in Figure 2-3.

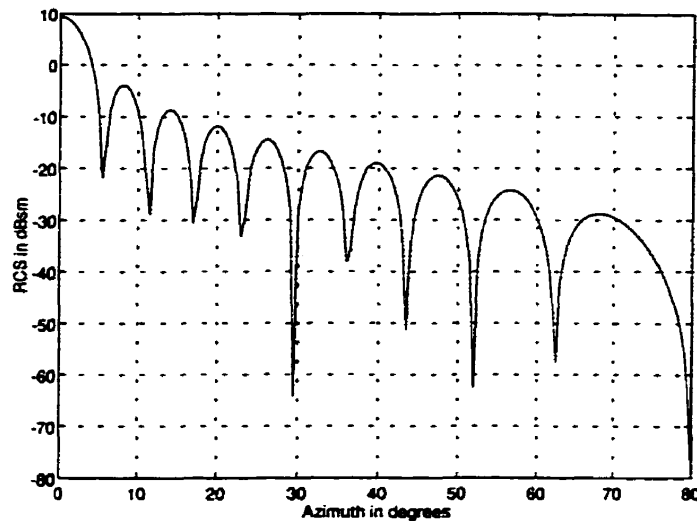


Figure 3-4 MATLAB X-Y Plot of the Radar Cross Section Results for a 6.5" by 6.5" Flat Plate

RAPPORT's results are nearly identical to those corresponding to the physical optics trace in Figure 2-3. The horizontal polarization results calculated by RAPPORT are not shown here as they are identical to the ones presented for the vertical polarization case. There is generally no drastic difference between the vertical and horizontal polarization results but only in instances where the geometry is identical for both polarizations are the results identical. Such is the case for the flat plate analyzed in this section but not so of the CPF model. Comparing the experimental result curve illustrated in Figure 2-3 to the physical optics curve enables us to gain an appreciation for the ineffectiveness of physical optics as the angle of incidence moves away from normal incidence, 0°. The RCS away from normal incidence for a flat plate is much lower than it is at normal incidence which reduces the negative impact considerably. Unfortunately the

RCS of dihedral and trihedral corners is much more distributed in azimuth, rendering the lack of accounting for edge diffraction more prevalent for these shapes.

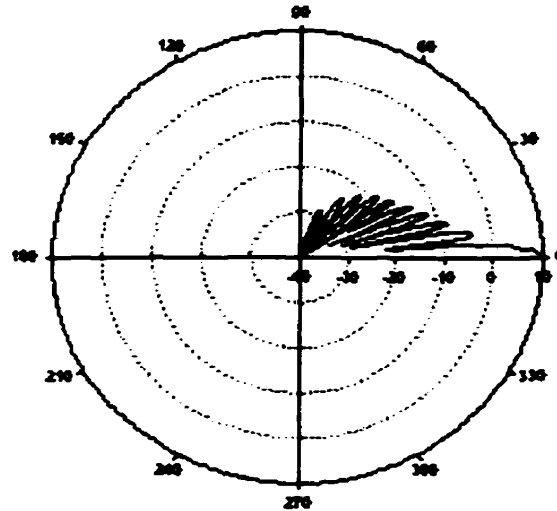


Figure 3-5 SIGMAPLOT Polar Plot of the Radar Cross Section Results for a 6.5" by 6.5" Flat Plate

The second phase of RAPPOR's performance evaluation consists of comparing it briefly with XPATCH. The most obvious difference between these two high-frequency prediction codes is user friendliness. XPATCH integrates with an X-Window graphical user interface which combines CAD-geometry pre-processing and analysis tools along with post-prediction analysis tools, making it an end-to-end prediction analysis package capable of displaying and examining three-dimensional color views of the analysis geometry [11]. XPATCH is obviously easier to use as it replaces all the software tools described in Figure 3-3.

XPATCH is an ongoing project which has seen considerably more funding than RAPPOR. It is intended to support the Aerospace Non-cooperative Target Recognition

(NCTR) program which seeks to develop Automatic Target Recognition (ATR) algorithms and processing hardware capable of positively identifying threat, neutral and friendly aircraft and ground vehicles. XPATCH is instrumental in producing the predicted radar signature templates for the identification algorithms at the heart of the process. The NCTR program will require in the order ten million radar signature templates to be compiled. These computations are being performed on very high speed machines yet will still take years to complete [12].

Efforts to improve XPATCH are expected to continue to be funded well into the year 2010. These improvements or upgrades include integrating the method of moments (MoM) to the algorithms used to compute the radar signature [12]. The version of XPATCH provided to DREO was based on the shooting and bouncing ray technique (SBR) which is essentially equivalent in function to the ray tracing used by RAPPORT to ascertain shadow and blockage checking on the geometry, although somewhat different in application. Once the SBR process is complete, XPATCH uses physical optics to calculate the RCS of the object. As with RAPPORT, XPATCH can account for multiple reflections but has the added feature of being able to include edge diffraction by applying a physical theory of diffraction algorithm in its code [11].

A very rudimentary comparison between XPATCH and RAPPORT was made at DREO using the perfectly conducting flat plate described earlier and a model of the CPF. The flat plate results of the XPATCH simulation were similar to the GTD curve of Figure 2-3. The XPATCH results are evidently better away from normal incidence than the ones predicted by RAPPORT using only physical optics for the simple reason that XPATCH has the ability to account for edge diffraction. Sample comparisons were also made using the CPF model. The results using a "maxsize" of 0.001 compared well with the one's obtained from XPATCH except for a few

notable discrepancies at two specific angles. The reduction of “maxsize” to 0.0001 all but eliminated the discrepancies at the two angles of interest and overlaying the two sets of results indicated a clear correlation. Although the comparison was not extensive, it did provide a greater degree of confidence in the results produced by RAPPOR by virtue of the high correlation with the results generated by XPATCH. The results produced by XPATCH would be expected to be the more accurate by virtue of accounting for edge diffraction. It is interesting to note that the XPATCH simulation performed at DREO was approximately 600 times slower than the one using RAPPOR, which took approximately 80 minutes.

The increased computational time observed in the preliminary comparison was not in itself sufficient to detract from its use for this project. Aside from the fact that DREO had not been able to succeed in getting XPATCH to function properly at the start of this project, it has one serious drawback in the prescribed application. XPATCH was intended to predict the RCS of airplanes and ground vehicles, not ships. Given that DREO was provided with the software without the ability to alter the source code, it has remained unsuitable for the purpose of this project. The primary limitation of XPATCH is that it does not allow for the inclusion of a ground plane in the calculations. This is obviously not an issue for airplanes but the surface of the sea acts as a ground plane and cannot be ignored. The comparisons between the two software packages was thus made with RAPPOR omitting the calculations for the sea-water ground plane. The primary advantage of RAPPOR over XPATCH revolves around the fact that several improvements were made to the source code to account for the ground-plane reflections. These improvements include the ability to account for a perfectly conducting ground plane and allowing the sea-water characteristics to be frequency dependant.

Overall, XPATCH is easier to use, includes edge diffraction and is being improved continuously while RAPPORT is faster and accounts for the sea-water ground-plane. Fortunately the models generated for RAPPORT can easily be adapted for simulation using XPATCH which leaves the door open to future developments.

CHAPTER 4 RESULTS

The purpose of this chapter is to enumerate the results of the RCS simulations performed on the various iterations of the CPF model. The measured RCS of most military vehicles such as ships or airplanes is classified and the RCS of the CPF is no exception. The RCS results predicted by RAPPORT will consequently not be related in this document to the known RCS of the CPF but rather compared to the baseline model and the subsequent modifications to it. This will provide insight into the impact of geometry on the RCS of complex objects like ships.

4.1 BASELINE MODELS

There were two baseline models available from which to initiate this project. The first model was obtained by DREO from National Defense Headquarters in a file format compatible with AutoCAD. This model was likely intended to be an architectural representation of the CPF, containing details which were superfluous for RCS analysis and in some cases even cause for errors. These details included lines depicting major watertight bulkheads inside the hull structure which are of no relevance to the RCS. Ideally, only the outer surface of conducting structures contribute to the scattering of energy and an object such as a solid sphere would provide an identical RCS profile to that of a hollow sphere for example. Using this assumption, considerable time was expended at DREO to make the first baseline model suitable for RCS analysis by removing a multitude of extraneous lines and in other cases adding lines to form facets. In the end, the outer hull and structure of the ship were modeled entirely using triangular facets.

The second baseline model was generated by converting a wire-grid model of the CPF

into a facet model using DIDEDEC. The model was originally built by LCdr J.B. McLachlan for the purpose of his master's thesis [13]. LCdr McLachlan entered the vertices coordinates from scale drawings of the CPF primarily by employing a digitizing tablet interfaced to DIDEDEC.

From the outset of this project, it was recognized that the two baseline models might be unsuited for RCS analysis in their original conditions as both had been intended for other purposes. The validity of the model used as the baseline for the CPF will be discussed in the next chapter. Figure 4-1 is a scale representation of the CPF similar in detail to the one utilized in this project to input vertices into AutoCAD except of a smaller scale. Figure 4-2a depicts baseline model # 1 prior to making it compatible for RCS analysis, Figure 4-2b is the same model except that hidden lines are not shown and Figure 4-2c represents the model after conversion into a facet model. The difference between Figure 4-2a and Figure 4-2b provides an indication of the number of lines which were extraneous in the original model, especially in the hull. Aside from having removed several lines and formed facets with the entire structure, the model in Figure 4-2c was cropped at the waterline. As is the case with most electromagnetic problems involving ships, the waterline acts as the ground plane and thus removing the structure below it is not only convenient in most cases but necessary as well.

At quick glance, baseline model # 1 appears to be a reasonable representation of the CPF in Figure 4-1, at least for the details shown. What is less obvious is that the overall length of this baseline is 133.6 meters instead of the actual 134.2 meters and that some of the details are not particularly accurate. The most obvious flaw is in the slope of the forward aspect on the structure between the superstructure and the funnel but there are other details less obvious to the naked eye which make the model's utility questionable. Combined with the fact that the source or accuracy

of the model could not be confirmed, it was deemed more appropriate not to use it as baseline.

The baseline model which was used for RCS analysis of the CPF in this research is shown in Figure 4-3, baseline model # 2. Although it was originally intended to be used as a wire-grid model, this baseline was deemed to be a more accurate representation of the CPF. For instance, the angle of the funnel top is much closer to reality as are the flight deck and the structure between the funnel and the superstructure. The after end of the hull bottom appears to be more detailed in baseline model # 1 but in fact baseline model # 2 is a better representation. The number of facets used to describe the second baseline model was also much smaller which contributed to simplify the addition of details and reduced the computational time dramatically. It is important to note that the model shown in Figure 4-3 was not simply the result of a direct DIDECON conversion of LCdr McLachlan's wire-grid model. Initial efforts at DREO constituted dedicating some time making necessary adjustments, most notably the removal of the wire antennas which are at the basis of radiation pattern simulations but insignificant in RCS predictions.

Despite considerable efforts, the converted wire-grid model used as the baseline was not entirely accurate. For instance, the overall length of the model was 134.4 meters instead of 134.2 meters, the error likely arising from the level of accuracy achievable by the digitizing process of scale drawings. Based on RCS theory, this 20 centimeter difference was not deemed significant in the overall RCS prediction of the ship. This assumption was based on the fact that the difference in the broadside RCS of a flat plate the length of the CPF would be insignificant as a result of a 20 centimeter variance. On the other hand, a variance of this type on the angle of a perfect dihedral or trihedral corner could change the RCS rather significantly. The biggest

complication caused by the above mentioned inaccuracies was the fact that the baseline model coordinates were rarely exactly the same as on the scale drawings. For example, the mast structure was referenced to a very specific coordinate on the top of the superstructure in the drawings yet the inclusion of the mast onto the baseline model resulted in the mast not matching up with the existing structure. This forced the modification of either the detail being added or of the structure it was to be appended on. To facilitate the process of adding details to the model, the point of origin on the baseline was relocated using a translation feature in AutoCAD to make it the same as the reference used on the ship's drawings.

4.2 RCS OF THE BASELINE MODEL

The RCS prediction of the baseline model was performed using numerous combinations of the different features available in RAPPORT even though the inaccuracies of the baseline model precluded the analysis of the results from producing significant observations. The exercise was intended as a means of gaining a better appreciation for the analysis process as well as investigate the impact of changing the variables on a ship-like object as opposed to simple objects like flat plates. These simulations included varying:

- a. the frequency;
- b. the azimuth angle;
- c. the elevation angle;
- d. the polarization;
- e. the number of reflections; and
- f. the value of "maxsize".

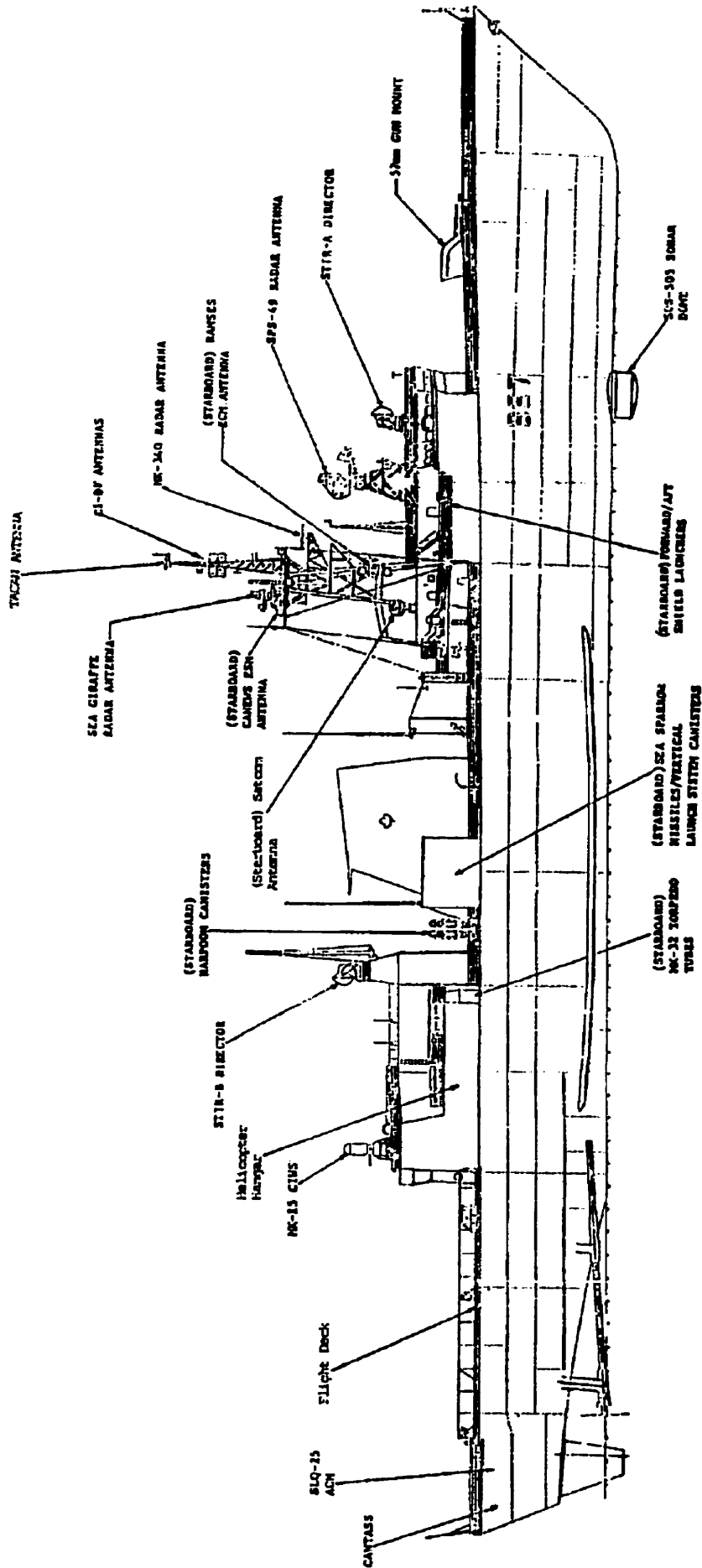


Figure 4-1 Scale Drawing of the Canadian Patrol Frigate

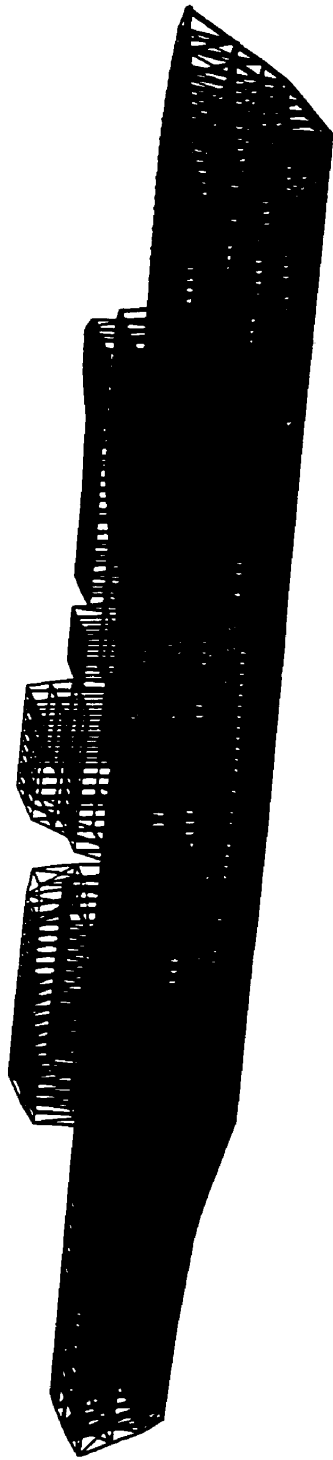


Figure 4-2a Canadian Patrol Frigate Baseline Model # 1 - Prior to Manipulation for Radar Cross Section Analysis

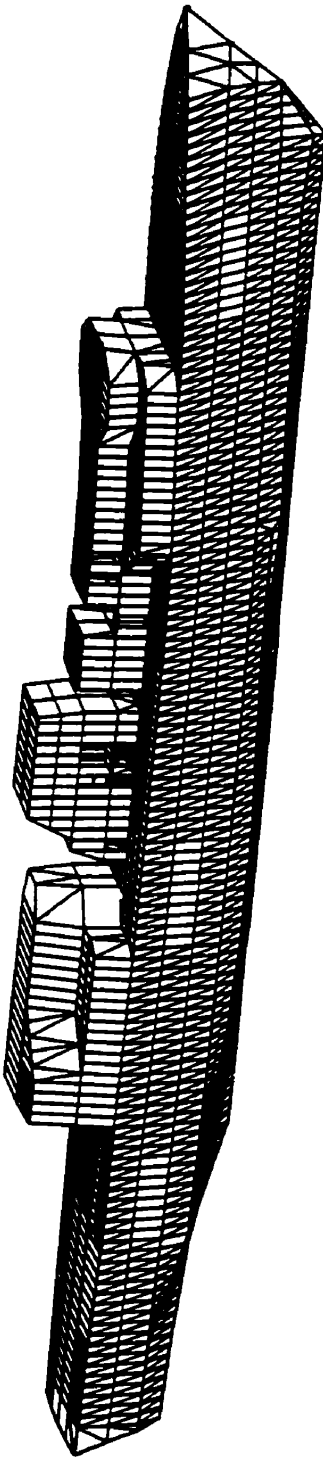


Figure 4-2b Canadian Patrol Frigate Baseline Model # 1 - Prior to Manipulation for Radar Cross Section Analysis with Hidden Lines

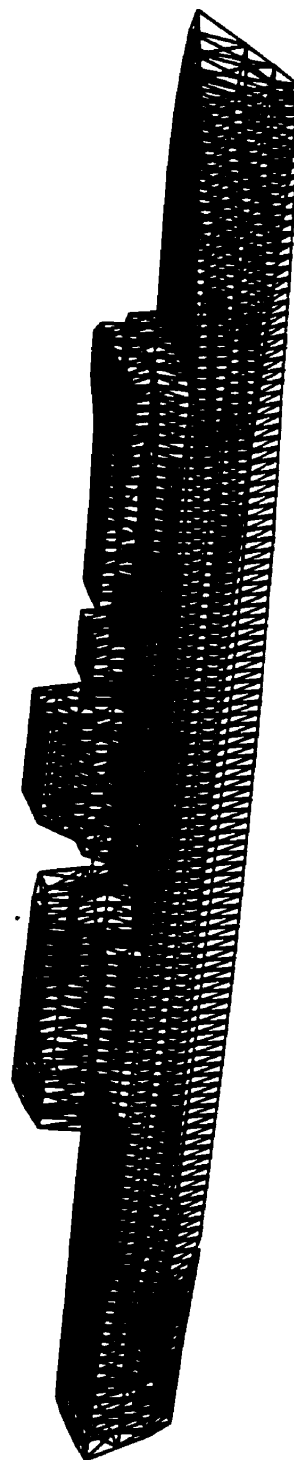


Figure 4-2c Canadian Patrol Frigate Baseline Model # 1 - After Initial Conversion into FACETS File

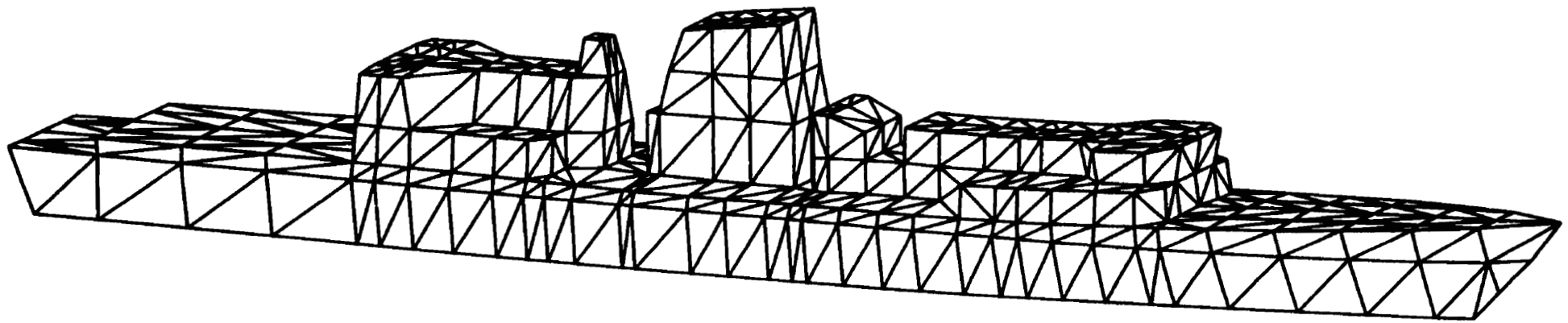


Figure 4-3 Canadian Patrol Frigate Baseline Model # 2 with Hidden Lines

The RCS prediction of the baseline model depicted in Figure 4-3 is shown in Figure 4-4 with the applicable *.rpi parameter file.

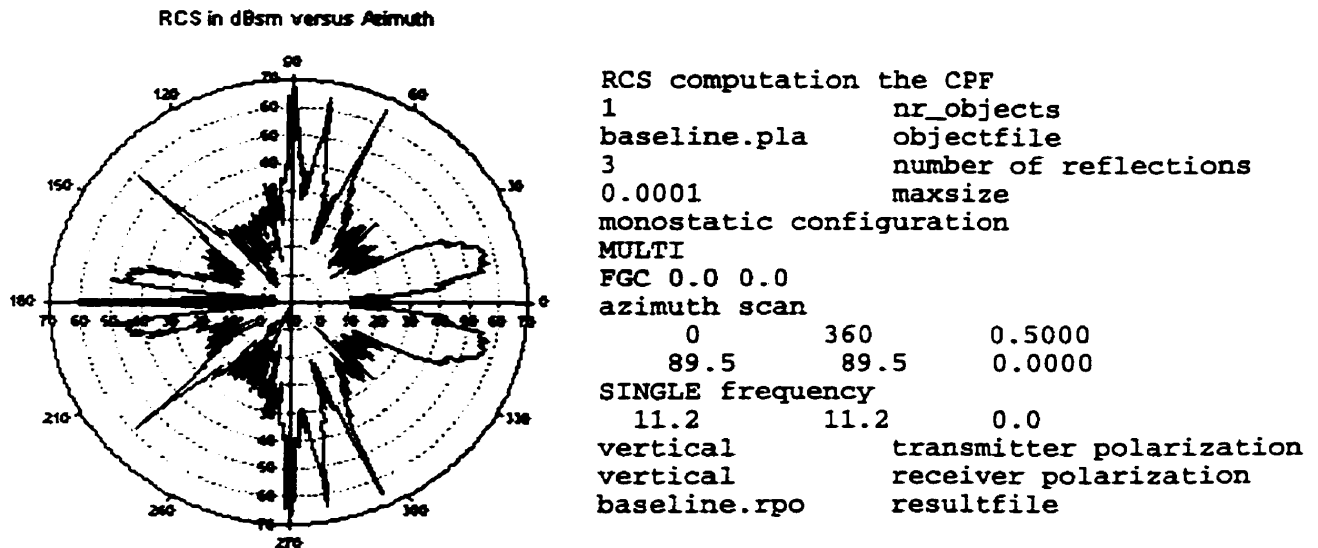


Figure 4-4 Radar Cross Section of the Canadian Patrol Frigate Baseline Model and Parameter File Information

The elevation angle was chosen as 89.5°, corresponding to a 0.5° angle above the horizon, to coincide with the approximate angle of the RCS measurement facilities located at Osbourne Head Gunnery Range (OHGR) near Halifax, Nova Scotia [14]. The frequency was selected to coincide with results from the Thorn-EMI measurements performed on the scale model of the CPF [7,8]. The OHGR facility measurements were taken at several frequencies including 11 GHz which is close enough to 11.2 GHz for the purpose of this project. Although Figure 4-4 eludes to the results being RCS, they are in fact MULTI with FCG 0.0 0.0 which means that the RCS was predicted assuming a finitely conducting ground plane with frequency-dependant sea-water dielectric parameters in accordance with reference [15].

The OHGR and Thorn-EMI measurements are both classified SECRET and cannot be used for comparison in this document. Qualified users can refer to the results of the Thorn-EMI

scale modeling measurements [7,8] or to the full-scale measurements performed on the CPF [14,23]. To provide some sense of figure-of-merit, the results can be compared to the RCS of the large auxiliary ships measured on Chesapeake Bay shown in Figure 2-8. By taking measurements of several ships from the same location, the following empirical formula for the RCS of a naval ship was proposed [6]:

$$\sigma = 52 f^{1/2} D^{3/2} \quad (4.1)$$

where f is the frequency in MHz and D is the full-load displacement in kilotons. This formula represents the average of the median RCS at low grazing angles in the port bow, starboard bow and quarter aspects, excluding the broadside peaks, for various wavelengths and ship displacements [6]. Assuming a ship displacement of 5 kilotons for the CPF at a frequency of 11.2 GHz or 11,200 MHz, the RCS would be approximately 66 dBsm. To put this value in perspective, an RCS of 1 mi² is equal to 64.1 dBsm. Assuming that the actual RCS of the CPF is relatively constant with azimuth as it is in Figure 2-8 for the auxiliary ship, it is rather obvious that the accuracy and level of detail included in the baseline model was inadequate to provide suitable results. At some azimuth angles, the RCS was below -10 dBsm which is nowhere near the 66 dBsm calculated using equation (4.1).

There were eighteen primary modifications made to the baseline model to attempt to fill the azimuths where the RCS was well below the 66 dBsm calculated. These modifications included in Table 4-1 represent the heart of this research and are covered in the following section.

Modification	Description
a	changing the waterline location
b	adding the solid structure supporting the mainmast
c	adding a solid structure to simulate the lattice mainmast
d	changing the solid mainmast structure to a beam mast structure
e	adding a flat plate without thickness on the starboard side of the boat deck, dimensions as per the general arrangement drawings
f	adding thickness to the starboard side boat deck flat plate
g	adding four of the eight VLSS canisters on the starboard side
h	adding a flat plate with thickness on the port side of the boat deck, dimensions as per the profile drawings
i	adding the other four VLSS canisters on the starboard side
j	adding the eight VLSS canisters on the port side boat deck
k	adding the port aft structure to the hangar
l	modifying the port aft structure of the hangar added in 'k' and the slope on the port side of the hangar top
m	modifying the aft end of the hangar to include a perfectly vertical door
n	modifying the hangar door slope to match that of the hangar aft end
o	adding the CIWS mount
p	adding the funnel tail
q	cropping the bottom of four VLSS canisters on the starboard side, making them free-standing
r	cropping the bottom of the other four VLSS canisters on the starboard side

Table 4-1 List of Modification to the Baseline Model

4.3 RESULTS OF THE BASELINE MODIFICATIONS

The results presented in this section were predicted using the same parameters as indicated in the *.rpi file of Figure 4-4 with the exception of the value of “maxsize” which was set at 0.001. The first set of results addresses the waterline of the ship. The baseline model had a waterline of 4.3644 meter when in fact the CPF waterline is considered to be at 5 meters, although this value does vary depending on the amount of fuel, stores, water and ammunition carried on board at any given time. The difference in the RCS results between the models with waterlines at 4.3644 meter and 5 meters was not significant, as shown in Plot 4-1. The average difference in RCS over 360° in 0.5° increments was 0.22 dB. The most significant aspect of the results depicted by Plot 4-1 is the fact that the difference is distributed over the entire azimuth. This is significantly different from the results which will be presented below where the subsequent modifications present a generally localized impact on the RCS. It is interesting to note that although some azimuth angles have peaks as high as 18 dB, there is no obvious area over which an RCS improvement or reduction is noticeable. This is interesting given the fact that the surface area of the ship has been reduced by the change in waterline yet the overall RCS has increased slightly. The change in waterline certainly did not fill the gaps in the RCS plot of the baseline model where the levels were well below 66 dB. This lack of improvement made it more apparent that filling the gaps would likely require adding large dihedral or trihedral corners missing from the model or a very large number of small details.

Some references elude to the fact that the RCS of complex objects is largely dominated by upper deck structures like the superstructure and the likes [14]. Other references claim that

dihedral and trihedral corners dominate the RCS of such objects [9]. Modification 'b' was included as a first step towards filling the forward quarters of the RCS plot. Figure 4-5 illustrates the added structure.

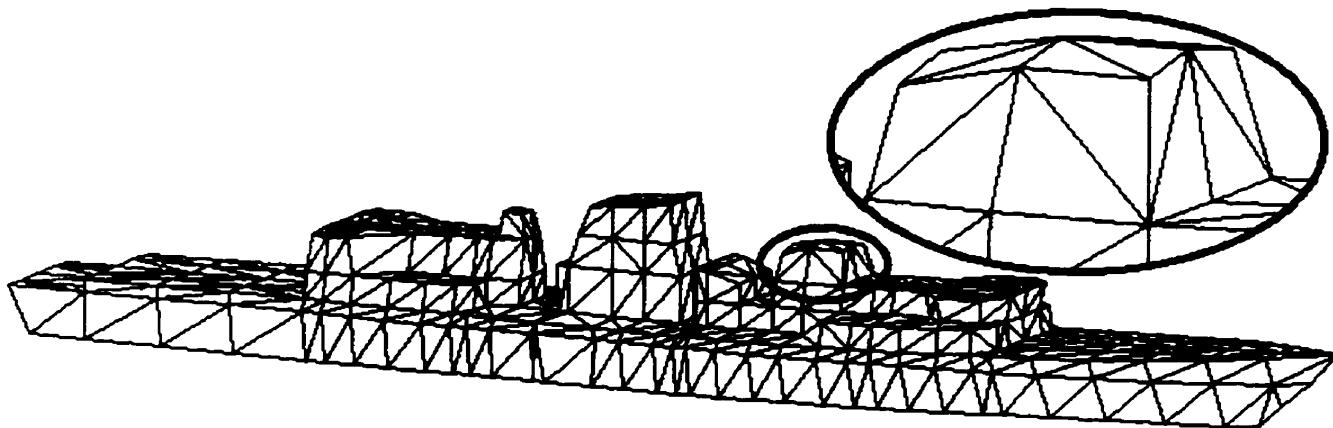


Figure 4-5 Mainmast Supporting Structure Modification (modification 'b')

The box-like structure added on top of the superstructure did not impact the RCS significantly for the simulations of interest. As depicted in Plot 4-2, there were only two azimuths where a significant improvement was made and that only over a very narrow area. The overall change in RCS from this modification was a mere 0.06 dB. As expected, the addition of the flat surface area of this structure forward was noticeable on the plot but such was not the case on both sides and astern. The lack of impact astern can be attributed to the blockage of the funnel at the elevation angle chosen while the sides of this added structure failed to bring forth any significant contribution by virtue of the smaller area they pose relative to the ship's sides. The contribution of the forward part of the structure could be incorrectly attributed to the dihedral shape formed with the top of the superstructure given the fact that this shape should have resulted in a wider area of impact, certainly with a 90° angle instead of the current angle.

The narrow spike returns seen on Plot 4-2 are more indicative of the contribution one would expect from a flat surface.

Modification 'c' was added to the model in an attempt to further investigate the significance of details well above the waterline. The mast is a complex structure formed of several beams supporting a myriad of different antennas. The small size of the details forming the mast and its components made it impractical to model thoroughly. The solid structure was thus designed to estimate an equivalent return by overemphasizing the surface area up to the top antenna platform to offset the absence of the structure above the top platform and of the antennas, in particular the Sea Giraffe search radar reflector due to its large physical size.

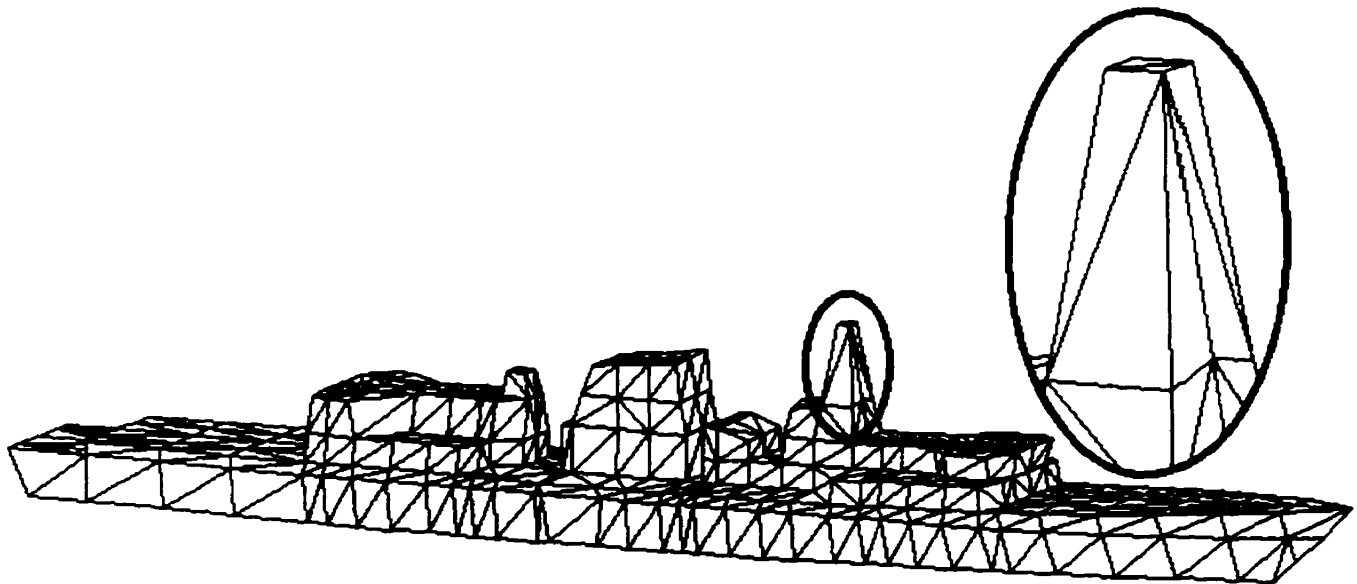


Figure 4-6 Solid Mainmast Modification (modification 'c')

The addition of modification 'c' did not significantly alter the RCS of the model. This was somewhat surprising given the surface area that this added structure manifested. After the results of modification 'c', it was not surprising to see the minimal impact resulting from

modification 'd' which consisted of changing the solid mast for one formed of beams. It is interesting to note however that modification 'c' brought forward an overall average increase in RCS of 0.01 dB while modification 'd' improved the solid mast return by 0.09 dB. Granted the difference is academic, it illustrates the fact that the shape of an object can be more important than its surface area. On the other hand, the contribution from flat plates such as those presented by the solid mast areas would only be significant at normal incidence to the plates. This would justify how a smaller dihedral surface area could have more of an impact than a larger flat surface.

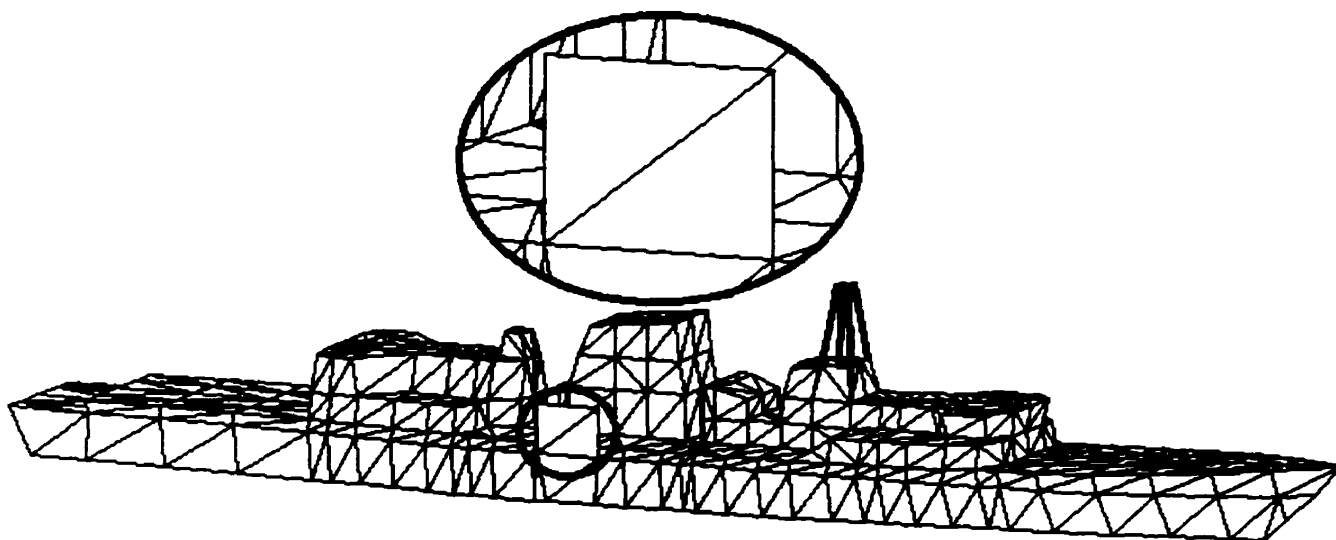


Figure 4-7 Addition of the Starboard Side Boat Deck Flat Plate (modification 'e')

The top of the superstructure contained numerous details yet almost all of them were omitted from the baseline model. The lack of evident change in the RCS from the mainmast modifications was deemed to be a suitable indication that perhaps the details more likely to impact the RCS were in another area of the ship. The focus thus turned to investigating the boat deck area. The most obvious omission from the baseline model on the boat deck was that of the

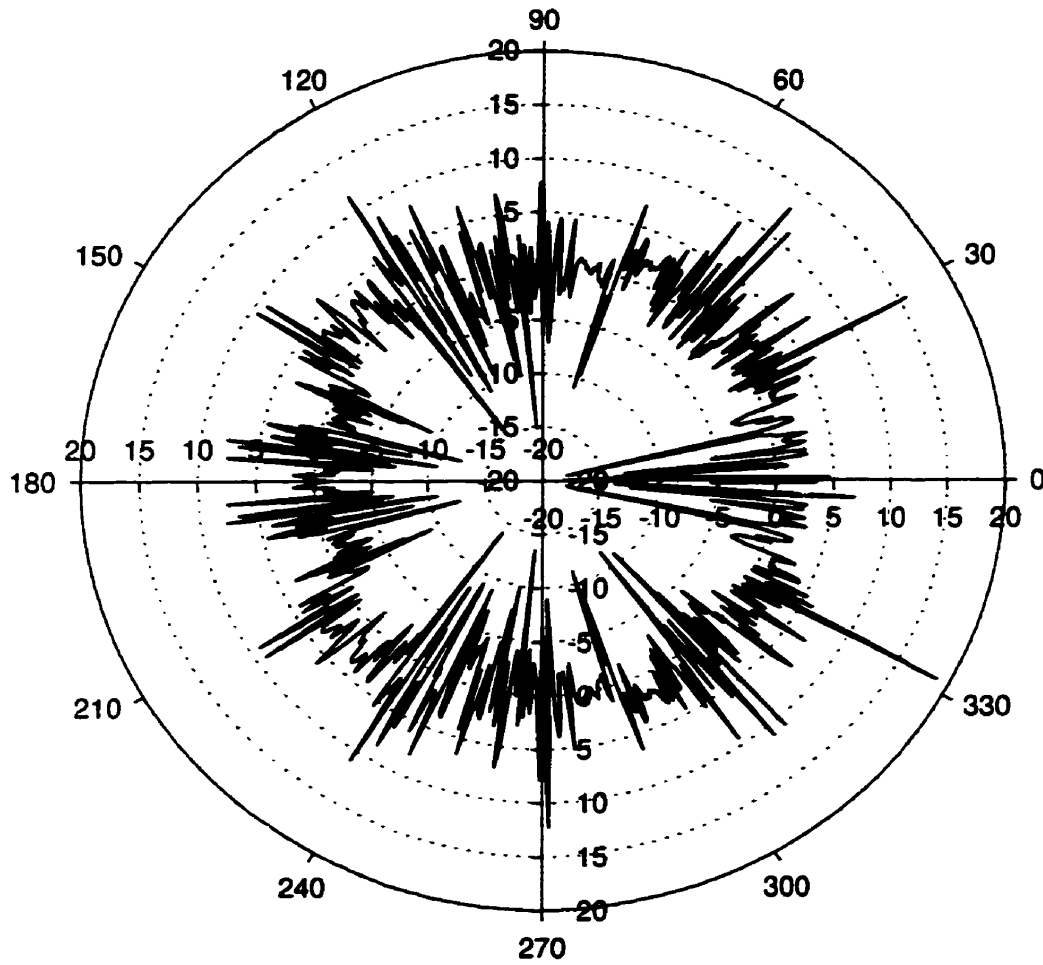
flat plates protecting the VLSS launcher area on each side. The flat plate added to the starboard side boat deck seen in Figure 4-7 was first modeled without thickness. The impact of modification 'e' seen in Plot 4-5 appears to be phenomenal, increasing the overall average RCS by an astonishing 29.57 dB. The only difficulty is that the model of the flat plate is actually flawed. One of the guidelines set into JUNCTION in converting the model into a format suitable for RAPPORT is that each edge can be shared by no more than two facets, or triangles in this case. The ship's side at the boat deck is modeled with a small flat surface depicting a slight drop in angle between the hull and the deck. Although it is not obvious from looking at Figure 4-7, the flat plate was added directly overtop the hull side on the boat deck. The slope of the corner formed between the deck and the hull was such that there was no way to include the plate in the model without forming three triangles with the bottom edge of the plate.

The flawed model was left intact to show the significance of correctly modeling the object being analyzed. What should have resulted in a minor improvement turned into a 29.57 dB increase in RCS. The impact was above 40 dB over large aspects in all four quadrants which is obviously far too much.

Modification 'f' targeted the significance of proper modeling by giving the correct thickness to the same flat plate and thus alleviating the multiple edge sharing phenomena. It also served to verify that JUNCTION and RAPPORT were utilizing the correct outward normal for the flat plate in estimating the RCS. By giving the flat plate the proper thickness, there could be no confusion in assigning the direction of the outward normals by JUNCTION which might occur for a plate without thickness. Modification 'f' was not compared to modification 'e' as the latter was flawed but rather against modification 'd'. The result of the modification was a

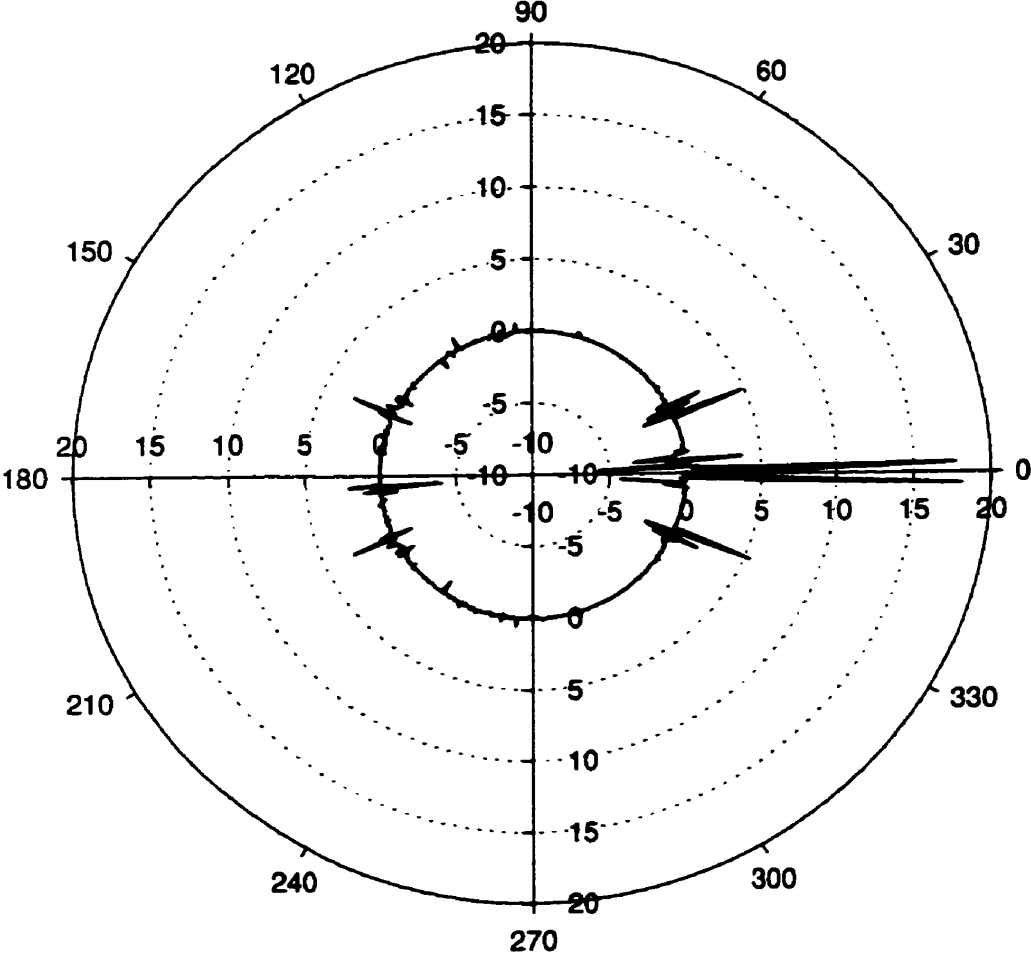
3.31 dB average overall increase in the RCS. It is relatively obvious to see from Plot 4-6 on which side of the ship the flat plate was added based on the significant increase in return between 180° and 360°. The thickness of the plate could be partially responsible for the increases close to 0° and 180° but in all likelihood the variance is due entirely to reflections caused by the plate with the funnel and the sea-surface. The exception would be broadside, at 270°, where the surface area of the flat plate could have been expected to impact the RCS but such was not the case as the contribution does not appear to have been significant enough relative to the overall area of the ship's side.

RCS Difference in dB versus Azimuth
Impact of changing the waterline location



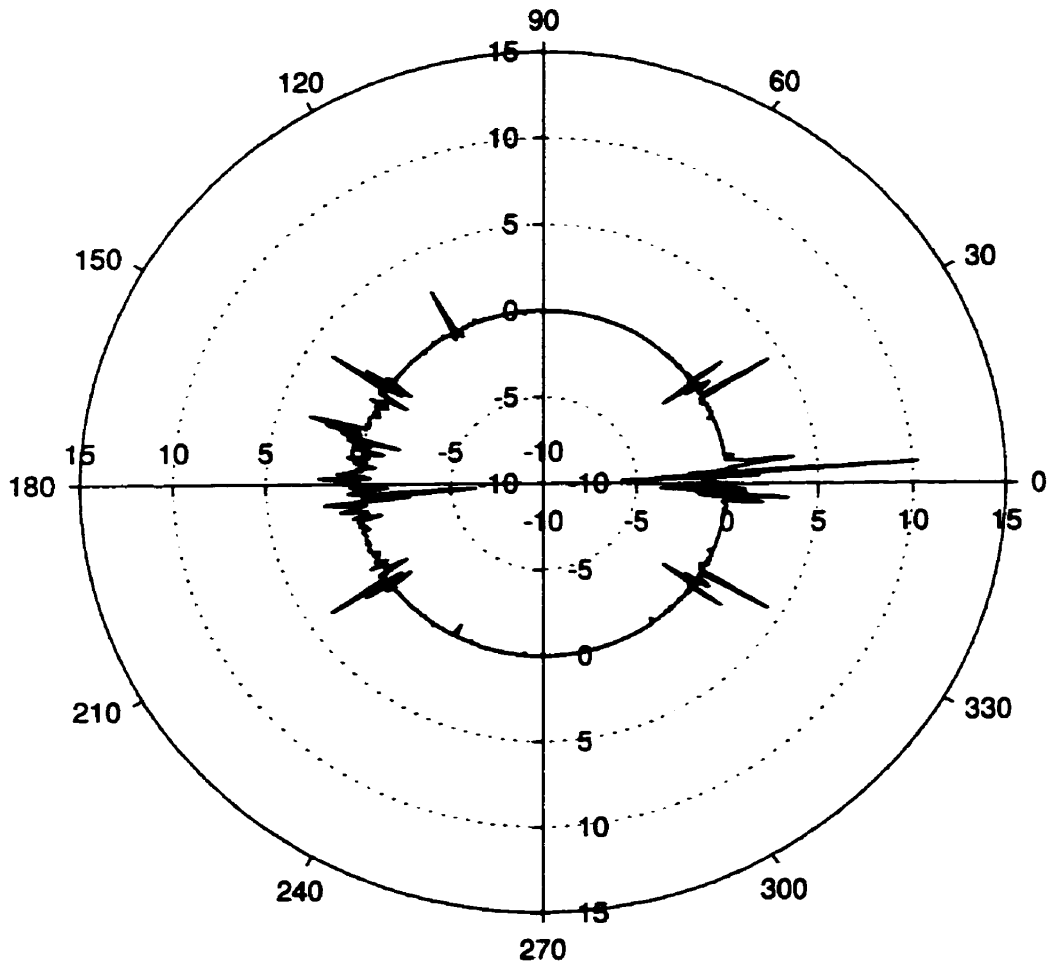
Plot 4-1 Radar Cross Section Difference Between Modification 'a' and Baseline Model of the Canadian Patrol Frigate

RCS Difference in dB versus Azimuth
Impact of adding the mainmast base



**Plot 4-2 Radar Cross Section Difference Between Modification 'b'
 and Modification 'a' of the Canadian Patrol Frigate Model**

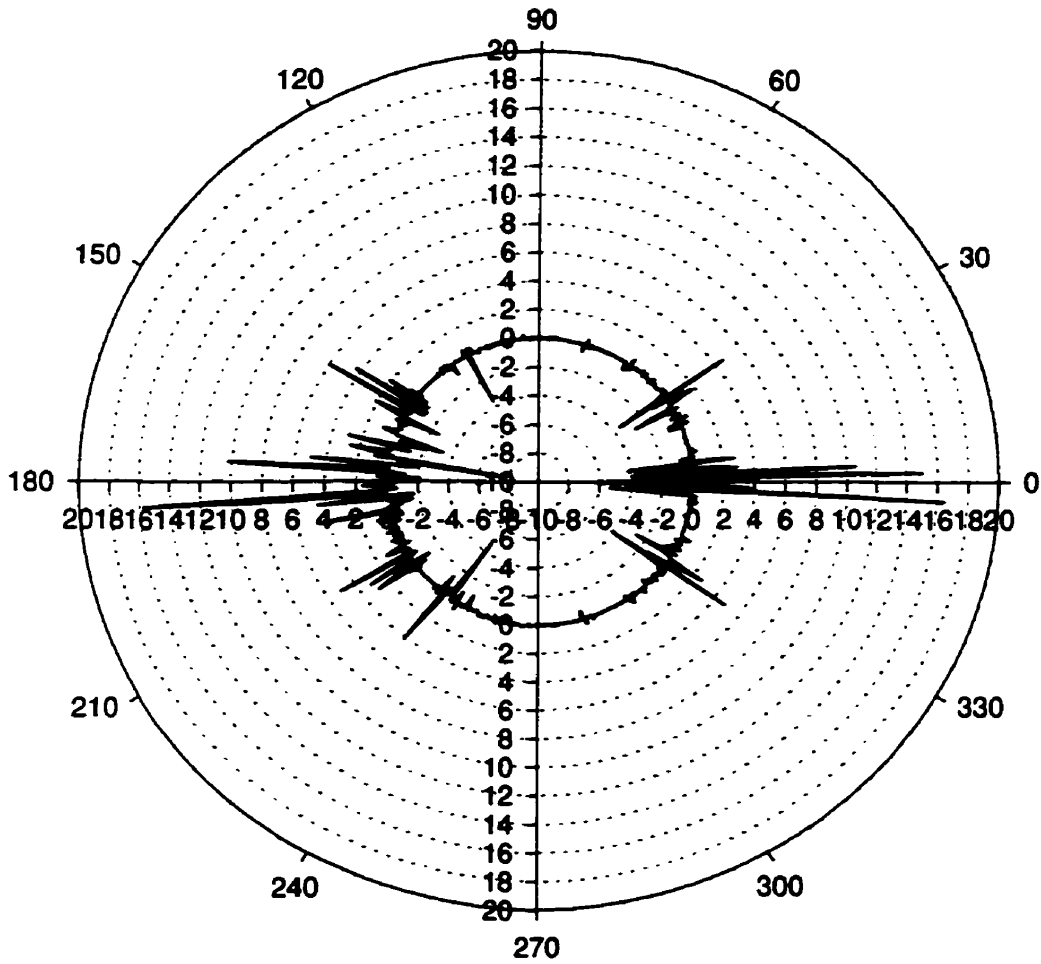
RCS Difference in dB versus Azimuth
Impact of adding a solid mainmast



**Plot 4-3 Radar Cross Section Difference Between Modification 'c'
and Modification 'b' of the Canadian Patrol Frigate Model**

RCS Difference in dB versus Azimuth

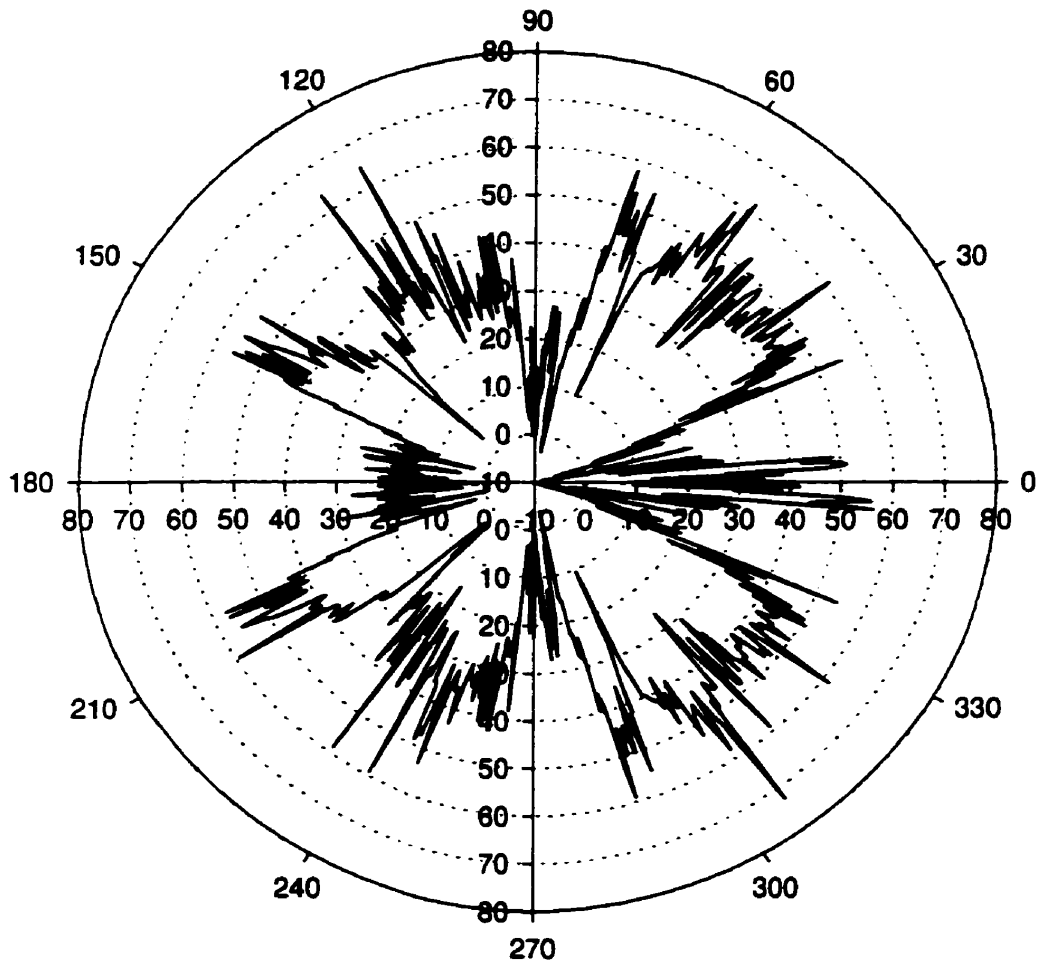
Impact of changing the mainmast from solid to lattice



Plot 4-4 Radar Cross Section Difference Between Modification 'd' and Modification 'c' of the Canadian Patrol Frigate Model

RCS Difference in dB versus Azimuth

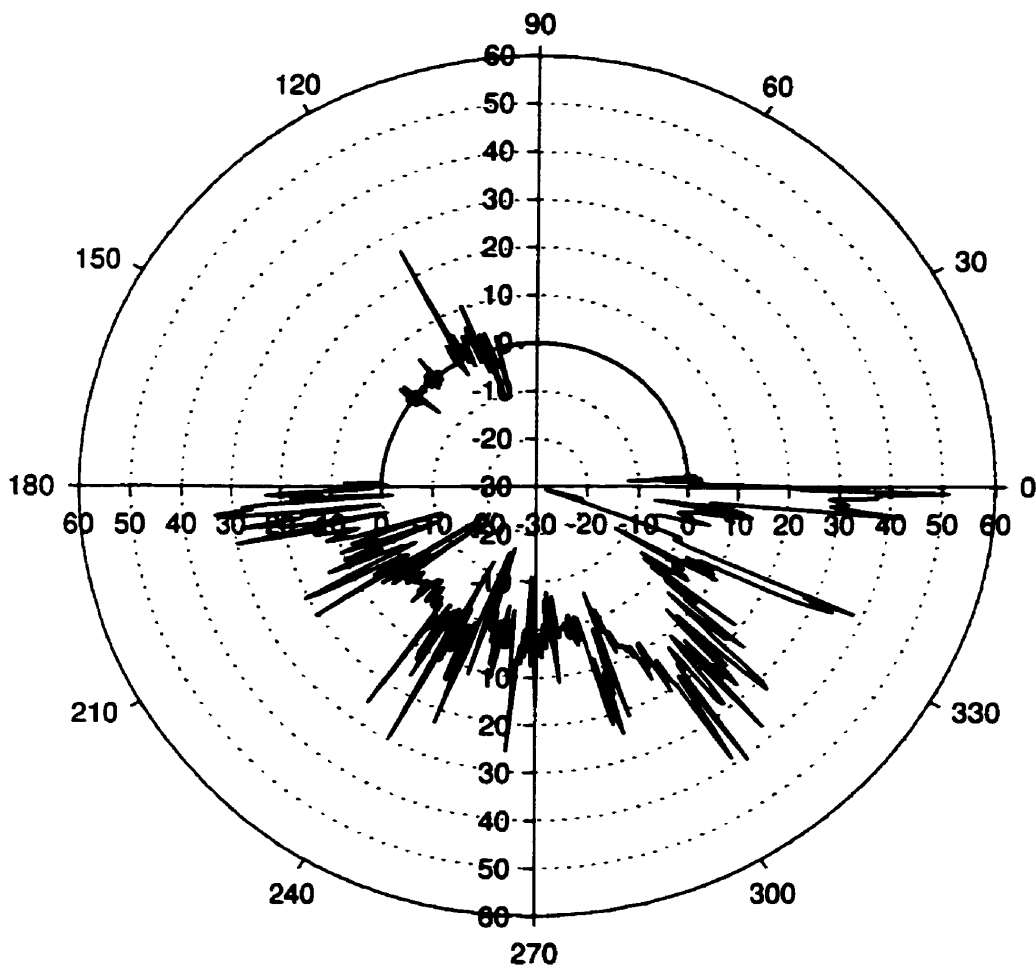
Impact of adding a flat plate without thickness on the STBD Side Boat Deck



Plot 4-5 Radar Cross Section Difference Between Modification 'e' and Modification 'd' of the Canadian Patrol Frigate Model

RCS Difference in dB versus Azimuth

Impact of adding a flat plate with thickness on the STBD Side Boat Deck



Plot 4-6 Radar Cross Section Difference Between Modification 'f' and Modification 'd' of the Canadian Patrol Frigate Model

Modification 'g' was included to model some of the details behind the flat plate on the boat deck. A complete VLSS launcher consists of eight rectangular canisters with tubes connected to the bottom of each canister to take the exhaust during launches and direct it upwards between the canisters. There are four such cylindrical tubes in a row for the eight canisters supported by a beam-like structure. It was not practical to model the complete launcher at this stage without a better appreciation for the potential impact on the RCS. The first iteration of the VLSS modeling was simplified by making the four canisters start from the deck, thus ignoring the exhaust tubing under the canisters, and omitting all the supporting brackets and beams. The top view coordinates of the canisters were reasonably accurate but the canisters themselves were simplified in the modeling due to complexity issues. As can be seen in Figure 4-8, the number of lines required to include the four canisters into the model was quite significant. Each canister was formed of eighteen lines and took nearly half that many to merge with the boat deck. The result of the modification on the RCS was quite apparent, in particular in the forward starboard quadrant where a 20 to 30 dB increase was noticeable over nearly 45°. Overall the average RCS was increased by 2.47 dB over a relatively concentrated area as there was virtually no impact outside the 45° window seen in Plot 4-7. The primary mechanism responsible for the return in the forward starboard quadrant seen in Plot 4-7 is likely multiple reflections resulting from the interaction between the sides of the VLSS canisters and the funnel. It would be interesting to investigate the impact of applying RAM to the side of the funnel and confirm that indeed multiple reflections are at the source of this highly localized return.

Modification 'h' was developed to assess the impact of the difference between the general arrangement drawings and the profile drawings. Both were part of the same set of

drawings but represented distinctive views or aspects of the ship, producing slightly different dimensions. The discrepancy between the drawings was intriguing enough to justify further investigation. The comparison of Plot 4-8 with that of Plot 4-6 is somewhat misleading in that the addition of the plate and four canisters on the starboard side may have had a slight impact on the port side return. Nevertheless the increase in RCS from the addition of the flat plate on the port side was consistent with that of the starboard side with a 3.36 dB increase as opposed to 3.31 dB to starboard. As expected, the impact of this modification to starboard was minimal. The return seen in Plot 4-8 differs from the return of Plot 4-6 although some of the general features are consistent, like the 20° window in the forward quadrant where clearly the modification is having an impact.

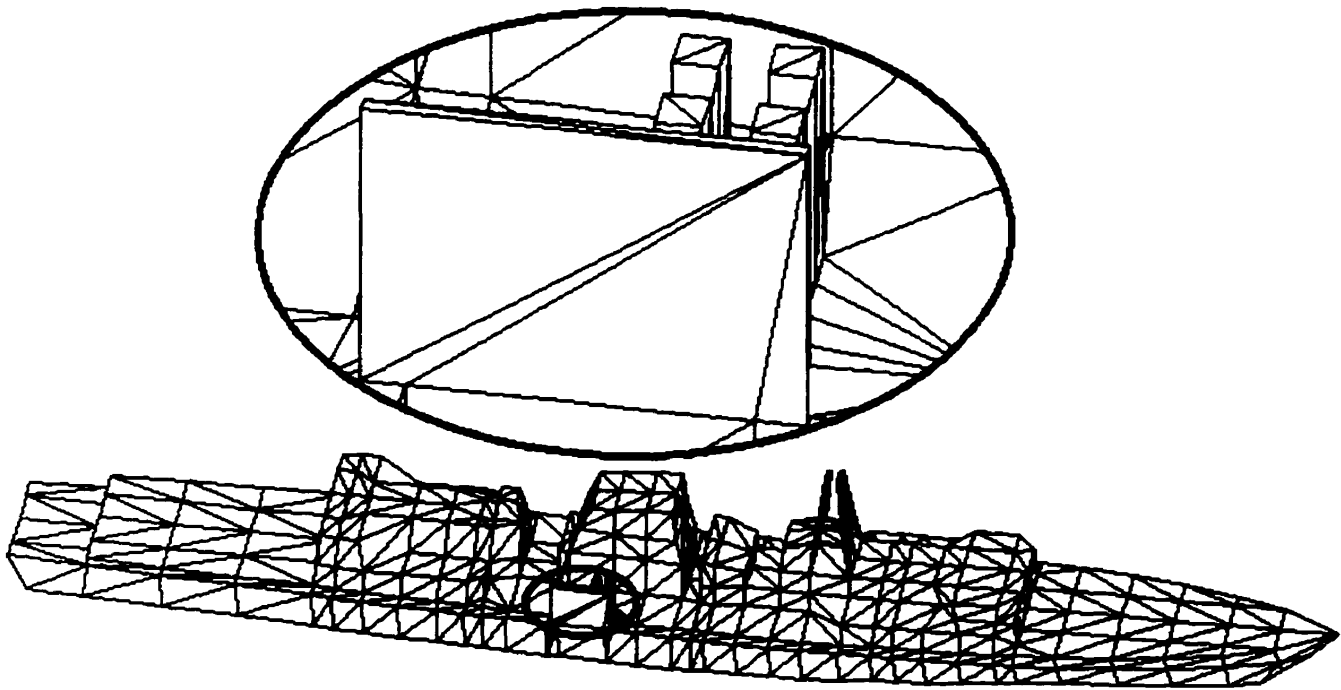


Figure 4-8 Addition of Four VLSS Canisters on the Starboard Side (modification 'g')

The impact of modification 'i' had been expected to be as significant as that of modification 'g' but such was not the case. The modification increased the RCS in the aft starboard quadrant but over a much smaller azimuth range. The RCS increases and decreases were almost all narrow spikes as opposed to continuous variances although clearly the impact was most felt in the aft starboard quadrant as expected. The overall change in RCS from this modification was a mere 0.26 dB as opposed to the 2.47 dB noted from the addition of the four forward canisters on this side. The return on the port side was not surprisingly essentially unchanged.

The addition of the eight VLSS canisters on the port side, modification 'j', was done in a single step using the profile drawings as opposed to the two steps taken on the starboard side using the general arrangement drawings. The impact of the modification was different although consistent with that obtained on the starboard side. For instance, Plot 4-10 paints the picture of a strong return over a wide window in the forward port quadrant, a significant number of spikes with no substantial overall increase in the aft port quadrant and finally little change to starboard, all features which were observed as a result of the same modifications on the opposite side of the ship. The overall result is an average increase of 2.52 dB.

The next modification was directed at addressing the low levels in the two aft quadrants of the previous simulations. The CPF baseline modeled the aft end of the hangar as a flat plate and omitted the structure on the port aft side. This missing structure presented a significantly large dihedral profile with the hangar aft end even if it wasn't at 90°. The first iteration of this detail is shown in Figure 4-9. The impact of this modification was felt almost entirely in the aft starboard quadrant, resulting in a 0.80 dB overall average increase in RCS. As expected due to

obstruction from the hangar itself, Plot 4-11 indicates nil impact over a window of more than 180° forward. The thrust of the improvement was felt over a 10° window corresponding to the bore sight of the non-ideal dihedral corner formed by this additional structure.

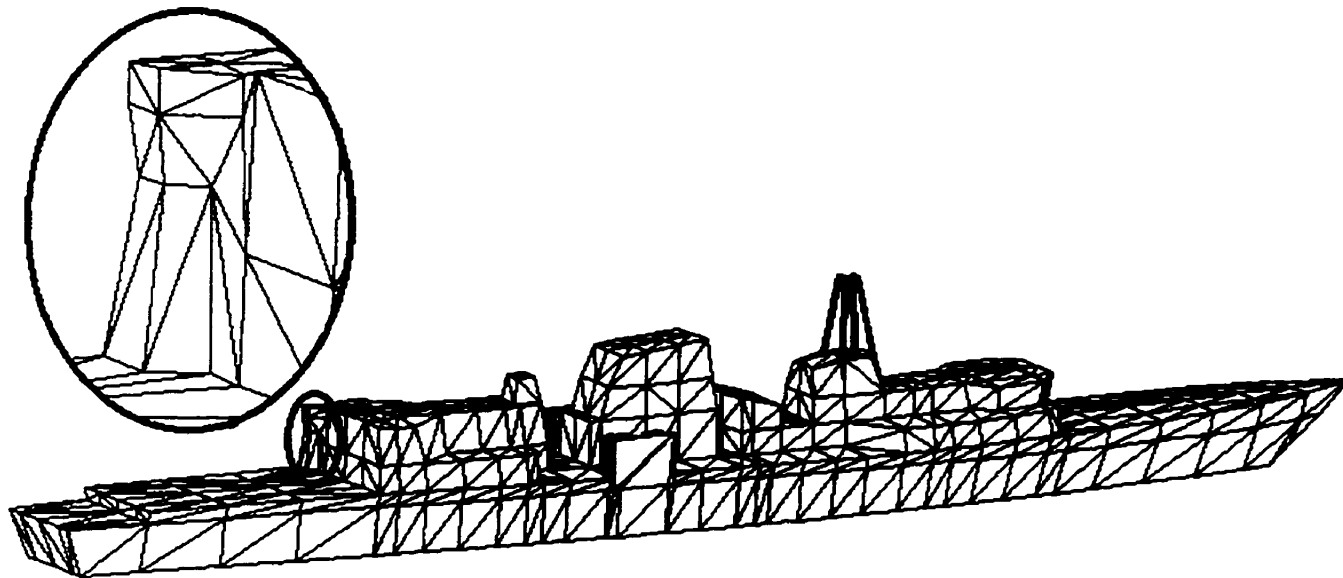
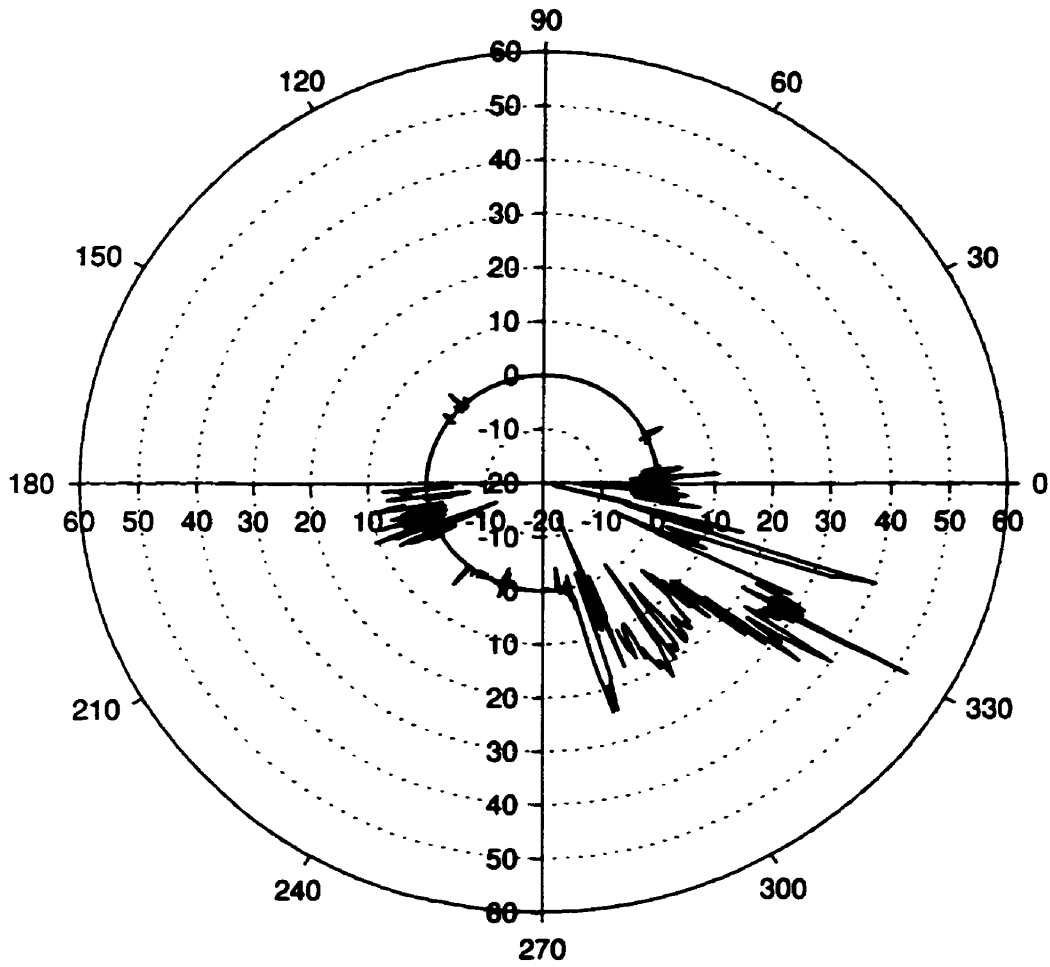


Figure 4-9 Addition of the Hangar Port Aft Structure (modification 'k')

RCS Difference in dB versus Azimuth

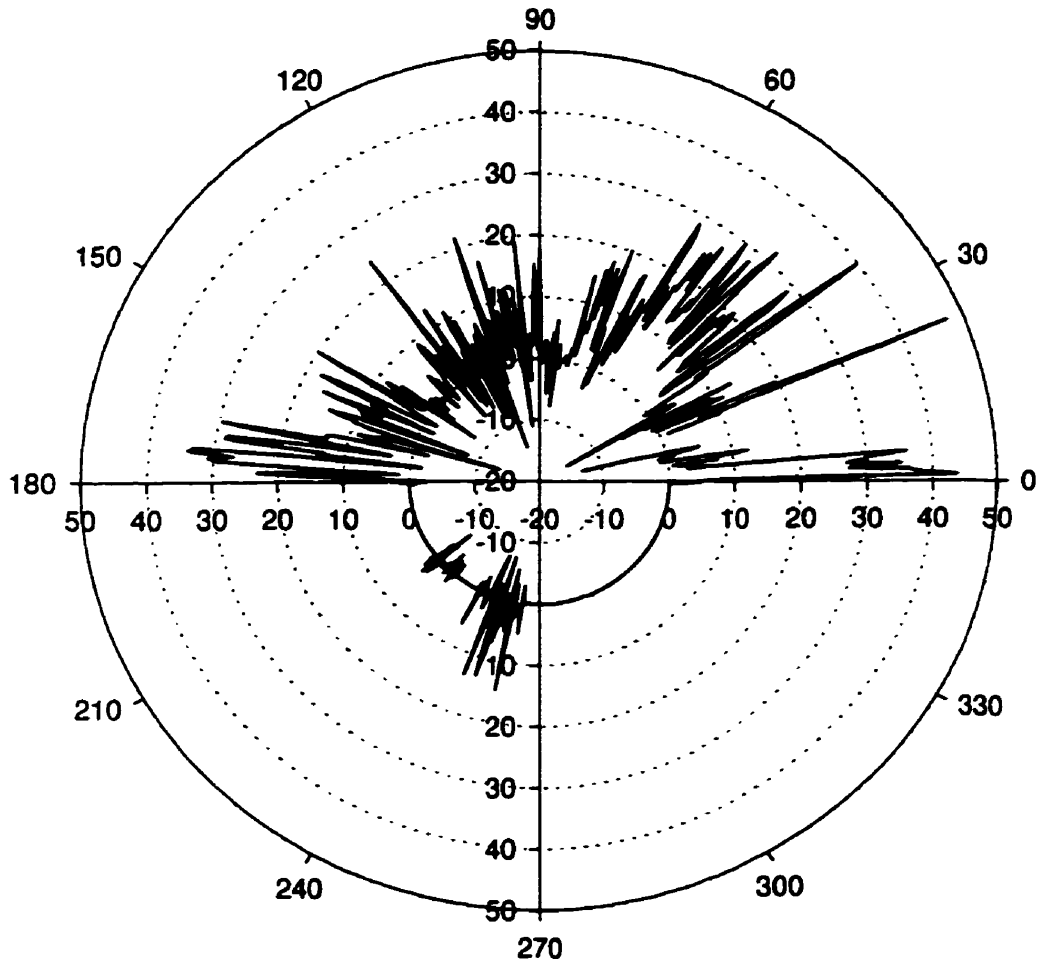
Impact of adding 4 VLSS canisters on the STBD Side Boat Deck



Plot 4-7 Radar Cross Section Difference Between Modification 'g' and Modification 'f' of the Canadian Patrol Frigate Model

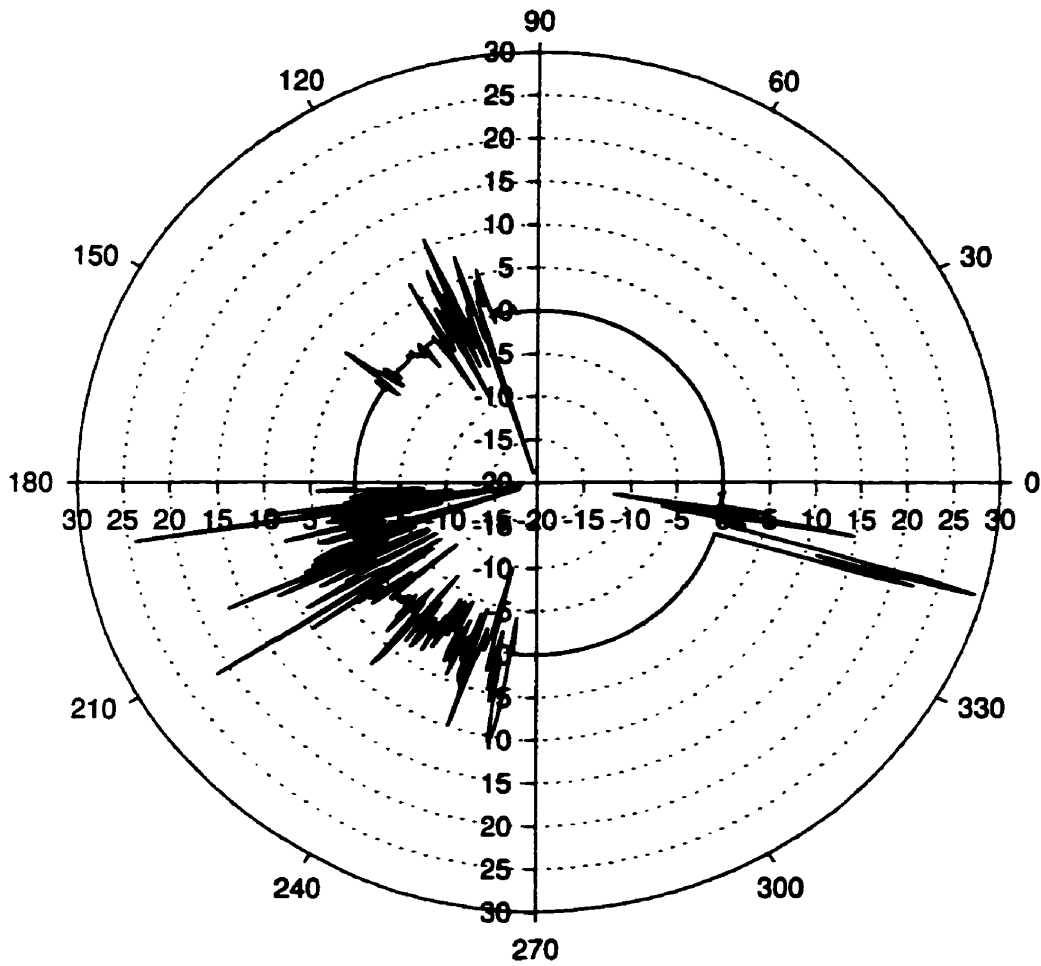
RCS Difference in dB versus Azimuth

Impact of adding a flat plate with thickness on the PORT Side Boat Deck



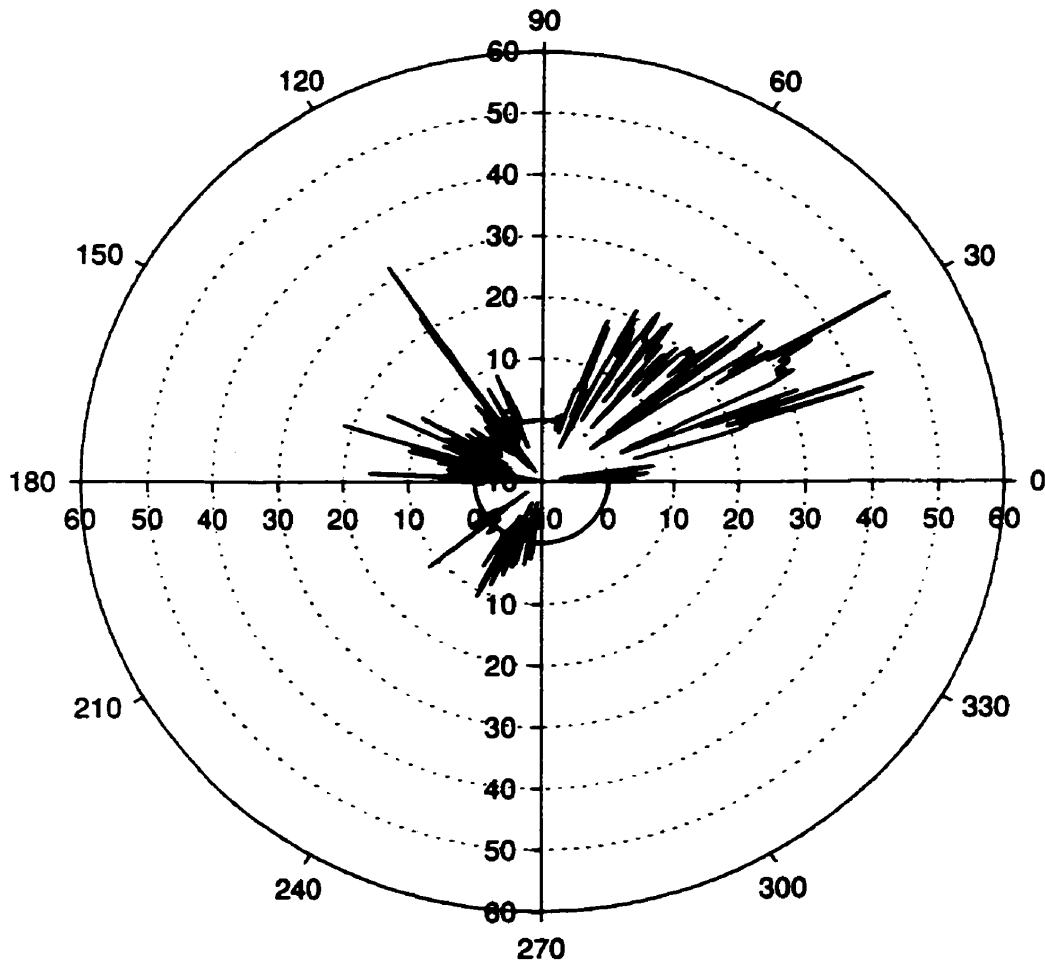
Plot 4-8 Radar Cross Section Difference Between Modification 'h' and Modification 'g' of the Canadian Patrol Frigate Model

RCS Difference in dB versus Azimuth
Impact of adding other 4 STBD VLSS canisters



**Plot 4-9 Radar Cross Section Difference Between Modification 'i'
and Modification 'h' of the Canadian Patrol Frigate Model**

RCS Difference in dB versus Azimuth
Impact of adding 8 PORT VLSS canisters



**Plot 4-10 Radar Cross Section Difference Between Modification 'j'
and Modification 'i' of the Canadian Patrol Frigate Model**

The details of modification 'k' were not easily converted from the drawings to the model in AutoCAD and after verifying the actual details onboard one of the CPFs, HMCS CALGARY, it was deemed appropriate to take a second look at this area of the model. It was soon realized that the hangar top had been initially modeled as being essentially symmetrical with respect to the centerline when in fact this was not the case. The structure hanging to port on top of the hangar should have actually been given a more pronounced downward angle than the one on the starboard side. This angle discrepancy also impacted the top of the structure added in modification 'k'. Modification 'l' was thus incorporated to address the slope error on the port side hangar top inherent in the baseline model as well as remodel the structure on the port side aft end of the hangar. The result was a much less pronounced increase in the RCS as the difference in return was limited to essentially a few spikes in the starboard aft quadrant. This would be indicative of the addition of flat surfaces as opposed to the return which appeared to be dominated by the dihedral of the previous modification. The overall impact of the return seen in Plot 4-12 was 0.05 dB which barely justifies the additional structure. Such might not be the case at different elevation angles where the interaction of this additional structure with the model could result in returns more indicative of dihedral or even trihedral shapes. The importance of the angles and the coordinates used to model the port aft structure of the hangar are evident by comparing Plot 4-12 with Plot 4-11.

The first attempt at adding the hangar door into the model was done with the assumption that the aft end of the hangar was perfectly vertical. The impact of the modification shown in Figure 4-10 was so astonishing that the modeling accuracy of this addition was challenged. There was indeed cause for concern as the hangar door was not given the same angle as the aft

end of the hangar which sits at 2.3° according to the drawings. The modeling error of the hangar door generated a significant increase over a very wide window astern, 100° to 265° , and nil impact elsewhere. The slight difference between the port and starboard side RCS shown in Plot 4-13, most noticeable between the return at 95° and 265° where the port side is null, can be attributed to the port aft end structure of the hangar. Overall this flawed modification had a significant impact on the RCS astern of the ship with an average increase of 10.94 dB.

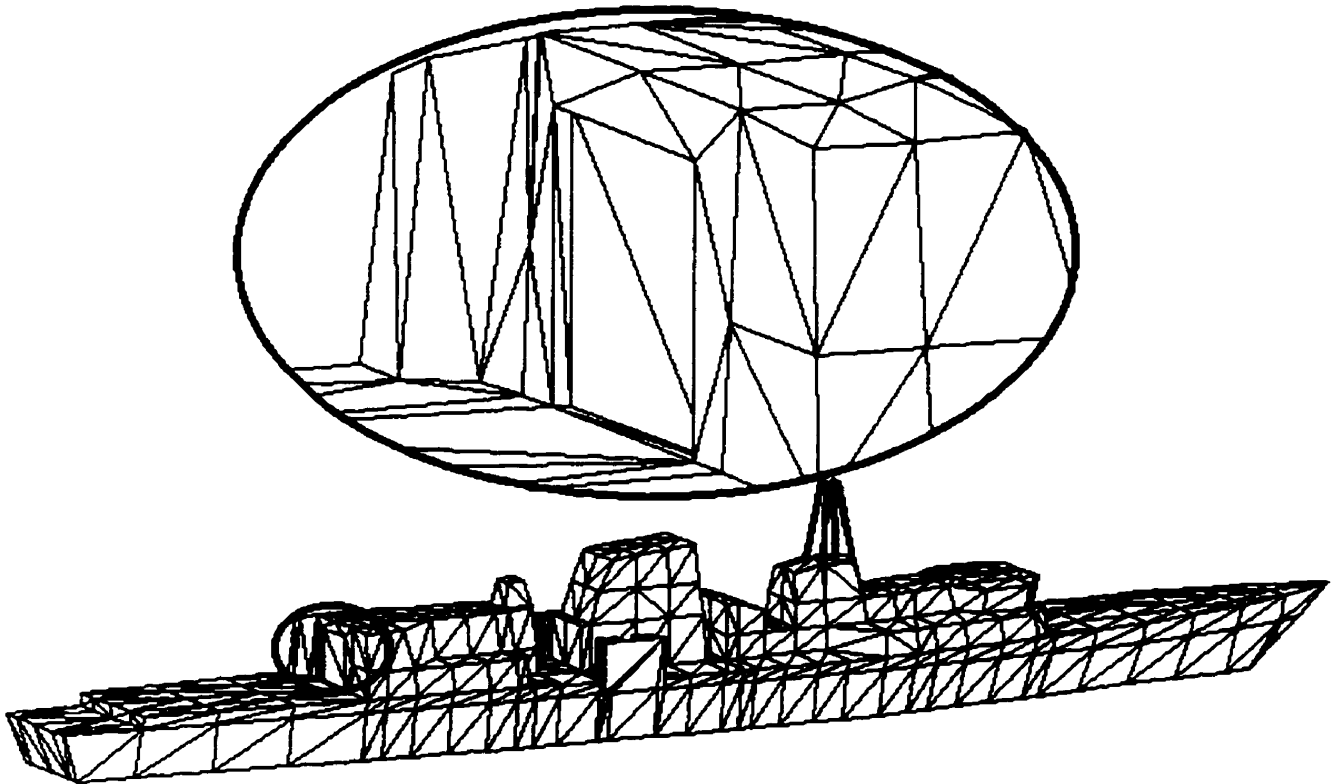


Figure 4-10 Modifications to the Hangar Aft End (modifications 'l' and 'm')

The 2.3° angle omitted from initial consideration in modification 'm' was addressed in modification 'n'. The difference between the two inclusions was so insignificant from a purely visual perspective that a separate figure illustrating the difference was not deemed necessary. The return depicted in Plot 4-14 is more indicative of the results expected from this modification.

From a purely geometrical point of view, the addition of the hangar door should offer no increase in surface area dead-astern and should not provide an increased RCS in azimuths where the hangar blocks the door from line-of-sight, that being forward. Furthermore, the primary consequence of the inclusion of the hangar door was the formation of two symmetrically tall yet shallow dihedral corners. The returns around 105° and 260° are more than likely the result of these dihedral corners. At higher angles, the two trihedrals formed by the flight deck and the hangar door dihedral may become factors but there was no evidence to support this hypothesis at the elevation angle chosen. The overall impact of this modification was 1.22 dB.

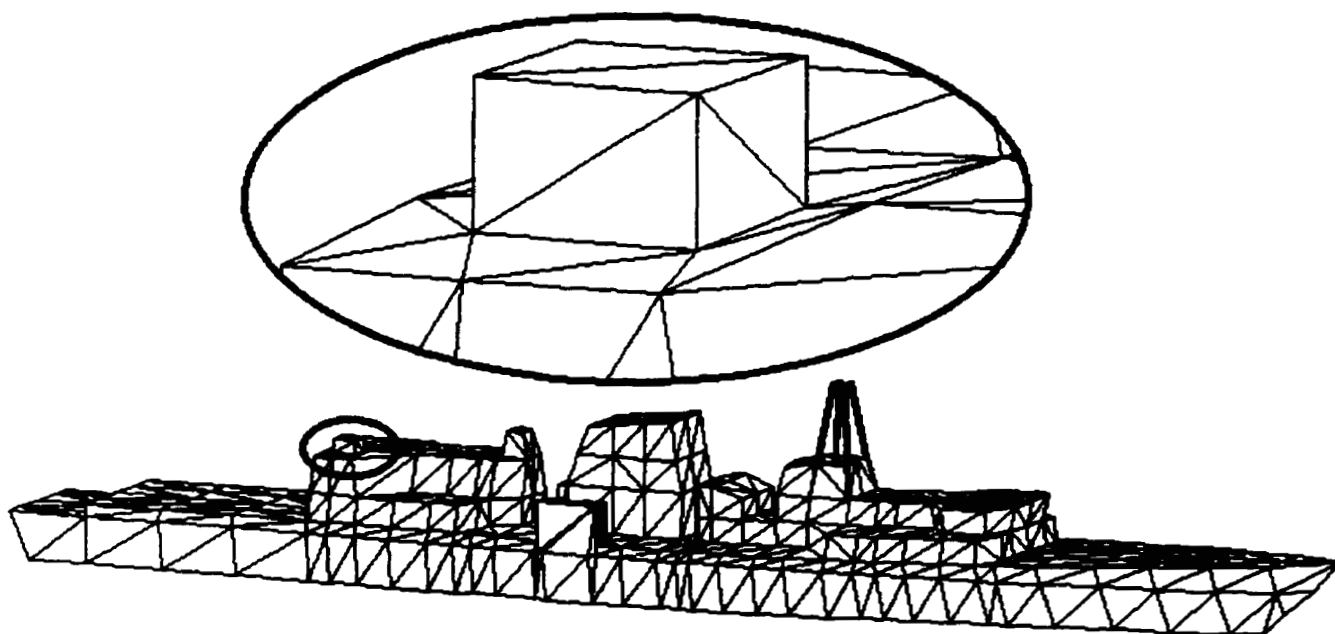
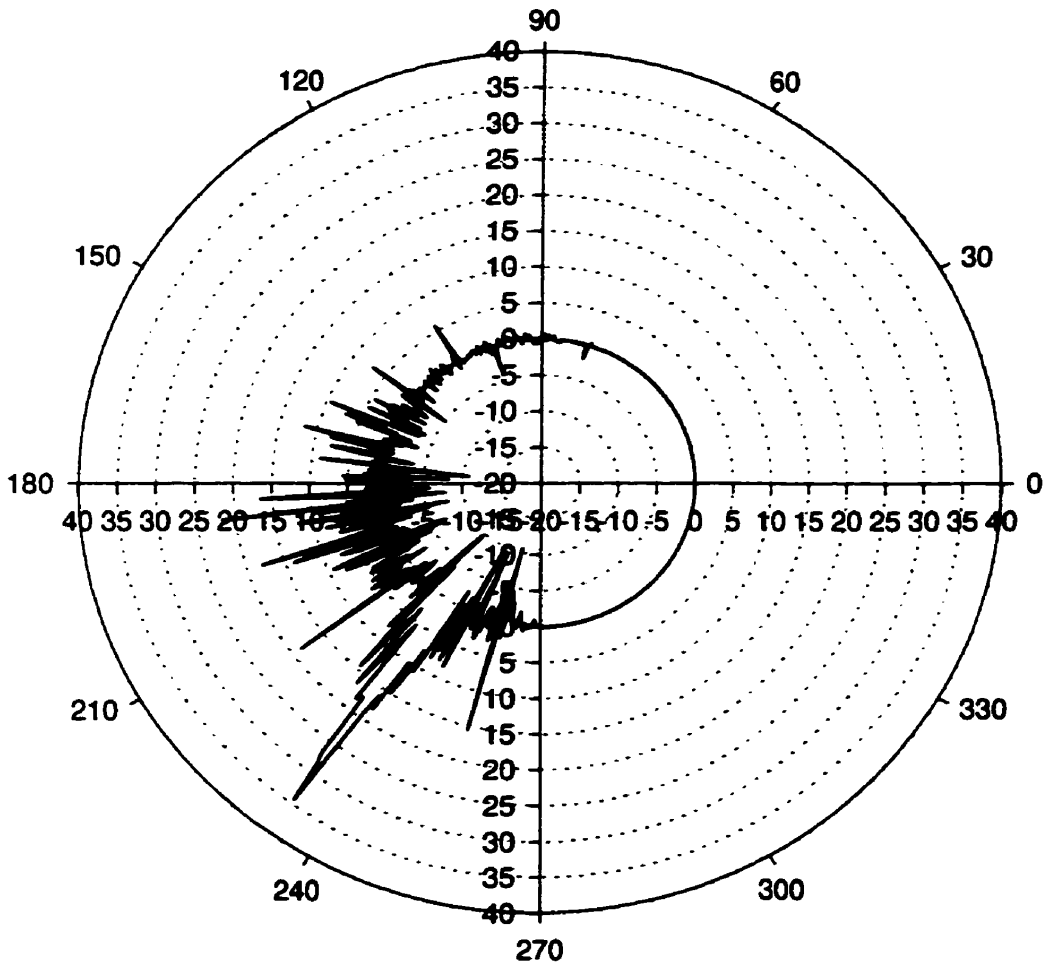


Figure 4-11 Addition of the Close-in-Weapon-System Mount (modification 'o')

RCS Difference in dB versus Azimuth

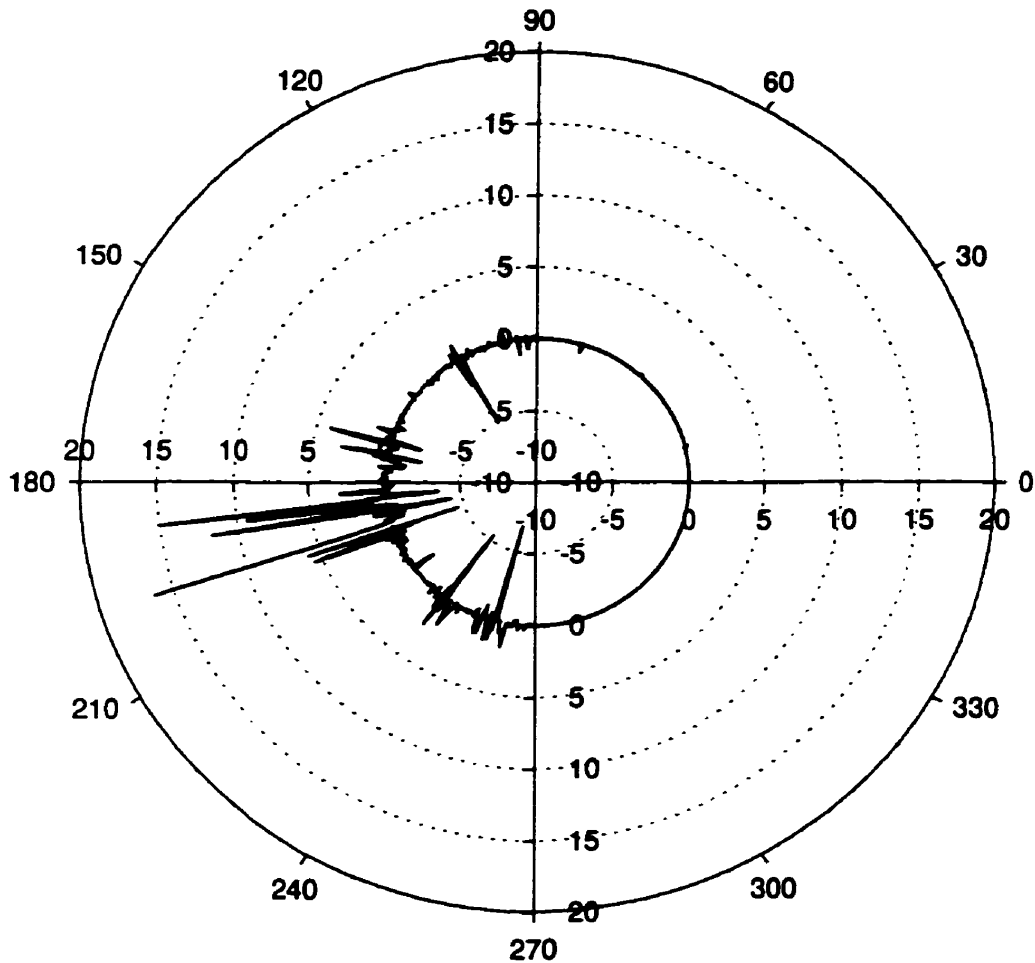
Impact of adding PORT AFT structure of the hangar



Plot 4-11 Radar Cross Section Difference Between Modification 'k' and Modification 'j' of the Canadian Patrol Frigate Model

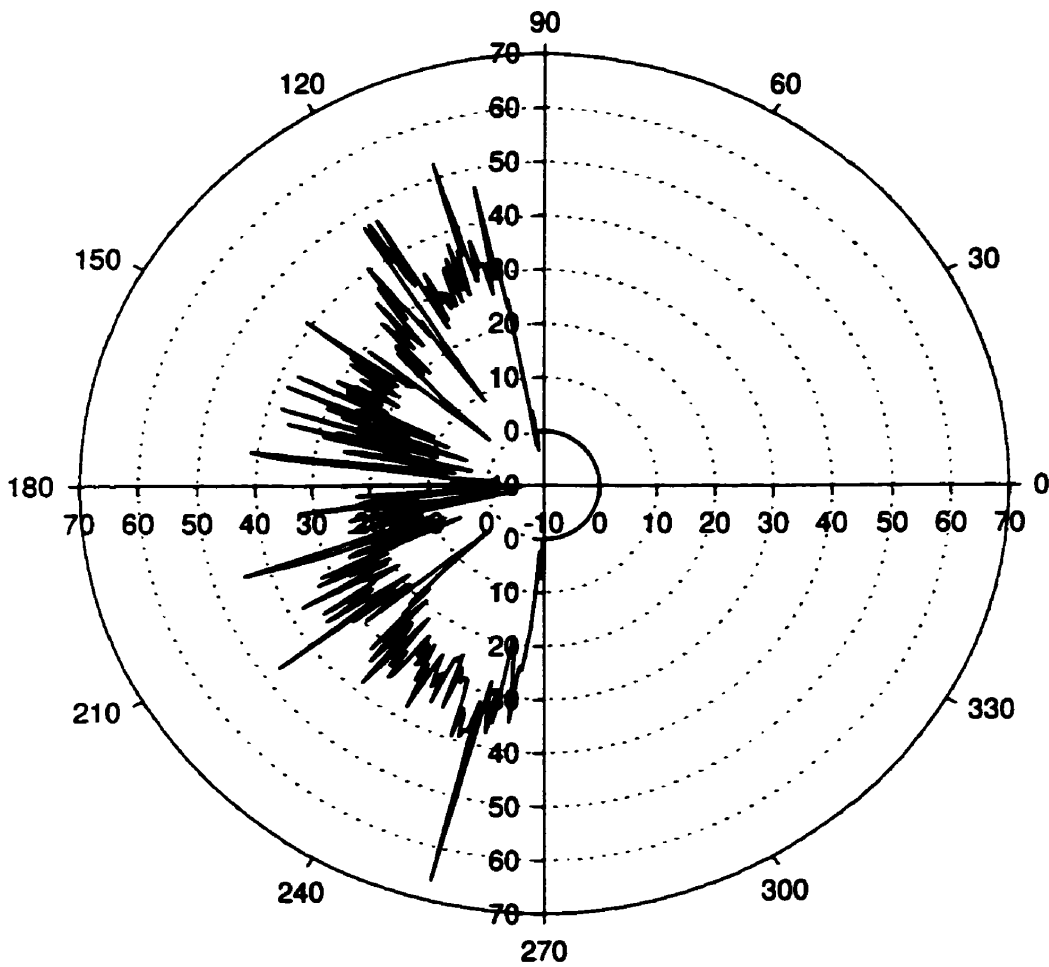
RCS Difference in dB versus Azimuth

Impact of modifying the PORT AFT structure of the hangar and the PORT TOP hangar slope



Plot 4-12 Radar Cross Section Difference Between Modification 'l' and Modification 'j' of the Canadian Patrol Frigate Model

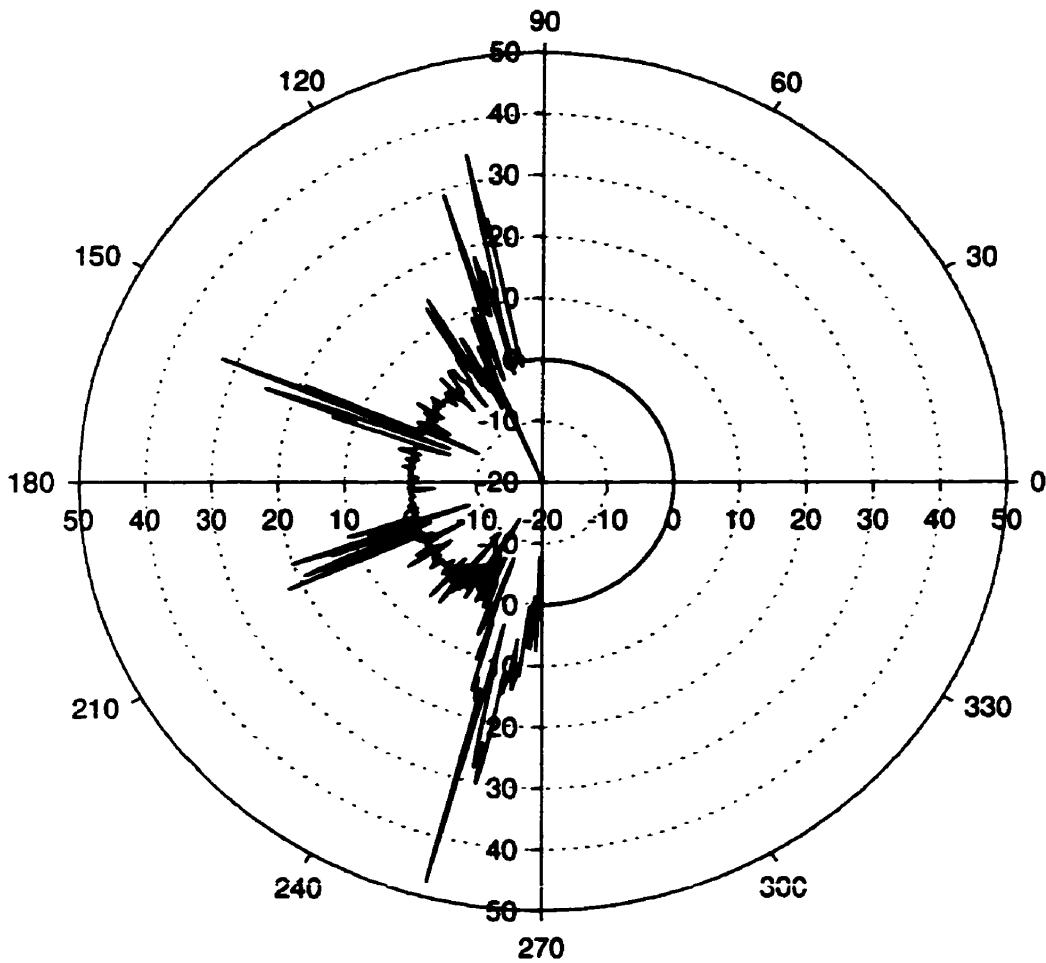
RCS Difference in dB versus Azimuth
Impact of adding a vertical hangar door



Plot 4-13 Radar Cross Section Difference Between Modification 'n' and Modification 'm' of the Canadian Patrol Frigate Model

RCS Difference in dB versus Azimuth

Impact of adding the hangar door (with the proper slope)



Plot 4-14 Radar Cross Section Difference Between Modification 'n' and Modification 'l' of the Canadian Patrol Frigate Model

In keeping with attempting to fill the low returns in the two aft quadrants, modification 'o' was included into the model. The CIWS is a fully-automatic gun with its own search and fire control radars to detect, classify and engage targets at very short ranges from the ship. The search and fire control radars are mounted overtop a mount located on top of the hangar on the CPF. Although the inclusion of the radar reflectors would provide an increase in return down the bore sight of the antennas, these details were omitted as the reason this structure was added was to assess the potential impact of the dihedrals formed by the mount itself with the hangar top. The modification made to the model for this detail was thus restricted to a basic box-like structure at the appropriate location. The impact at the elevation angle chosen was not particularly significant with an average increase of only 0.26 dB. This was lower than expected considering the 90° angle formed between the sides of the mount and the hangar top. The simplification of the mount structure was expected to over-emphasize the dihedral corners by ignoring the small details and rounded corners of the actual mount. Plot 4-15 indicates no particular area of impact to show for the modification. Again in this case the impact of the dihedral corners formed might be more prevalent at higher elevation angles where the return is closer to bore sight with the corners as opposed to looking down at the edges of the corners where the return more closely resembles that of a flat surface.

The next detail added to the model was the overhanging part of the funnel top. It was not expected to impact the RCS significantly even if the added surface area of the modification was worth consideration. The result was a decrease of 0.004 dB which for all intent and purpose can be considered as negligible. Aside from the spike at approximately 155°, the difference in RCS return shown in Plot 4-16 was insignificant for all azimuths.

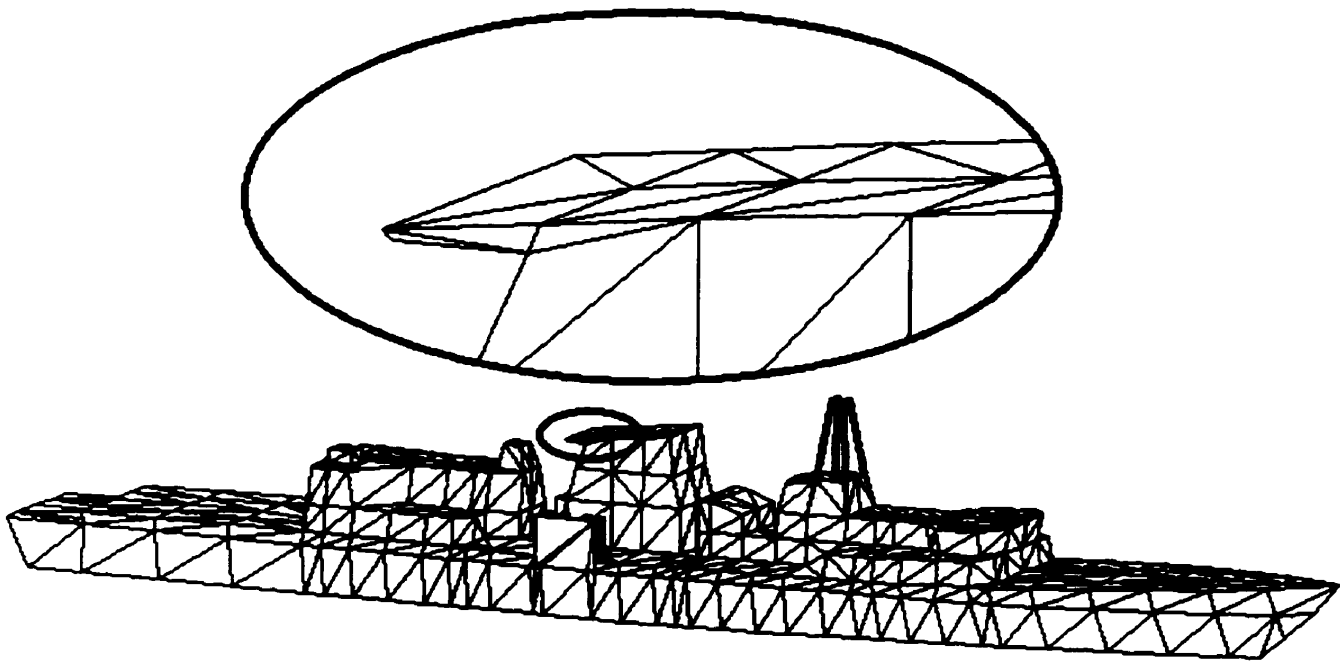


Figure 4-12 Addition of the Funnel Tail (modification 'p')

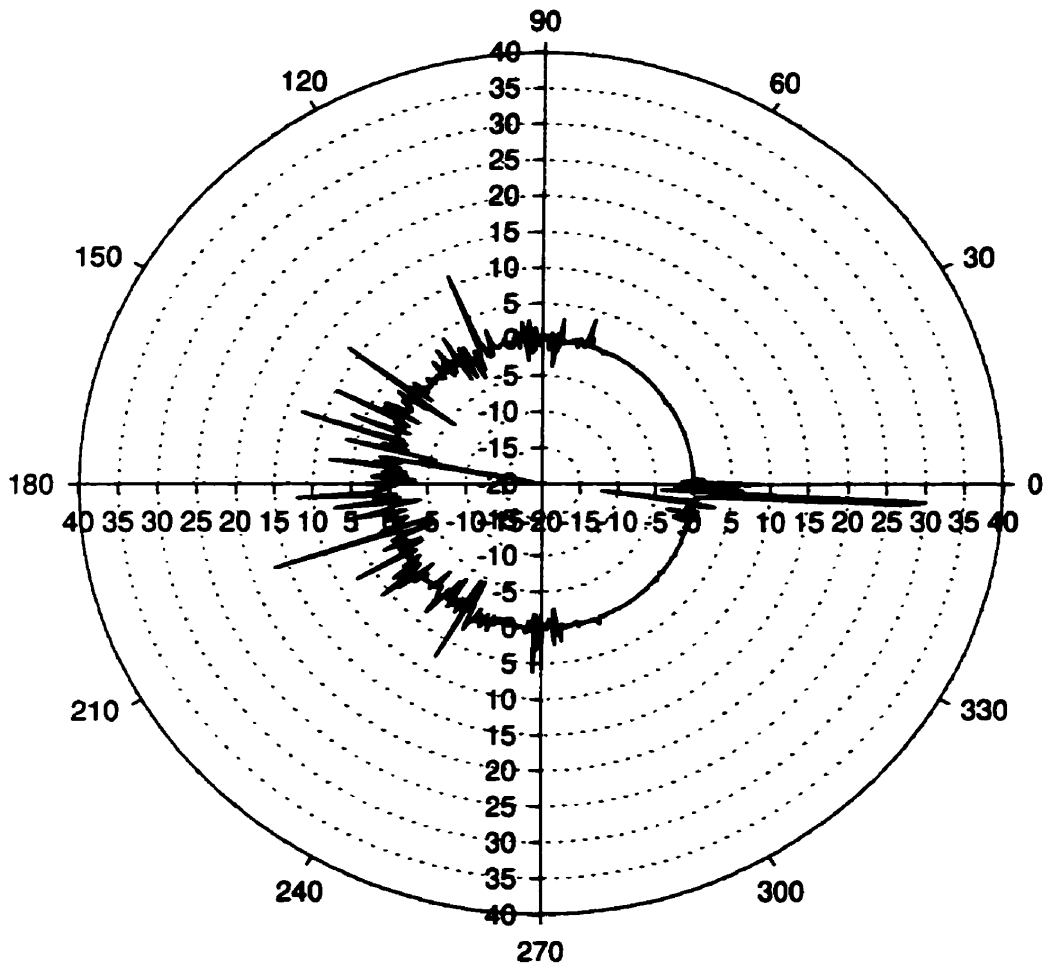
The modifications made to the model on the boat deck had the most significant impact on the RCS thus far. Additional effort in this area was thus deemed appropriate. The VLSS canisters modeled earlier had been simplified by allowing them to start at deck level and disregarding the exhaust tubing between the bottom of the canisters and the deck. As mentioned earlier, rounded surfaces like tubes are very difficult to model using triangles. Modifications 'q' and 'r' thus simplified the VLSS canisters by making them free-standing and excluding the portion between the canisters and the deck. The first part of the investigation addressed the four aft canisters on the starboard side. Plot 4-17 indicates clearly the impact of this modification in the aft starboard quadrant. The overall result of this change to the model was an average increase of 1.85 dB. The second part of the investigation addressed the other four canisters on the starboard side. The results of this modification were somewhat unexpected. Aside from the fact that cutting the bottom of the four forward canisters on the starboard side increased the average

RCS a striking 3.80 dB over the modification of cutting the four aft canisters, the areas of impact were highly localized and could easily be mistaken as being in the wrong quadrants. Plot 4-18 shows two primary areas of impact. On the starboard side, the return was increased not forward but aft. Even more surprising is the large return on the port side, at approximately 120°, which could only be explained as resulting from multiple reflections originating on the starboard side.

The results of the eighteen primary modifications made to the CPF are presented in Table 4-2 and are discussed further in the following chapter.

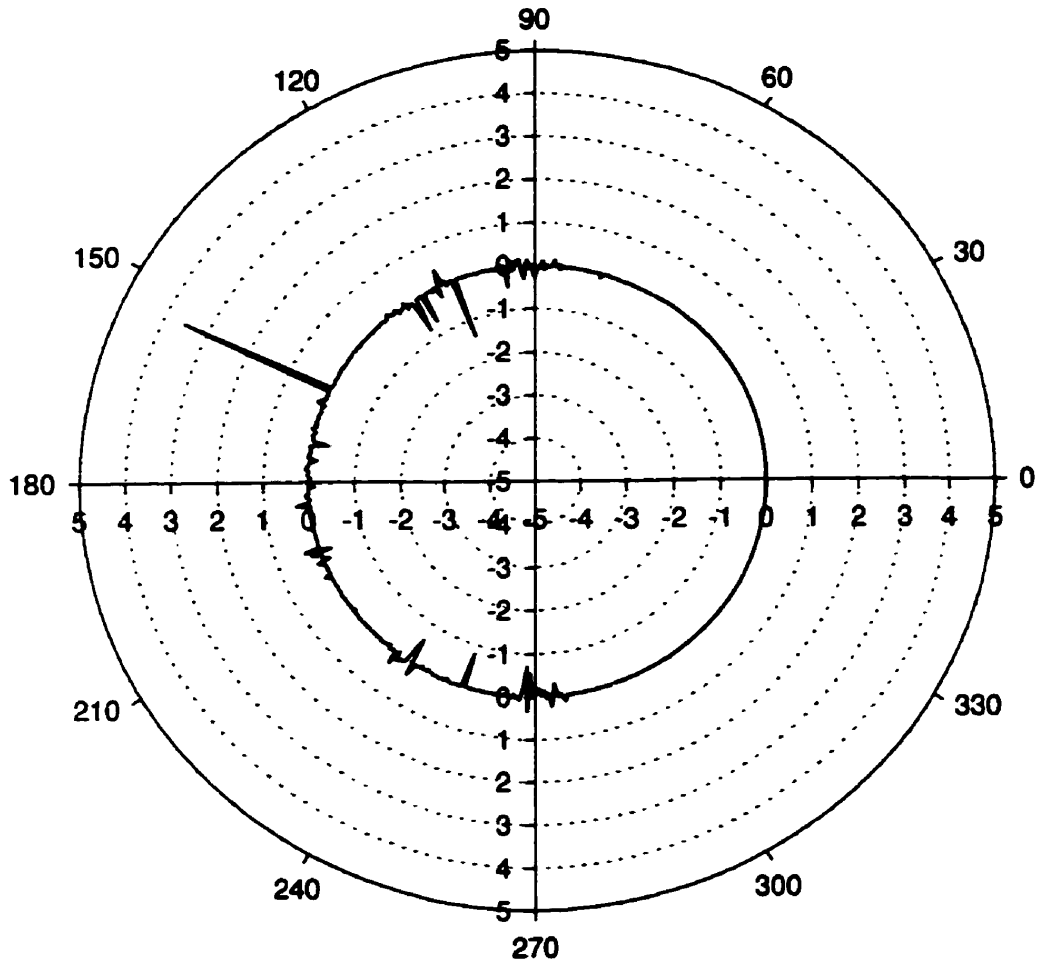
RCS Difference in dB versus Azimuth

Impact of adding the CIWS mount



Plot 4-15 Radar Cross Section Difference Between Modification 'o' and Modification 'n' of the Canadian Patrol Frigate Model

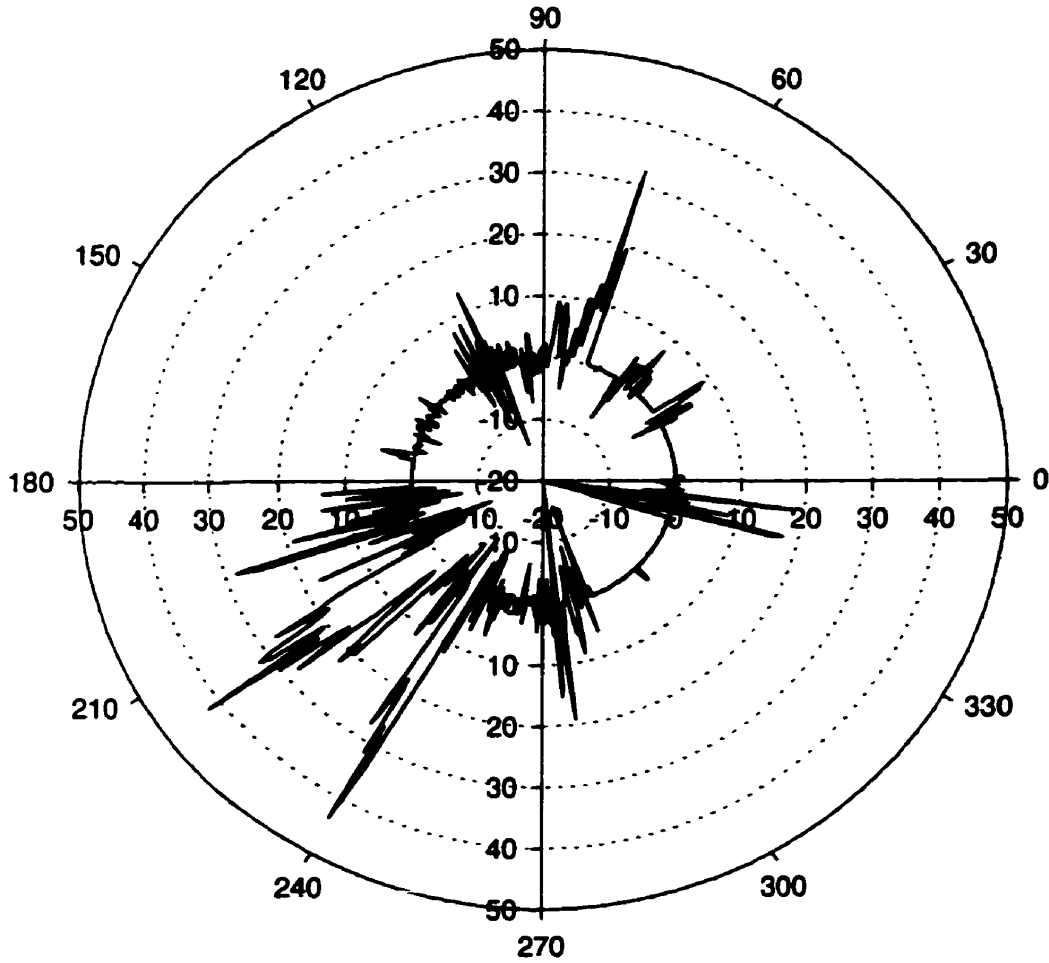
RCS Difference in dB versus Azimuth
Impact of adding the Main Funnel Tail



Plot 4-16 Radar Cross Section Difference Between Modification 'p' and Modification 'o' of the Canadian Patrol Frigate Model

RCS Difference in dB versus Azimuth

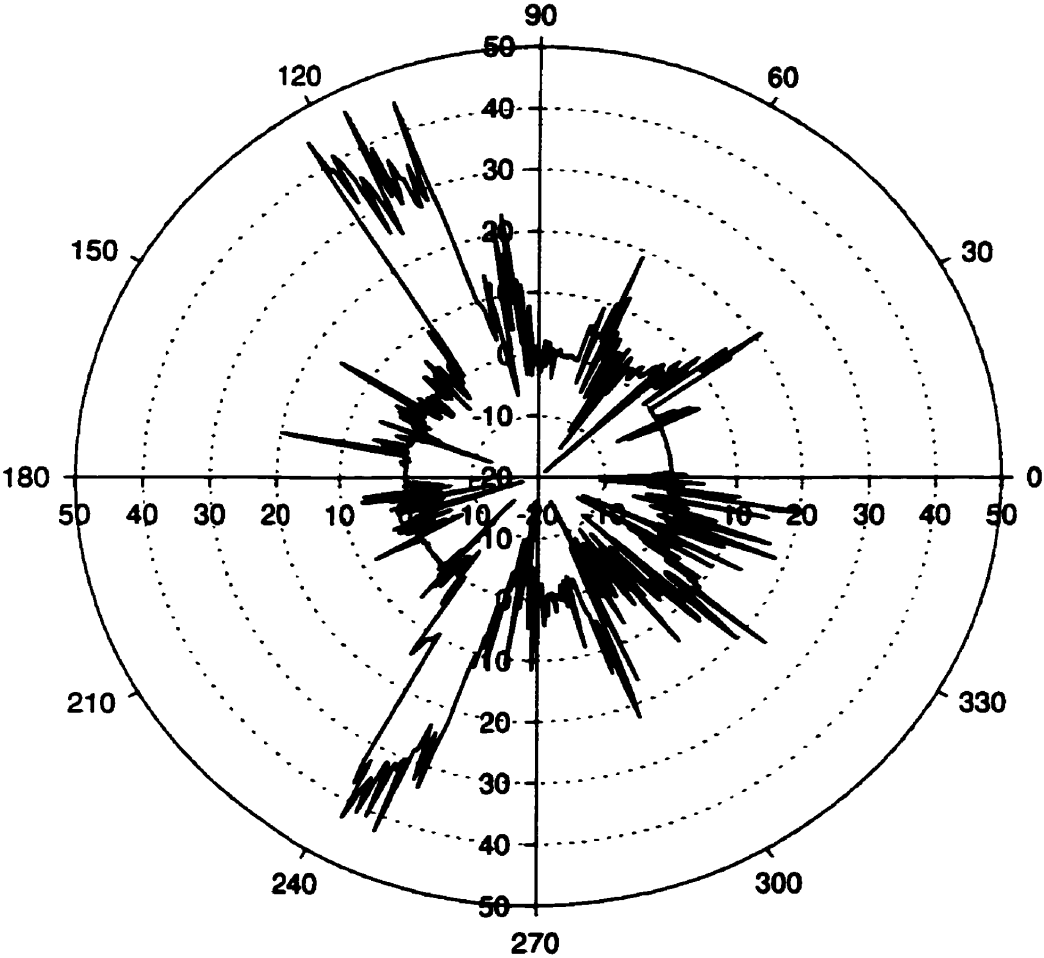
Impact of cropping the bottom of 4 STBD VLSS canisters



Plot 4-17 Radar Cross Section Difference Between Modification 'q' and Modification 'p' of the Canadian Patrol Frigate Model

RCS Difference in dB versus Azimuth

**Impact of cropping the bottom of
other 4 STBD VLSS canisters**



**Plot 4-18 Radar Cross Section Difference Between Modification 'r'
and Modification 'q' of the Canadian Patrol Frigate Model**

Model A	Model B	RCS difference: Model (B-A) dB	Nature of Modification
baseline model	modification 'a'	0.22	change in the waterline location
modification 'a'	modification 'b'	0.06	addition of mainmast base
modification 'b'	modification 'c'	0.01	addition of solid mainmast
modification 'c'	modification 'd'	0.09	change of solid mast for lattice mast
modification 'd'	modification 'e'	29.57	addition of a flat plate without thickness on the starboard side boat deck in accordance with the general arrangement drawing
modification 'd'	modification 'f'	3.31	addition of a flat plate with thickness
modification 'f'	modification 'g'	2.47	addition of 4 VLSS canisters on the starboard side boat deck
modification 'g'	modification 'h'	3.36	addition of a flat plate with thickness on the port side boat deck in accordance with profile drawings
modification 'h'	modification 'i'	0.26	addition of the other 4 VLSS canisters on the starboard side
modification 'i'	modification 'j'	2.52	addition of the 8 VLSS canisters on the port side boat deck
modification 'j'	modification 'k'	0.80	addition of the port side aft structure of the hangar
modification 'j'	modification 'l'	0.05	modification of the port side aft structure of the hangar and the port side hangar top slope
modification 'm'	modification 'n'	-9.72	modification of the hangar door slope from vertical to one matching the hangar aft end
modification 'l'	modification 'n'	1.22	inclusion of the hangar door with a slope to match the hangar aft end
modification 'n'	modification 'o'	0.26	addition of the CIWS mount
modification 'o'	modification 'p'	-0.004	addition of the funnel tail
modification 'p'	modification 'q'	1.85	cropping the bottom of 4 VLSS canisters on the starboard side
modification 'q'	modification 'r'	3.80	cropping the bottom of the other 4 VLSS canisters on the starboard side
baseline model	modification 'r'	19.47	overall impact of modifications

Table 4-2 Impact of modifications on the RCS

CHAPTER 5 DISCUSSION

The initial aim of this research was to generate a CAD model of the CPF suitable for RCS analysis using RAPPORT. This model could then be used to ascertain the effectiveness of radar cross section reduction techniques such as shaping or the application of radar absorbent material. The key to being able to draw useful results from this effort was to improve the baseline model of the CPF to the point of making the predicted RCS as close as possible to the measured results. This task proved to be a formidable challenge and was altered for a more achievable goal of investigating the impact of geometry on the RCS of a complex object. The primary reason for the change of objective was simply the underestimating of the model building process. The majority of the efforts put forth in this research were dedicated to constructing objects in AutoCAD only to find out that the baseline model chosen was not accurate enough to eventually provide the expected results. The first aim of this chapter is to assess the suitability of the process proposed in Chapter 3 in predicting the RCS of a complex object like a warship. The second aim looks at evaluating the impact of geometry on the RCS of complex objects.

5.1 VALIDATION OF THE PROCESS

The first part of this research consisted of translating the RCS analysis process used by TNO and DREO from one based on UNIX or DEC-ALPHA platforms to one based on a personal computer system. Given the fact that the Royal Military College (RMC) and DREO are located approximately 150 kilometers apart from each other, it was recognized from the outset of this research that a means of reducing the travel requirement to produce results was highly desirable.

There were two primary options available to perform the function of converting the ship's drawings into a digital format. The first option was to interface a digitizing table with a computer running DIDEK and input the drawing vertices one at a time. This option was quickly discarded as a digitizing table could not be obtained in a suitable time frame. It is pertinent to mention that the accuracy of this method relies heavily on the ability of the user to precisely position the cross-hairs of the cursor or mouse on the appropriate vertices on the drawings as well as the scale of the drawings. Larger scale drawings make it less likely that the coordinates will be incorrectly entered although these drawings tend to come in several sheets which in itself is a potential for errors in calibrating the reference point of each sheet.

The second option available to build the CPF model was to input the drawing vertices into DIDEK or AutoCAD manually. This approach offered many advantages as it would allow for the use of many automated features to simplify the process such as mirror imaging, copying and pasting of objects. The scale of the drawings was equally important in this case as the errors relating to lifting-off the coordinates and the measurements increased as the scale decreased. Smaller scale drawings also make the task of correctly identifying small objects or details more challenging. The real benefit of this method is that drawings generally have several reference points where coordinates are given with a high degree of certainty. Measurements to other points or coordinates on the drawings are often given with respect to these reference points which reduces the requirement to extrapolate or convert scaled measurements manually. The use of a digitizing table does not easily allow one to differentiate between reference points and other points which are less accurate, thus increasing the probability of propagating errors during the conversion from drawings to CAD tool. The obvious disadvantage of the manual method is that

it is extremely time consuming and as with any repetitive process lends itself to human errors which could have a more or less noticeable impact on the final product.

A copy of AutoCAD Release 13 was available at RMC while DREO provided a copy of the most recent version of DIDEDEC for the purpose of this research. Although using AutoCAD to generate a model was easier and more accurate than the first option, building a model of this magnitude was no simple task. As the level and number of details increased, the level of complexity associated with making modifications to the model increased considerably. It was unfortunate that the CAD tools utilized by Saint John Shipbuilding (SJSJL) to construct the CPFs were not compatible with AutoCAD or DIDEDEC. The initial conception of the CPF was made in the late 1970's and early 1980's with the help of what would be termed today as a basic two dimensional CAD software package. Although DIDEDEC has the capability of merging a pair of two-dimensional views into a three-dimensional view which could subsequently be massaged for RCS analysis, the file formats of the available two-dimensional views were not conducive to this approach.

The design of future replacement warships or submarines will almost certainly make use of modern CAD tools with the ability to output files in one of the formats which AutoCAD can import. In the meanwhile, efforts are being staffed in NDHQ to tender a contract to an engineering firm capable of converting the current two-dimensional drawings of the CPF into a three-dimensional model in a file format compatible with AutoCAD and/or DIDEDEC. With concise guidelines for the generation of the CPF model, this effort could provide a true appreciation for the level of accuracy achievable in predicting the RCS of warships in Canada with the application tools proposed in this research. Successful continuation of this research

relies heavily on the generation of a more accurate model of the CPF. Failure to obtain a model from a contractor would warrant dedicating efforts towards producing an algorithm which will allow the two-dimensional digital drawings of the CPF to be converted to a format suitable for input into AutoCAD and/or DIDEK. A quick investigation into the probability of accomplishing such an endeavor was done at the beginning this research and deemed risky but the possibility of attempting this effort should not be discarded without further examination.

The next decision made early into this research was with respect to the benefits of converting JUNCTION and RAPPORT into PC-compatible applications. Using the versions available at DREO was considered but would have necessitated frequent travel or having the simulations sent by email and returned on completion, constituting a serious burden in the long term for DREO. On the other hand, it was feared that the amount of memory required by RAPPORT to perform the RCS calculations might preclude it from being able to function on a PC at all. The possibility of converting the programs using FORTRAN 77 on both the UNIX based Hewlett Packard workstations and the SOLARIS based SUN workstations at RMC was investigated. Based on the number of users on both these systems, an insufficient knowledge base in the specific area of interest and the priority this project would be afforded by the respective network managers, the decision was made to proceed with attempting to convert the files for execution on a PC. This decision was further precipitated by the fact that a Windows version of Microsoft FORTRAN 90 was available at RMC and had been used extensively by the author for a course in Numerical Techniques in Electromagnetics. This much improved version of FORTRAN had been compared to WATFOR 77, Microsoft FORTRAN 77 as well as the UNIX version of FORTRAN 77 on the Hewlett Packard workstations at RMC and proven to be

much more flexible with respect to memory allocation in addition to fostering easier to use debugging and programming tools. Converting RAPPOR to a PC based platform would have the added benefit of facilitating classified research further along in the process.

The effort to convert JUNCTION and RAPPOR to function on a PC using FORTRAN 90 was successful. The only significant concessions required were related to a minor memory allocation limitation and a relatively large reduction of computational speed, in the order of 10 folds. The "limit.h" file of RAPPOR Version 3.0 contains the limits of the eight global arrays declared by FORTRAN which dictate the amount of memory required to execute the program once compiled. For instance, the value of "MAX_NR_PATCHES" was set at 1,500,000 by DREO and at 60,000 by TNO in their compilation of the program. At 60,000, the PC version was set close to the maximum available memory for this purpose yet sufficient to run most RCS prediction simulations. For instance, the simulations executed using a "maxsize" equal to 0.001 generated approximately 2,400 patches for the CPF model constructed in this research. Decreasing "maxsize" to 0.0001 resulted in RAPPOR describing the same model using approximately 21,000 patches and any value smaller than 0.0001 was not practical to run on the PC version. Fortunately a value of 0.001 for "maxsize" was small enough to determine the impact of changing the geometry of the model. Consequently, most simulations were performed on the PC version of RAPPOR at RMC.

The opportunity to submit files to DREO by email was used on occasion to validate results. This was particularly beneficial in cases where the results appeared to be flawed as it served to provide a second opinion on the accuracy of both the model and the process from drawings to result plots. This was easily accomplished as the output file formats of AutoCAD,

DIDEC, JUNCTION and RAPPORT were all completely interchangeable between the PC and DEC-ALPHA versions. To further simplify comparisons, the use of the different hardware platforms generated identical results which took away any doubt of errors being present when discrepancies were noted. This was not the case initially as modifications were required to the source code to rectify deficiencies which resulted in disparities between the two platforms. The use of DREO's facilities was equally beneficial in running simulations using "maxsize" of 0.0001 to validate the results obtained with 0.001 as it represented a considerable times savings to do so once models had been finalized and verified at RMC. Based on the dimensions of the CPF, 0.0001 was considered the physical optics lower limit of "maxsize" and thus the memory limitations and the increase in calculation time inherent in the PC were not a serious issue. That is not to say that the value of "maxsize" was not important. In fact to the contrary, tests conducted on several models indicated clearly a marked difference between the results obtained using 0.01 and 0.001 for "maxsize". The difference between 0.001 and 0.0001 was not nearly as significant and only impacted the level of detail of the curves on the polar plots as opposed to the location of major returns.

The importance of the number of reflections considered in estimating the RCS was also investigated. Taking an infinite number of reflections into account would idealize the returns calculated at the cost of increasing the computation time needlessly. Several different simulations were performed to investigate this feature and the results indicated a notable difference between the returns for single bounce to those using two reflections. Experiments were conducted using up to eight reflections and showed that three reflections were sufficient to accurately account for multiple bounce contributions to the RCS.

Overall, the process described in Chapter 3 was found suitable for analyzing the RCS of complex objects like the CPF. The primary limitation of this process was the complexity of converting the information from the drawings to the computer. The digitizing of drawings is a laborious exercise which ultimately determines the achievable accuracy of the RCS prediction process. It is true that increasing the number of reflections and reducing the value of “maxsize” improves the exactitude of the results but both constitute a marked increase in computational time. The run-time for a simulation similar to the one described in the parameter file of Figure 4-4 using a “maxsize” value of 0.001 was in the order of minutes while the same run on a 90 MHz PC with 16 MB of memory exhausted nearly four hours. Running the same simulation using a “maxsize” of 0.0001 took days to run using the PC version of RAPPORT. It is expected that the generation of a complete CPF model would comprise a far greater number of facets and necessitate the use of a platform more powerful than a PC to produce results. On the other hand, power and network failures at DREO resulted in a simulation run using a “maxsize” value of 0.00001 to take several months. Fortunately the results of this simulation were requested more out of interest as they theoretically exceeded the physical optics limit. The use of the PC could nevertheless prove valuable as the RAPPORT simulation was the only computationally time consuming part of the overall process proposed in Chapter 3.

It is expected that the benefits gained from generating a more precise model of the CPF would enable for a more accurate assessment of the limitations intrinsic to RAPPORT’s use of physical optics in the RCS prediction of complex objects. As discussed in Chapter 2, RCS prediction techniques do not account for all scattering mechanisms. In using physical optics, RAPPORT accounts only for the simplest of cases which may be the reason for the results not

comparing favorably to the expected values. It is possible that edge diffraction and other mechanisms will need to be accounted for in RAPPORT's source code but the probability of providing a significant impact on the results appears unlikely based on theory. Figure 2-3 indicates a minimum of 10 dB difference between physical optics and experimental results beyond 70° from normal incidence on a flat plate. This 10 dB minimum is not that significant in itself but the variance becomes nearly 40 dB or more when compared to the maximum return at 0°. It is this 40 dB difference which makes it very likely that the overall contribution of including edge diffraction in the prediction process is not at the source of the low levels obtained in the simulations.

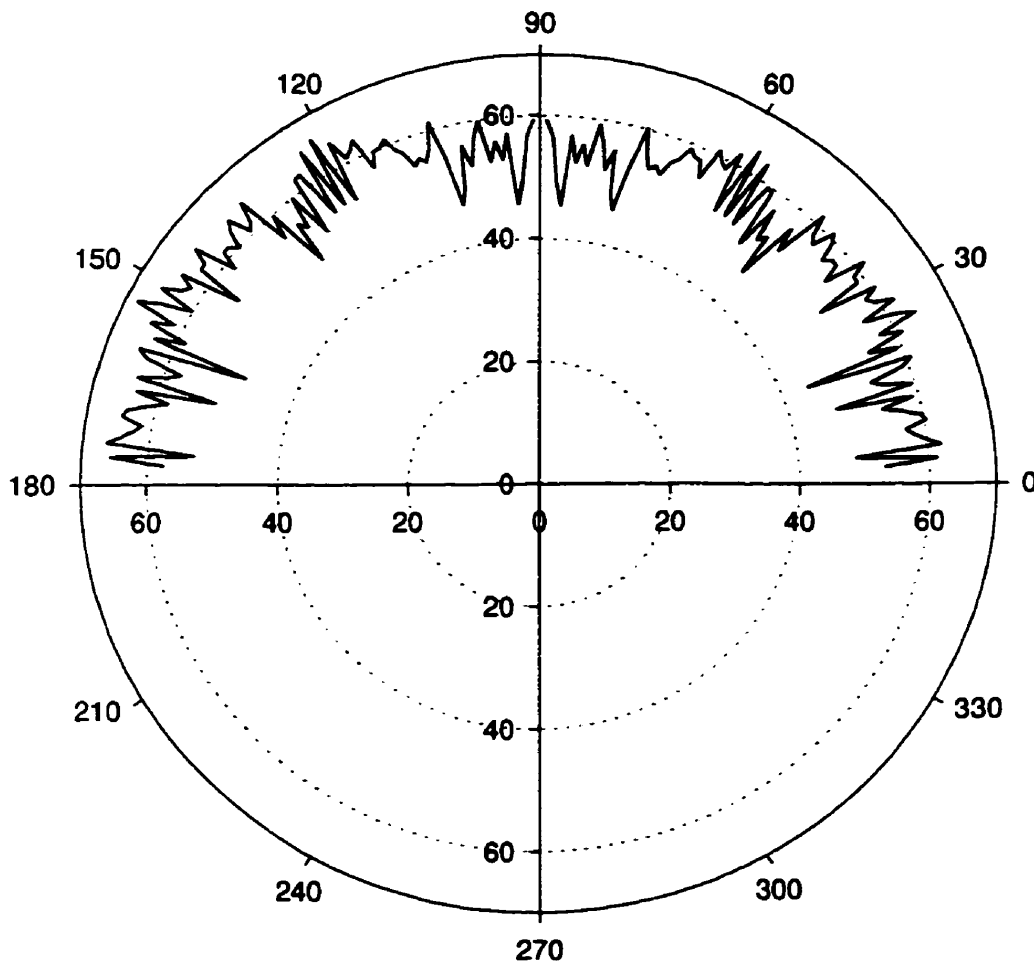
Aside from the geometrical aspects of the model, the physical characteristics also play an important role in determining the RCS of an object. These characteristics, including the conductivity of the surface, were not investigated in this research. The results of this research simply made use of DREO's efforts in investigating the impact of including frequency-dependant sea-water dielectric parameters in the prediction process [15]. Although RAPPORT has the ability to assign different characteristic parameters to each facet of the model, failure to achieve a high enough level of accuracy in the model renders utilizing this feature a futile effort.

5.2 REVIEW OF RESULTS

The most important step in producing accurate results is without a question the generation of a model as exact as practically possible to reality. At the beginning of this research, much effort was dedicated to identifying which details would fill the gaps in RCS identified in the baseline model. One of the basic assumptions made from the beginning of this research was that

slight discrepancies in the dimensions of the details being modeled on the CPF would not impact the RCS significantly. This is the case for simple objects considered separately such as flat plates but it was not so for a complex object like the CPF. This was not obvious from some of the initial results obtained. For instance, the change in waterline by over 0.5 meter had a mere 0.22 dB impact on the RCS yet it represented a reduction in the surface area on each side of the ship of nearly 80 meters². To put things in perspective, this is equivalent to the dimensions of a 9 meter by 9 meter flat plate which constitutes a relatively large object, even on a ship the size of the CPF. Equally interesting was the meager 0.06 dB increase in RCS resulting from the addition of the mast base given that it represented a surface area of nearly 75 meters² looking horizontally around the added structure. On the other hand, the initial error in modeling the hangar door as perfectly vertical instead of given it the requisite 2.3° slope presented a 10.94 dB increase in the overall RCS even though there was effectively no increase in surface area. It is not being suggested that the surface area is the only factor impacting on the RCS of an object although it is certainly most pertinent. The point being made is that the shape of the object and the elevation angle at which it is being analyzed play a much bigger role than does the surface area in certain circumstances. This was not particularly unexpected as clearly from Table 2-1 the impact of both these factors is apparent. What turned out to be somewhat of a surprise was the fact that the areas where these factors would be more prevalent were not easy to ascertain. The impact of even slight changes in dimensions or angles in some areas had significant impacts while almost non-existent in others. The knowledge of the hierarchy of scattering shapes was not as important a factor in the micro-object modeling process as it was in the macro sense. In other words, it was far less important to consider the relative merits of including a dihedral shaped

RCS in dB versus Elevation



Plot 5-1 Radar Cross Section versus Elevation of Modification 'k'

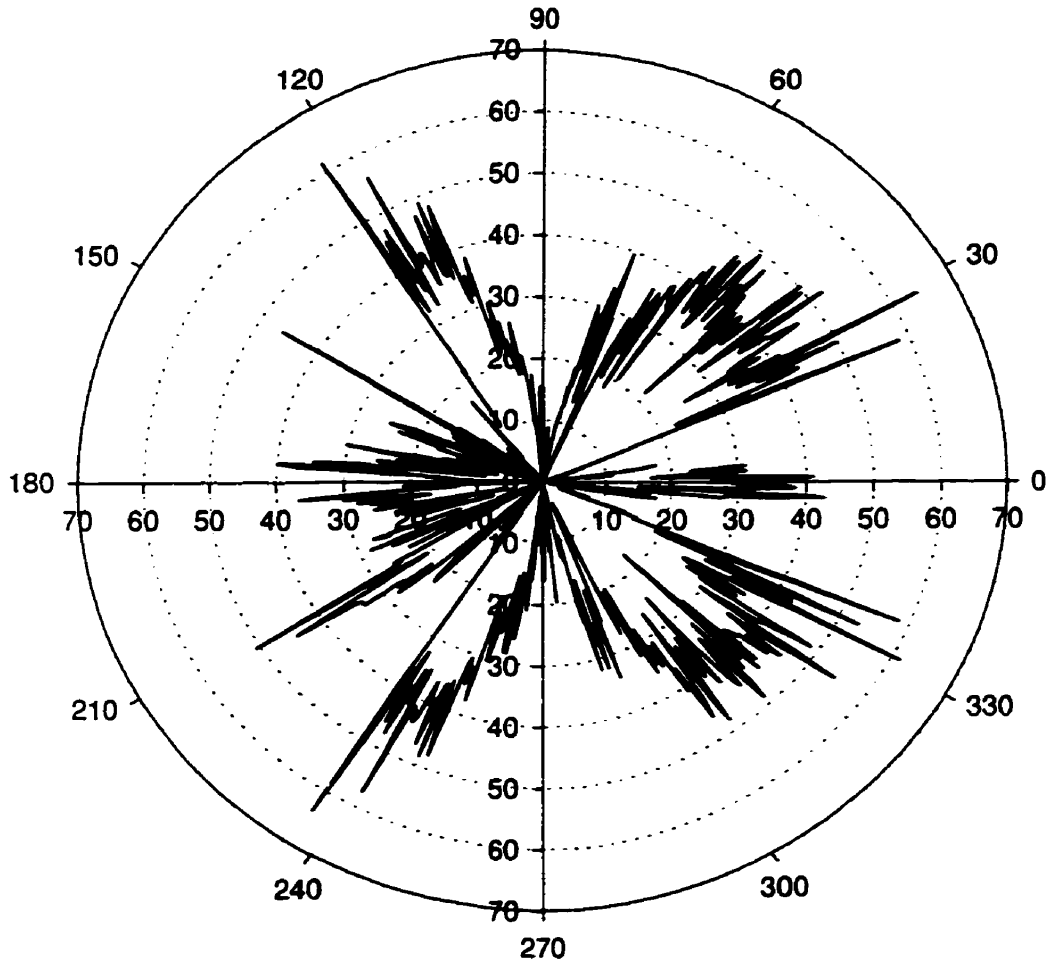
object as opposed to a trihedral than it was to consider the interaction or impact on the inclusion of the object into the larger model. This was the case on the boat deck where reducing the VLSS canister length in modification 'r' actually increased the RCS even if in theory the surface area had been reduced. In this case, it was the contribution from the reflections created by the space between the bottom of the canisters and the deck which brought about the difference. The 3.8 dB increase in the RCS level resulting from this modification was the most significant one made to the model aside from the errors made with the flat plate on the both deck and the hangar door angle, modifications 'e' and 'm' respectively.

The elevation angle was also worth serious consideration in assessing the impact of adding objects or changing the geometry of the model. Although these results are not specifically documented in Chapter 4, the RCS varied with elevation angle in a similar fashion as it did with the azimuth angle. The difference being that the RCS variation with elevation angle was not nearly as severe except near 0° , 90° and 180° . On a simulation run performed using the model depicting modification 'k' at an azimuth angle of 180° , the RCS did not exhibit any significant spike-like features as shown in Plot 5-1 except at 0° , 90° and 180° where the signal levels fell outside the 0 to 70 dB range of the plot.

The effort of generating a model of the CPF with an RCS closely resembling that of the actual measured results is not simply a case of making the individual objects which constitute the ship fit to fill the gaps in the RCS plot. It is very important to construct the model in such a manner as to achieve a level of certainty in not only the comparison between the results but in the ability to extrapolate the process in including objects. This is the only means of ensuring that the prediction process is able to evaluate the impact of changing the geometry of the ship without

RCS Difference in dB versus Azimuth

Impact of all modifications on
the CPF Baseline Model



**Plot 5-2 Radar Cross Section Difference Between Modification 'r'
and Baseline Model of the Canadian Patrol Frigate Model**

requiring measurements. This would be beneficial in determining the impact of not only RCS reduction techniques but also in assessing the impact of changes in the waterline as a result of load characteristics or the addition of an antenna during a deployment for example.

The possibility of having the modeling inaccuracies described above account for all the gaps in the CPF RCS plot is unlikely. Should a refined model of the CPF be generated, it is expected that its ideal representation of objects will remain a factor in the achievable accuracy of the results. Taking the funnel of the CPF as an example, there are cooling grids on the top forward corners as opposed to being perfectly flat plates as modeled in this research. A maple leaf sits on the middle of the funnel and the metal surface suffers from a rippling phenomenon. The corners of the funnel are to a certain extent rounded as opposed to perfectly square and finally the angle between the funnel and the deck may not be exactly as depicted in the drawings or the model. It is believed that the ideal representation of objects over-emphasizes certain areas of the return such as broadside while de-emphasizing others. It is conceivable that some of the large spikes inherent in the return of the current AutoCAD representation of the CPF would be smoothed-out by the details omitted or oversimplified in the model. The overall average RCS would not likely be changed but would differ in appearance.

The ideal representation of smaller objects cannot be avoided completely due to the size limitations imposed by physical optics. In the main mast for example, not only are the beams constituting the structure very small, they have features which are almost impossible to model. Such is the case with the oval penetrations on the mast beams because such shapes are difficult to accurately represent with triangles, especially at these small sizes. A quick analysis of Figure 4-4 reveals that the baseline model RCS has several spikes which would be indicative of large flat

areas. It is possible that some of these narrow spikes are the result of ideal modeling which as stated above presents an oversimplified representation of the ship. The impact of changing the geometry of a flat plate even slightly was touched upon in Chapter 2. In essence, the simplistic approach to modeling the ship using only flat triangular facets may offer certain non-ideal characteristics. In reality, what appears to be a flat surface area may in fact have slight irregularities or a multitude of small objects mounted to it such that the return is less of a spike and more distributed. As indicated previously, depicting smaller objects increases the complexity of the model significantly and results in increased computation time. Without the benefit of the error checking capabilities provided by JUNCTION, ensuring the accuracy of the details modeled would have been practically impossible.

Overall, the modifications made to the baseline model of the CPF resulted in an average RCS increase of 19.47 dB. This increase excludes the erroneous impacts of the modifications which were modeled either improperly, as was the case with the VLSS flat plate without thickness and the vertical hangar door angle, or to emphasize the impact of certain features like the solid mainmast and the VLSS canister length. The impact of cropping the 8 VLSS canisters on the port side could easily be added to the 19.47 dB already implemented which would amount to an additional 5.65 dB, assuming a response similar to the one observed on the starboard side.

The results of the modifications made to the baseline model are shown in Plot 5-2. The improvements were clearly localized. The forward quadrants show nearly 40 dB improvement over a 40 degree span around approximately 45° and 315°. In the aft quadrants, several spikes are located approximately 30° on either side of dead astern with two 20° wide windows of nearly 40 dB improvement at approximately 115° and 245°. Notwithstanding the fact that the baseline

model accuracy was found to be insufficient in allowing subsequent modifications to provide truly valid results for radar cross section reduction purposes, some interesting conclusions can nevertheless be made in this respect. Given the impact of the modifications made to the boat deck area, the VLSS structure in its entirety is worth considerable attention. Only the hangar door modification was even close to being worthy of consideration for radar cross section reduction purposes based on the modifications implemented. Having said that, the modifications made relating to the VLSS were in all cases simplifications of reality with the exception of the flat plate which is believed to be a close approximation. Notwithstanding the uncertainty over the actual impact of the VLSS on the overall CPF RCS, it is worth noting that it was the formation of dihedral and trihedral corners which had the most significant impact on the overall RCS. These areas can be found throughout the ship around common areas like hatches and doors for example. These types of details appear to be more likely to impact the RCS than the objects located high above the waterline given their greater interaction with the surrounding structure and the ground. As a result, it is suggested that future modeling efforts of the CPF not pay too much attention to masts although their base structures should clearly be included given their obvious interaction with the remainder of the ship from a wave reflection perspective.

CHAPTER 6 CONCLUSION

The initial aim of this research was to build a model of the CPF suitable for RCS analysis. This model could then be utilized to ascertain the effectiveness of radar cross section reduction techniques such as the application of radar absorbent material or shaping. After determining that the possibility of automatically converting the available two-dimensional electronic drawings of the CPF into a three-dimensional file format compatible with AutoCAD was low, the decision was made to focus efforts towards one of two baseline models available at DREO. Notwithstanding the fact that both baselines were considered of average precision from the beginning, based on RCS theory it was felt that the level of detail was sufficient to achieve the desired results.

After much time and effort, the initial assumptions pertaining to modeling precision had proven to be invalid. The fact that the level of detail would increase the validity was never in question but the extent to which this was true was somewhat unexpected. The scope was thus adapted partway through the research to that of investigating the impact of geometry on the RCS of complex objects. In all, eighteen primary modifications were made to the baseline model chosen to attempt to fill the gaps in the RCS. Although an overall average improvement of nearly 20 dB over the baseline model was achieved with these modifications, it was the significance of rigorously modeling the details which was most notable.

This research made it apparent that in order to make any use of the results produced by the process proposed in Chapter 3, a means of automatically converting ship's drawings into a format suitable for input into AutoCAD or DIDEK was essential. It is considered fundamental

that such a model of the CPF be generated as the next step in this research to confirm RAPPORT's ability to accurately represent the RCS of the CPF. The primary complication of such an endeavor will be the modeling of smaller objects. The use of physical optics by RAPPORT limits the size of the smallest lines depicting the shape of the objects forming the model to no less than approximately one wavelength. It is possible that this limitation will prevent the results from attaining the desired accuracy. The other potential limitation arises from the omission of edge diffraction in the algorithm used by RAPPORT to calculate the RCS. The effort to achieve a model precise enough to successfully investigate the effectiveness of radar cross section prediction techniques using numerical modeling may indeed rely on improvements to either RAPPORT or XPATCH.

The journey towards the aim of this research also provided some secondary benefits. The conversion of the process used by both TNO and DREO relied on high-powered computer platforms. This research was conducted almost exclusively on a 90MHz personal computer with a mere 16 MB of memory. The PC version was not surprisingly slower in computing the RCS of a complex object like the CPF but was nevertheless able to prove its usefulness. This was particularly so as all input and output file formats of the various software tools described in Chapter 3 were compatible between the PC-version at RMC and the DEC-version at DREO. Given that the results of the CPF RCS are ultimately classified, this becomes an important contribution as it allows unclassified work to be conducted by a contractor or academic institution such as RMC on the model using a personal computer and leave the actual compilation of results to the defense agency, in this case DREO. Otherwise this type of research will continue to progress at a seemingly slow rate in Canada because of the security precautions

inherent in such efforts. It is worth noting that the validity of the model was in large part dependant on the error-checking features built into the modified version of JUNCTION. It is not considered likely that a contractor could build a precise model of the CPF without some exposure to the complete process described in Chapter 3 and using these error-checking features.

REFERENCES and BIBLIOGRAPHY

- [1] "United States Naval & Shipbuilding Museum Online", <http://www.us-salem.org/features/mysteries/ans02.htm>, on web site 3 November 1997.
- [2] E.F. Knott, J.F. Shaeffer and M.T. Tuley, "Radar Cross Section" Artech House, Norwood, MA, 1985, pp. 14-15, 47-50, 116-152 and 174-192.
- [3] A. Tappan, "www.seawolf.com", <http://www.seawolf.com/navy/usn/cru/sc21.jpg>, on web site 3 November 1997.
- [4] "U.S. Navy: Welcome Aboard", <http://www.chinfo.navy.mil/navpalib/ships/carriers/g-washington/refuel3.jpg>, on web site 3 November 1997.
- [5] "United States Naval & Shipbuilding Museum Online", <http://www.us-salem.org/navhist/canada/current/halifax/calgary1.jpg>, on web site 3 November 1997.
- [6] M.I. Skolnik, "Radar Handbook", Second Edition, McGraw-Hill, New York, 1990, pp. 11-12 to 11-31.
- [7] J. Darke and R. Porter, "Radar Backscatter Multi-Source Mathematical Model of a Canadian Patrol Frigate at J-Band Using Horizontal Polarization" UK SECRET UK/CAN EYES ONLY, Thorn EMI DMP.10703 Issue 2, June 1988.
- [8] G. Villis, "J-Band Backscatter RCS Measurements and Scatterer Location for CPF Halifax", UK SECRET UK/CAN EYES ONLY, Thorn EMI PO 103903, December 1989.
- [9] M.G.E. Brand, "Radar Signature Analysis and Prediction by Physical Optics and ray Tracing: The RAPPORT code for RCS Prediction", Netherlands Organization for Applied Scientific Research, TNO Report FEL-95-A097, June 1996.
- [10] M. Dion, S. Kashyap and A. Louie, "A Sophisticated CAD Tool for the Creation of Complex Models for Electromagnetic Interaction Analysis", Defense Research Establishment Report 91-16, Ottawa, June 1991.
- [11] D.J. Andersh, S.W. Lee, F.L. Beckner, M. Gilkey, R. Schindel, M. Hazlett and C.L. Yu, "XPATCH: A High Frequency Electromagnetic Scattering Prediction Code Using Shooting and Bouncing Rays" in Proc. 10th Annual Review of Progress in Applied Computational Electromagnetics, vol. 2, pp. 424-433, March 1994.
- [12] "XPATCH Success Story: Aerospace Noncooperative Target Recognition (NCTR) Program", <http://hpcweb.nosc.mil/hpc/xpatch/xpatch.html>, on website 5 June 1997.

- [13] J.B. McLachlan, "Electromagnetic Modeling of Complex Structures", Royal Military College of Canada, Kingston, Ontario, 1991.
- [14] C. Harrison, "Data Reduction and Analysis of HMCS Halifax RCS Data", Atlantis Scientific for Defense Research Establishment Ottawa, Contract Number W7714-3-0142, Report Number 324, August 1994.
- [15] S. Kashyap and A. Louie, "Radar Cross Section of Objects on Sea Water", Defense Research Establishment Ottawa, Report to be published.
- [16] A. K. Bhattacharyya and D. L. Sengupta, "Radar Cross Section Analysis & Control", Artech House, Norwood, MA, 1991.
- [17] A. Stewart, "Ship Radar Signature Control", Defense Research Establishment Ottawa Technical Note 90-12, May 1990.
- [18] D. Bird, "Target RCS Modelling", in Proc. IEEE 7th National Radar Conference, pp. 74-79, March 1994.
- [19] V. Stein, "RCS Prediction Models Based on PO and PTD and State of Validation", in Proc. Electromagnetic Wave Propagation Panel Specialists' Meeting, AGARD-CP-501, pp. 12-1 to 12-13, May 1991.
- [20] O. Weiland and J. Wendiggensen, "Aspects of Radar Cross Section Calculation for Targets of Complex Structure", in Proc. Electromagnetic Wave Propagation Panel Specialists' Meeting, AGARD-CP-501, pp. 13-1 to 13-11, May 1991.
- [21] I. De Leeneer and E. Schweicher, "RCS calculations of 3-dimensional objects, modeled by CAD", in Proc. Electromagnetic Wave Propagation Panel Specialists' Meeting, AGARD-CP-501, pp. 14-1 to 14-9, May 1991.
- [22] J. Warner, E. M. Starczewski and R.V. McGahan, "A Comparison Between Bistatic Radar Cross Section Prediction Codes", TTCP Report KTP-5-4, October 1991.
- [23] K. Wheaton, "RCS Reduction Plan for Halifax Class Ships", SECRET, Operational Research Division of Maritime Command Headquarters, Halifax, NS, Research Note RN 1/95, January 1995.
- [24] G. W. Hermann, "Radar Cross Section Measurements Conducted with Canadian Frigate Halifax Sept. 25, 1991", SECRET, Naval Research Laboratory, Washington, DC, NRL/MR/5360--93-7341, July 1993.

- [25] S. Kashyap and K. Wheaton, "Radar Signature Reduction", presentation package for brief at the Technology Investment Strategy Workshop, Ottawa, 9 October 1996.
- [26] DND Drawing Number 8455591, Hangar Structure, 1:50 scale.
- [27] DND Drawing Number HAL 8555564, General Arrangement of Inboard Profile, Outboard Profile and Decks, 1:50 Scale.
- [28] DND Drawing Number 8156014, Mast Structure, 1:25 and 1:10 Scale.